

CIRCULATING COPY
Sea Grant Depository

LOAN COPY ONLY

**Validation Studies of Models TEA and ELA
in Boston Harbor and Mass Bay**

E. Eric Adams, Douglas J. Cosler, John K. MacFarlane,
Keith D. Stolzenbach, Philip M. Gschwend and Anne M. Okamura

MITSG 90-247

90-27

MIT Sea Grant College Program
Cambridge, Massachusetts 02139

Grant Number: NA86AA-D-SG089
Project Number: RC-14/RC-16
November 1990

Abstract

The two-dimensional models TEA and ELA are being used to help site a diffuser outfall in western Massachusetts Bay to convey sewage effluent from the MWRA's proposed secondary treatment plant on Deer Island. This model validation study complements the siting effort by comparing measured tidal and low-frequency currents in western Mass Bay against simulation with TEA and by comparing the measured concentrations of halocarbon tracers, discharged from the existing Deer and Nut Island outfalls, against corresponding simulations with ELA. An extensive sensitivity study is also performed to identify the sensitivity of simulated concentrations to outfall location, pollutant decay rate, model representation of tidal and low-frequency currents, dispersion, near-field representation and treatment of the open boundary. This study follows previous model validation effort in Boston Harbor reported by Kossik et al. (1986)

Acknowledgments

This work, project number RC-14 and RC-16, was funded (in part) by the MIT Sea Grant College Program under federal grant number NA86AA-D-SG089, from the National Sea Grant College Program, National Oceanic and Atmospheric Administration, U.S. Department of Commerce.

This report was submitted to Camp Dresser & McKee Inc. in September 1987, first revised in December 1987 and revised again in March 1988. At the time the report was written, the authors were all affiliated with the MIT Department of Civil Engineering R.M. Parsons Laboratory.

Related reports

Tracing and Modelling Pollution Transport in Boston Harbor, by Richard F. Kossik, Philip M. Gschwend and E. Eric Adams. MITSG86-18. 227pp. \$5. Order from the MIT Sea Grant College Program, 292 Main St., Bldg. E38-368, Cambridge, MA 02139.

Table of Contents

ABSTRACT	i
1 INTRODUCTION	1
1.1 Project Objectives	1
1.2 Brief Review of TEA and ELA	1
2 MODEL SENSITIVITY STUDIES AND CHANGES	4
2.1 Base Case	4
2.2 Outfall Location, Low Frequency Currents, and Decay Rate	6
2.3 Open Boundary Conditions	8
2.4 Tidal Currents and Dispersion Coefficients	9
2.5 Near Source Representation and Dilution	11
2.6 Grid Refinement	13
2.7 Conclusions Based on Sensitivity Studies	13
3 ANALYSIS OF CURRENT METER DATA AND RELATIONSHIP TO TEA SIMULATIONS	16
3.1 Tidal Components	16
3.2 Low Frequency Currents	19
4 HALOCARBON TRACER STUDY	21
4.1 Background	21
4.2 Details of April 27, 1987, Survey	22
4.3 Results	23
4.4 Qualitative Observations	24
4.5 Model Calibration	28
4.6 Discussion	31
5 SUMMARY AND CONCLUSIONS	33
6 REFERENCES	36

1. INTRODUCTION

1.1. Project Objectives

This report describes work performed by MIT to validate the numerical models TEA and ELA to field data collected in western Mass Bay. The validation study thus complements earlier validation work performed on Boston Harbor and described in Kossik et al. (1986). The models TEA and ELA are being used by Camp, Dresser & McKee, Inc., (CDM) in their analysis of potential outfall sites for the new secondary treatment plant for the MWRA.

In close cooperation with CDM, a number of changes have also been made to the model and the grid to better simulate potential impacts. This report describes the model changes and results of the validation study.

1.2. Brief Review of TEA and ELA

The purpose of this report is to present results which address the validity of the models' application. Hence, only a brief discussion concerning the two programs is given below; additional information is provided in the discussion of the sensitivity studies, and in other references.

TEA is a two-dimensional harmonic finite element circulation model. In its complete non-linear form, TEA solves the following depth-averaged continuity and x and y momentum equations

$$\frac{\partial \eta}{\partial t} + \frac{\partial}{\partial x}[u(h+\eta)] + \frac{\partial}{\partial y}[v(h+\eta)] = 0 \quad (1.1)$$

$$\frac{\partial u}{\partial t} + u \frac{\partial u}{\partial x} + v \frac{\partial u}{\partial y} - fv = -g \frac{\partial \eta}{\partial x} + \tau_x^s / \rho(h+\eta) - \tau_x^b / \rho(h+\eta) \quad (1.2)$$

$$\frac{\partial v}{\partial t} + u \frac{\partial v}{\partial x} + v \frac{\partial v}{\partial y} + fu = -g \frac{\partial \eta}{\partial y} + \tau_y^s / \rho(h+\eta) - \tau_y^b / \rho(h+\eta) \quad (1.3)$$

where $h(x,y)$ is mean water depth, $\eta(x,y,t)$ is water surface elevation above the mean, $u(x,y,t)$, $v(x,y,t)$ are x and y velocity components, f is the Coriolis parameter, g is the acceleration of gravity, τ_x^s , τ_y^s are the x and y components of surface (wind) stress, $\tau_x^b = \rho c_f |u| u$, $\tau_y^b = \rho c_f |u| v$ are the x and y components of bottom friction, and $|u| = (u^2+v^2)^{\frac{1}{2}}$.

The model can be driven by prescribed elevations on open (ocean) boundaries, by prescribed fluxes (e.g., rivers) on land boundaries, and by prescribed shear stress on the surface. Because the model is harmonic, all forcing functions are presumed to be the sums of periodic components. (Note that steady forcing can be modeled as a periodic forcing with zero frequency.) When the model is driven by forces on the boundary at a particular frequency, the primary response in the interior is at the same frequency. However, because of non-linearities, responses at additional frequencies are also created. Through an iterative procedure, the full non-linear model allows any number of such frequencies to be generated. However, the model may also be run in a linear mode in which non-linear terms are dropped (bottom friction is linearized) and hence the model responds only at the forcing frequency. An intermediate option allows operation in the linear mode, with response only at the forcing frequency, but with iteration in order to better approximate non-linear bottom friction. In the following these three modes are designated, respectively, non-linear, linear, and linear with iteration.

For more information, the major references to the model TEA are Westerink et al. (1984, 1985); additional references include Westerink et al. (1986a, b).

ELA is a 2-D transport model which can be coupled with TEA to solve the depth-averaged advection-diffusion equation

$$\frac{\partial c}{\partial t} + u \frac{\partial c}{\partial x} + v \frac{\partial c}{\partial y} = \frac{1}{h} \frac{\partial}{\partial x} \left[h D_{xx} \frac{\partial c}{\partial x} + h D_{xy} \frac{\partial c}{\partial y} \right] + \frac{1}{h} \frac{\partial}{\partial y} \left[h D_{yx} \frac{\partial c}{\partial x} + h D_{yy} \frac{\partial c}{\partial y} \right] + \theta \quad (1.4)$$

where $c(x,y,t)$ is concentration, D_{xx} , D_{xy} , D_{yx} , and D_{yy} are dispersion coefficients, and θ represents sources, sinks, and vertical boundary fluxes. In applications with a constant diffusion coefficient, $D_{xx} = D_{yy} = D$ and $D_{xy} = D_{yx} = 0$. ELA solves Eq. 1.4 using a split operator technique involving the backwards method of characteristics for advection, an implicit finite element scheme for dispersion, and local explicit calculations for source and sinks.

The major reference to ELA is Baptista et al. (1984), and additional references include Baptista et al. (1985, 1986), and Baptista (1987). Kossik et al. (1986) describes previous applications of the two models to Boston Harbor and is cited throughout this report.

As part of this project, several changes were made to ELA to improve program efficiency and accuracy. These changes include use of a new sparse matrix solver in the finite element calculations, development of an improved tracking technique for the advection step, procedures to handle advection near shorelines, and improved resolution near sources. The last is discussed in more detail in §2.5.

2. MODEL SENSITIVITY STUDIES AND CHANGES

Before embarking on a detailed calibration/validation effort, it was thought to be important to explore the sensitivity of simulated concentrations to variation in a number of parameters and input variables. In this way we could better understand which portions of the validation effort were most critical. While the sensitivity study was not exhaustive, it did cover most aspects thought to be important, and complements additional sensitivity shown in Kossik et al. (1986). The model parameters and inputs used in the sensitivity study are summarized in Table 2.1, which also identifies the numbers of corresponding figures showing output. Calculations for both TEA and ELA were performed with the grid shown in Figures 2.1a and b. Note that this grid does not include refinements to be used in final outfall simulations and described in §2.6. Hence this grid is designated "old."

2.1. Base Case

Run 1 is a base-case water column simulation by ELA for the existing conditions assuming a combined loading from the Deer and Nut Is. treatment plants of 13.4 Kg/day and a combined flow rate of 23 m³/s. Currents consist of only M₂ tides computed with the linear mode of TEA by prescribing sinusoidal variation in water level at the open boundary between Cape Ann and Provincetown. Decay is represented by a constant downward fall velocity (representing particle settling) or upward piston velocity (representing gas exchange) of 4 cm/hr (\approx 1 m/day). A constant far field dispersion coefficient of $D = 70 \text{ m}^2/\text{s}$ was used following calibration in Boston Harbor by Kossik et al. (1986). The outfalls were treated as two single points (one for each treatment plant). Near field mixing was computed using a dilution function derived from observation at the two outfalls (Metcalf & Eddy, 1979) of the form

$$S = 50.5|u| + 6.5 \quad (\text{Deer Is.}) \quad (2.1a)$$

$$S = 31.7|u| + 5.5 \quad (\text{Nut Is.}) \quad (2.1b)$$

where S = dilution and $|u|$ = absolute current speed in units of m/s. Intermediate field spreading (at scales up to several grid spacings) was handled by ELA's puff routine using a constant puff diffusion coefficient of $D_p = 1 \text{ m}^2/\text{s}$ estimated from diffusion diagrams based on the scale of the near field plume.

Output from this and all other runs is presented at a tidal phase of high slack after 200 time steps of $\Delta t = 3.1$ hours ($\Delta t \equiv \text{tidal period}/4$) or approximately 25 days. For most calculations this is sufficient for simulated concentrations to reach a condition of periodic steady state over most of the domain. Note that the length of simulation is not a major factor in terms of computational cost—provided that periodic (e.g., tidal) currents are used. This is because calculation of the feet of the characteristics, a time-consuming step, is only performed over the first cycle (i.e., the first four time steps in these examples), and results are saved for future cycles. Calculations assume background concentrations (due to sources other than the treatment plants) are zero. They also assume zero dispersive flux boundary conditions on the open boundary between Cape Ann and Cape Cod. (Sensitivity to the open boundary condition is described in §2.3.)

Figures 2.2a and 2.2b show simulated concentration contours ranging from over 300 parts-per-trillion (ppt) near the source down to 1 ppt. The absolute concentrations are meaningful only in the context of the specified loading. However, the spatial distribution of concentration and the absolute concentration relative to other runs can be used to gauge sensitivity.

2.2. Outfall Location, Low Frequency Currents, and Decay Rate

Runs 2-12 test sensitivity to source location, low frequency current, and decay coefficient. Because the model will be used to help distinguish impacts associated with candidate sites, sensitivity to outfall location is perhaps the most fundamental sensitivity study; differences in simulated concentration for different outfall sites can serve as a reference to gauge the sensitivity to other parameters or inputs. Outfall locations that are simulated are Sites 2 and Site 5 shown in Figures 2.1a and b. Note that these sites correspond approximately to those being considered by the MWRA. However, these runs should be viewed as sensitivity studies pursuant to the objectives discussed above, rather than "official" simulations for the candidate sites.

For these additional outfall sites, mass is introduced at a discrete point using puffs based on a constant dilution of $S = 50$ and a puff dispersion coefficient of $D_p = 70 \text{ m}^2/\text{s}$. Because the actual diffuser is expected to be of the order of 1500 m in length, the single-point representation is inadequate to resolve near-source concentrations even with the near field grid sub-division provision of ELA. Note that with a dilution of 50, concentration at the end of the near field should be approximately 135, yet only contours of order 50 ppt and below are resolved in the output. Procedures for improving near field resolution from a distributed (diffuser) source, for purposes of later simulation, are described in §2.5. For the present, however, attention should be focussed only on the 1- and 10-ppt contours.

Sensitivity to low frequency currents is important because these currents, while low in magnitude, provide net drift (advective flushing) in contrast with tidal currents which mainly "slosh back and forth." Also, because much of our validation study has to do with representing low frequency currents based on observations, it is important to test the extreme variation: "with and without net drift."

For these runs, a net drift to the south was created with linear TEA by superimposing a constant linear water level slope along the open boundary in addition to the M_2 forcing. The slope was based on water level being 10 cm higher at Cape Ann than at Provincetown. The corresponding tidal average velocities ranged from less than 1.0 cm/s at Site 1 to about 2.6 cm/s at Site 5. Sensitivity of net drift to various forcing functions using linear and non-linear TEA is discussed in more detail in §3. At this point the purpose is to show sensitivity of simulated concentration to a flow field which includes a steady drift of order 1-3 cm/s.

Sensitivity to decay is included by considering two values of k : the 4 cm/hr used in the base case and 1 cm/hr. Note that the former value yields a characteristic removal time (water depth/ k) of order 10 days at the existing outfalls where depth \approx 10 m to one month at the other sites where depth \approx 30 m. Characteristic removal times for the lower value of k are four times larger.

Comparison of Runs 1-12 shows reasonably strong sensitivity to all parameters varied. Note that when the simulated outfall site is moved from the existing sites to Sites 2 and 5, concentrations in Boston Harbor and other *inshore* locations decrease monotonically; conversely, locations *offshore* of the outfall show little variation. Net drift appears to influence the simulated concentration distributions to a greater extent than the absolute magnitude of concentration. Sensitivity to net drift increases with distance from shore because of the larger drift magnitude; hence, while concentrations in Boston Harbor show little sensitivity to net drift, concentration in Mass Bay can differ significantly due to this effect. Conversely, sensitivity to decay is found throughout the domain. Because of the interest in currents in later parts of this study, results from Runs 1 and 2 are used to plot in Figures 2.14a and b the spatial distribution of the ratio of simulated concentrations with and without a net drift based on the existing outfall and $k = 4$ cm/hr.

2.3. Open Boundary Conditions

The open boundary condition is important in transport calculations because it affects the flux of mass leaving and re-entering the domain. The split operator technique used by ELA, and the associated large time step generally allowable, places some restrictions on the type of boundary condition that can be employed.

The base case calculations prescribe $\frac{\partial c}{\partial n} = 0$ on the open boundary. This condition applies to both diffusion and to advection for inflow (i.e., if a characteristic line is backtracked to the open boundary, its concentration is set to the concentration at the boundary which was established by the previous diffusion step).

This condition is clearly non-conservative in the sense that mass is added at the boundaries. To test the magnitude of the error involved, Run 17 repeats the base-case (Run 1) calculations using a boundary condition of $c = 0$. (Similarly, Run 34 repeats Run 2 which includes a steady current.) The boundary condition of $c = 0$ also applies to both diffusion and to advection for inflow (i.e., if a characteristic line is backtracked to the open boundary, its concentration is set to 0). Clearly this condition errors in the opposite sense of removing mass from the system.

Figure 2.15 plots the ratio of simulated concentration for Runs 1 and 17 showing, as expected, that the boundary condition has essentially no effect in the harbor or near shore, but an increasing effect toward the open boundary. If one assumes that the errors associated with the two conditions are equal and opposite, then an error of less than 5% (with either condition) is made to the southwest of the 90% contour, representing a little more than 50% of the surface area of the domain. Note that Site 5 is located at about the 98% contour (~1% error). For most situations these errors are probably tolerable, but they may be unacceptable in the evaluation of distant outfall sites or in simulating

pollutants with small decay rates. In such situations, the remedy is either to extend the open boundary farther to the east or to incorporate a more realistic boundary condition reflecting the gradual decrease in concentration expected naturally as one moves further offshore.

It should be added that limited experimentation was done with a boundary condition approximating $\partial^2 c / \partial n^2 = 0$. Such a condition can not be established formally in ELA, but was approximated by assuming the boundary was a line of inflection in the concentration field and extrapolating for concentrations outside of this boundary. However, initial tests showed this procedure to be unstable with the large model time steps.

2.4. Tidal Currents and Dispersion Coefficients

The base case calculations assume that the only tidal motion consists of a constant M_2 tide. Because TEA operates in the frequency domain, it is well suited to generate a range of tidal harmonics including other astronomical constituents (e.g., N_2 , S_2 , K_1 , O_1), plus compound and overtides resulting from non-linear interaction among these constituents. However, practical considerations suggest that only the most important constituents be included. Existing data as well as data from the ongoing field study (§3) suggest that the dominant astronomical constituent, by far, is the M_2 tide. Hence the dominant non-linearities would be those leading to overtides of the M_2 such as the M_4 and M_6 . Accordingly, two simulations were made using input from the non-linear version of TEA. Run 25 was driven by M_2 tidal forcing only while Run 27 was driven by M_2 forcing plus a steady 10-cm tilt. In both cases 6 overtides of M_2 were computed. The simulated currents are discussed in more detail in §3 in connection with measured currents, but in this section we concentrate on the corresponding simulated concentrations. Because the non-linear model uses quadratic bottom friction (evaluated iteratively), we include for comparison

two additional runs, Runs 26 and 28, which are otherwise comparable but are made with the linear model with iteration.

Figures 2.16a,b and 2.17a,b show ratios of simulated concentrations made with ELA in which all harmonics are included (non-linear model) versus those in which only M_2 is retained (linear model with iteration) for conditions without and with a net drift respectively. The results clearly indicate the small effect of including overtides.

The other major tidal effect which is not simulated with the base case is the influence of other astronomical constituents. For example, the linear superposition of different semi-diurnal tides is responsible for the observed spring-neap variations in tidal amplitude. Because the period of this variation is of order two weeks, ELA can not use saved feet of the characteristic lines over this interval and would be substantially more expensive to run if this cycle were resolved.

As an *approximate* test of the sensitivity to this cycle, Runs 29 and 30 were performed using M_2 boundary forcing but with only 70% of the magnitude of the base case (simulating approximate conditions of neap tide in comparison with the average tide of the base case). Run 29 contained no steady drift while Run 30 contained a steady drift achieved with a 10-cm tilt. Ratios of simulated concentrations for corresponding runs with neap tide and average tide amplitude, presented in Figures 2.18a and b and 2.19a and b, show the relatively small effect of tidal amplitude.

Because the model dispersion coefficients reflect, to a large extent, *tidal* dispersion effects, dispersion coefficients may also be expected to vary on a spring-neap cycle. Depending on the specific dispersion mechanisms being considered, dispersion coefficients could be expected to depend on tidal velocity or tidal velocity squared. Run 31 was made with a dispersion coefficient of $49 \text{ m}^2/\text{s}$ or 30% less than the base case. Figures 2.20a and b show the ratio of simulated concentrations for Runs 31 and 17 showing sensitivity to

variation in the dispersion coefficient which can be expected over a spring-neap tidal cycle. These results, plus other sensitivity studies described in Kossik et al. (1986), indicate strong sensitivity throughout the model domain, suggesting the importance of calibration to field measurements (§4).

2.5. Near Source Representation and Dilution

ELA was originally written (Baptista, 1984) to model transport resulting from specified initial conditions (e.g., following an instantaneous discharge), or resulting from boundary inflows (e.g., a polluted river or shoreline discharge). In order to model a continuous discharge from a point source in the interior of the domain (e.g., the existing Deer and Nut Is. outfalls), a puff routine was developed (Adams et al., 1986), in which the introduction of mass is simulated by the release of overlapping (Gaussian) puffs. The initial size (standard deviation σ of the Gaussian distribution) of each puff is related to the prescribed dilution S and the discharge flow rate Q_0 according to

$$\sigma_0 = \frac{SQ_0}{\sqrt{12}h|u|} \quad (2.2)$$

In general, puffs are initially smaller (order of 10's of m) than the grid size (order of 100's of m) so that the puffs can not be resolved on the ELA grid. However, puffs grow ($\sigma = \sigma(t)$) in accordance with a prescribed diffusion law (e.g., obtained from an instantaneous dye study or from the literature) until they are large enough to be resolved by the grid, at which time they are mapped onto the grid. In addition, when a concentration print-out is desired, an option is available to locally sub-divide the triangular grid into successively smaller triangles so the relatively "new" puffs can be included in the presentation of concentration contours.

Current plans call for the outfall diffuser to have a length L of approximately 1500 m, which is significantly larger than the local grid size. If it is desired to resolve concentration near the outfall, the source can not be represented by a single point as has been assumed in the runs described above. In order to achieve better resolution, ELA has been modified so that the source can be represented by N equally spaced puffs released at a given time. As before, each puff is advected by local time-varying currents and can be diffused according to a specified puff diffusion law. Initial puff size is now specified such that puffs overlap laterally by one standard deviation, i.e.,

$$\sigma_0 = \frac{L}{N} \quad (2.3)$$

This is similar to the criterion for the puff release interval Δt_p , which relates overlap in the longitudinal direction according to

$$\Delta t_p \approx \frac{\sigma}{|u|} \quad (2.4)$$

The modified source representation for a diffuser can be contrasted with the representation of a point source in terms of the relationship between source size and dilution. For a *point source*, Eq. 2.2 computes the near field lateral plume dimension (σ_0) based on *prescribed* dilution (Eq. 2.1) along with discharge flow rate, water depth, and current speed. In simulating a *diffuser* outfall, the near field lateral plume dimension is identically the diffuser length, and dilution is implicitly based on this length as well as discharge flow rate, water depth, and current speed. In the limit of large N , and assuming the diffuser orientation is perpendicular to the prevailing current direction, dilution is thus

$$S = \frac{|u|Lh}{Q_0} \quad (2.5)$$

Remembering that S represents depth-averaged dilution, and that for current speeds above a threshold dilution becomes proportional to current speed, this formulation is consistent with the initial dilution model ULINE being used to compute near field concentrations at the edge of the mixing zone.

Run 21 uses the above procedure with $N = 3$ to simulate the discharge from Site 5 under conditions that are otherwise similar to Run 6. Comparison of the two runs (Figure 2.21) shows, as expected, significant differences near the source with diminishing influence at distance. Later sensitivity also suggested that more detail near the source could be obtained with larger values of N .

2.6. Grid Refinement

The "old" grid used in the above calculations involves increasingly larger nodal spacing with distance offshore. Hence nodal spacing at the proposed outer sites is greater than that at the inner sites. In an attempt to remove potential bias that this may have when comparing simulated concentrations for the various sites, a "new" grid was designed to provide more uniform spacing in the region encompassing the potential sites. Portions of the revised grid are shown in Figures 2.22a and b and Run 37 is a repeat of Run 17 using the new grid. Figure 2.23 shows that there is little difference in simulated concentrations. The new grid is to be used for future simulations.

2.7. Conclusions Based on Sensitivity Studies

The following conclusions were reached.

- Simulated concentration distributions are sensitive to low frequency currents. The primary area of sensitivity is the lower range of induced concentrations impacting Mass

Bay. Hence it is important to study the magnitude, direction, duration, and spatial distribution of low frequency currents contained in recent measurements.

- Conversely, relatively little sensitivity is seen to the precise representation of tidal currents—either the inclusion of overtides of the M_2 tide or the inclusion of multiple tidal species. In view of the added computational expense of including additional frequencies, it is recommended that the tide be represented by only the M_2 component, using the model in linear mode with interaction, and that effort be concentrated on representation of the low frequency components. See additional discussion in §3.

- As expected, concentrations are quite sensitive to the outfall location and the pollutant considered (characterized by the decay rate). This will hopefully provide a reasonable trade-off in evaluating sites.

- The present results, as well as those of Kossik et al. (1986), show strong sensitivity to dispersion coefficient as well. The sensitivity to both dispersion coefficient and decay rate increases the difficulty in calibrating ELA to field tracer studies.

- A procedure involving the use of *multiple* puffs per time step has been developed to reasonably represent concentrations near a diffuser outfall. This procedure, along with the new grid providing uniform resolution around proposed sites, should be used in future simulations. Additional sensitivity concerning the number of puffs should be conducted using the new grid with the actual sites in order to optimize this procedure.

- As one approaches the open boundary, sensitivity to specification of the open boundary condition increases and neither condition tested, $c = 0$ or $\partial c / \partial n = 0$, is accurate near the boundary. For the conditions tested, it is estimated that the error for either condition ranges from less than 0.1% at Site 2 to about 1% at Site 5. Future simulations should be made with care and, in order not to exaggerate impacts associated with distant

sites involving slow decay rates, an effort should be directed to improved representation of this condition.

Table 2.1
Summary of Sensitivity Studies

Run Grid	Circulation		Near Source Characteristics					Far Field Characteristics				
	Mode of TEA	Forcing	Site(s)	Source		Puff	Transport	Loss	Open	B.C.	Figure	
				Repr	Disp							Disp Coef
	a	b	D_p	D	k	$\frac{\partial c}{\partial n}$						
1 old	Linear	M ₂	DI NI	2	N=1 N=1	50.7 31.7	6.5 5.5	1 1	70	4.0	$\frac{\partial c}{\partial n}=0$	2.2a, ref1
2 old	Linear	M ₂ +steady	DI NI	2	N=1 N=1	50.5 31.7	6.5 5.5	1 1	70	4.0	$\frac{\partial c}{\partial n}=0$	2.3a,b; 2.14,ref
3 old	Linear	M ₂ +steady	DI NI	2	N=1	0	50	70	70	4.0	$\frac{\partial c}{\partial n}=0$	2.7a,b
4 old	Linear	M ₂ +steady	DI NI	5	N=1	0	50	70	70	4.0	$\frac{\partial c}{\partial n}=0$	2.11a,b
5 old	Linear	M ₂	DI NI	2	N=1	0	50	70	70	4.0	$\frac{\partial c}{\partial n}=0$	2.6a,b
6 old	Linear	M ₂	DI NI	5	N=1	0	50	70	70	4.0	$\frac{\partial c}{\partial n}=0$	2.10a,b
7 old	Linear	M ₂	DI NI	2	N=1	50.5 31.7	6.5 5.5	1 1	70	1.0	$\frac{\partial c}{\partial n}=0$	2.4a,b
8 old	Linear	M ₂	DI NI	2	N=1	0	50	70	70	1.0	$\frac{\partial c}{\partial n}=0$	2.8a,b
9 old	Linear	M ₂	DI NI	5	N=1	0	50	70	70	1.0	$\frac{\partial c}{\partial n}=0$	2.12a,b
10 old	Linear	M ₂ +steady	DI NI	2	N=1	50.5 31.7	6.5 5.5	70	70	1.0	$\frac{\partial c}{\partial n}=0$	2.5a,b
11 old	Linear	M ₂ +steady	DI NI	2	N=1	0	50	70	70	1.0	$\frac{\partial c}{\partial n}=0$	2.9a,b
12 old	Linear	M ₂ +steady	DI NI	5	N=1	0	50	70	70	1.0	$\frac{\partial c}{\partial n}=0$	2.13a,b

Table 2.1 (cont.)

Run	Circulation		Near Source Characteristics				Far Field Characteristics						
	Grid	Mode of TEA	Forcing	Site(s)	Source Repr	Dilution		Transport Loss	Disp Coef	Velocity	Open	B.C.	Figure
						$S=au+b$	D_p						
17 old	Linear	M_2	DI NI	N=1	50.5 31.7	6.5 5.5	1 1	70	4.0	c=0	2.15; 2.23b;ref		
21 old	Linear	M_2	5	N=3	2070	10	70	70	4.0	$\frac{\partial c}{\partial h}=0$	2.21		
25 old	Nonlinear	M_2	DI NI	N=1	50.5 31.7	6.5 5.5	1 1	70	4.0	c=0	2.16a, b		
26 old	linear (w/ iteration)	M_2	DI NI	N=1	50.5 31.7	6.5 5.5	1 1	70	4.0	c=0	ref		
27 old	Nonlinear	M_2 +steady	DI NI	N=1	50.5 31.7	6.5 5.5	1 1	70	4.0	c=0	2.17a, b		
28 old	linear (w/ iteration)	M_2 +steady	DI NI	N=1	50.5 31.7	6.5 5.5	1 1	70	4.0	c=0	ref		
29 old	Linear	$0.7M_2$	DI NI	N=1	50.5 31.7	6.5 5.5	1 1	70	4.0	c=0	2.18a, b		
30 old	Linear	$0.7M_2$ + steady	DI NI	N=1	50.5 31.7	6.5 5.5	1 1	70	4.0	c=0	2.19a, b		
31 old	Linear	M_2	DI NI	N=1	50.5 31.7	6.5 5.5	1 1	49	4.0	c=0	2.20a, b		
34 old	Linear	M_2 +steady	DI NI	N=1	50.5 31.7	6.5 5.5	1 1	70	4.0	c=0	ref		
37 new	Linear	M_2	DI NI	N=1	50.5 31.7	6.5 5.5	1 1	70	4.0	c=0	2.23a		

1 Reference runs are used for comparison with other runs in the sensitivity study

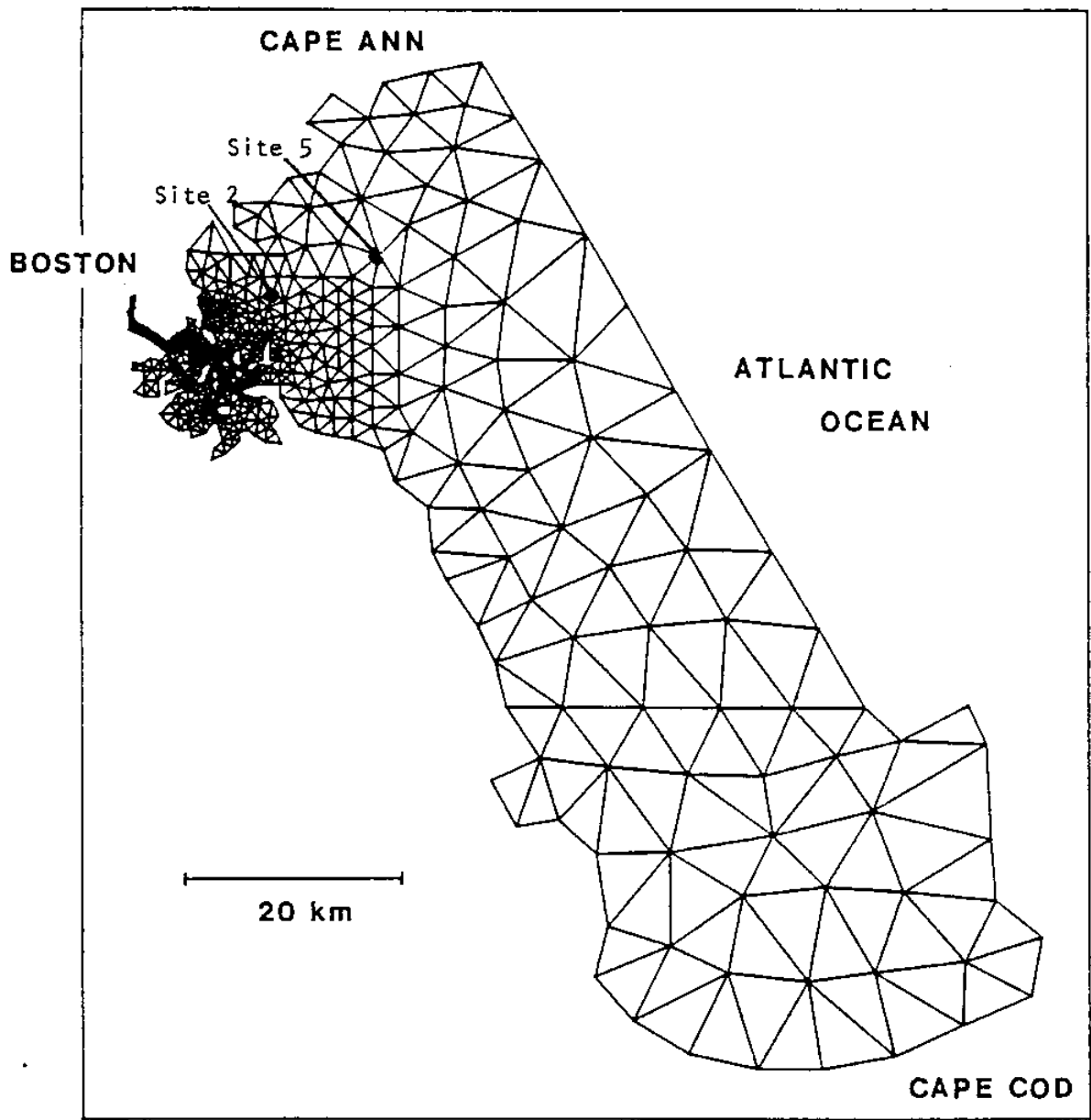


Figure 2.1a Finite element grid of Massachusetts Bay (old grid)

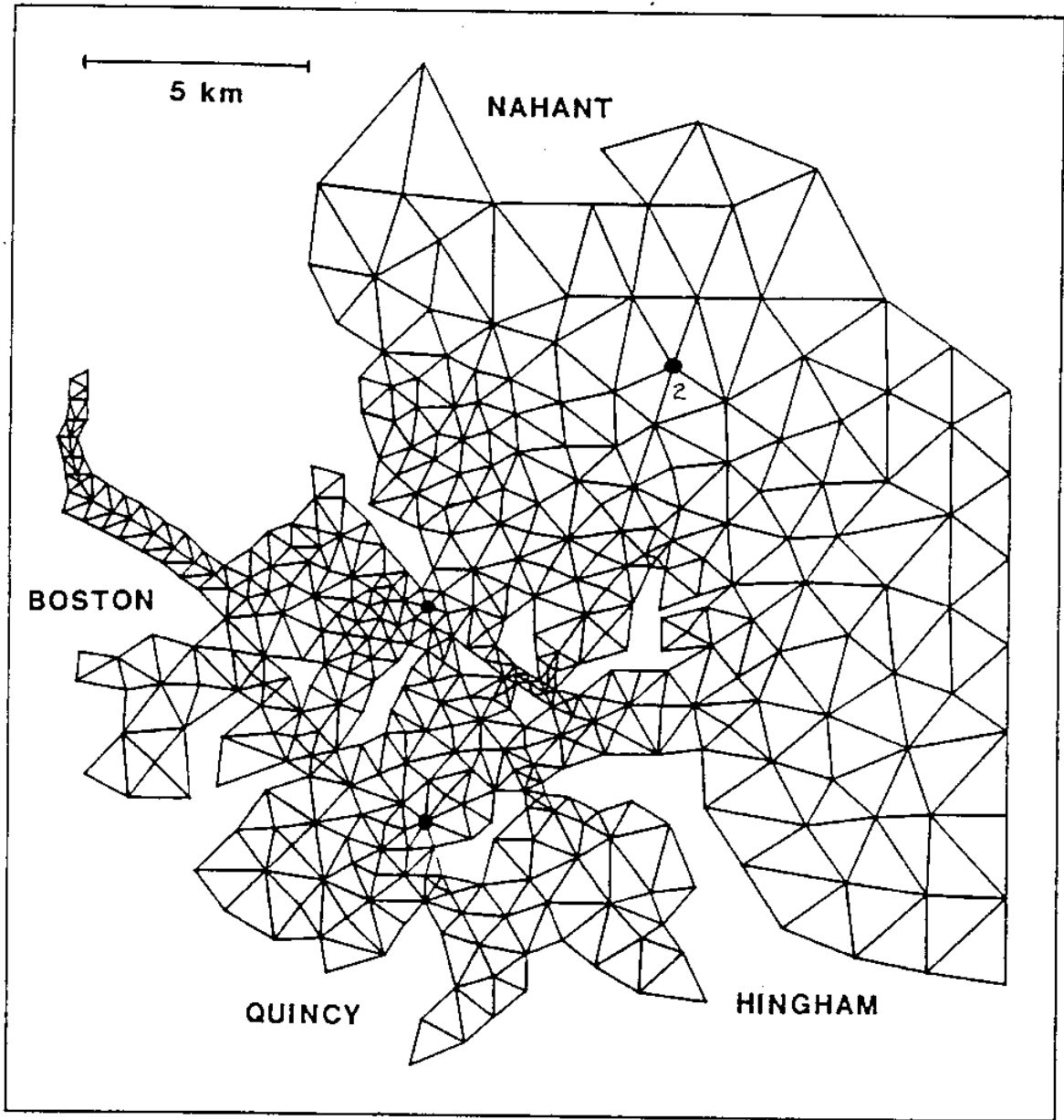


Figure 2.1b Finite element grid of Massachusetts Bay (old grid), detail of Boston Harbor

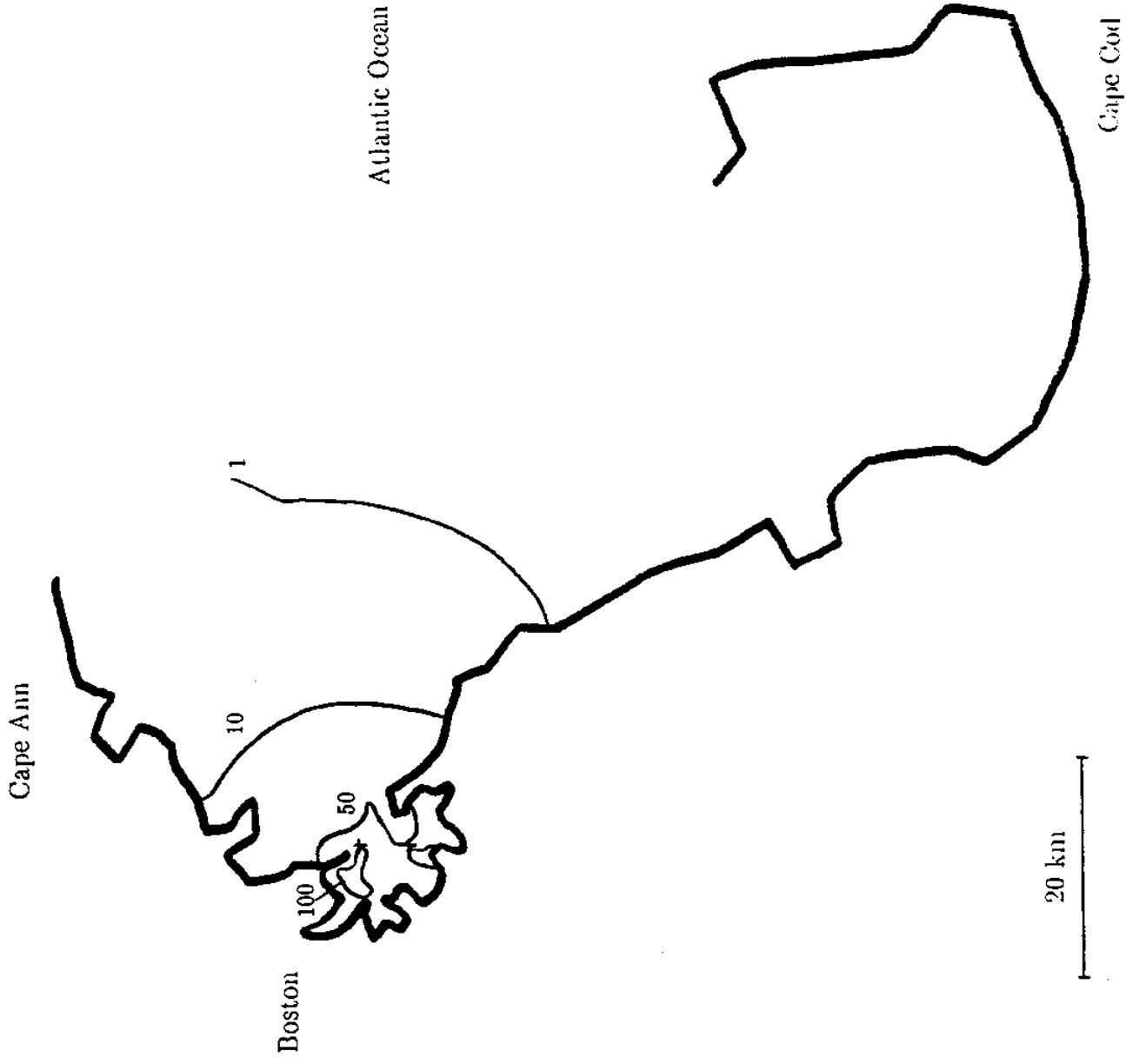


Figure 2.2a Simulated concentrations (ppt) for Run 1: Deer and Nut Is., tidal circulation only, $k = 4 \text{ cm/hr}$

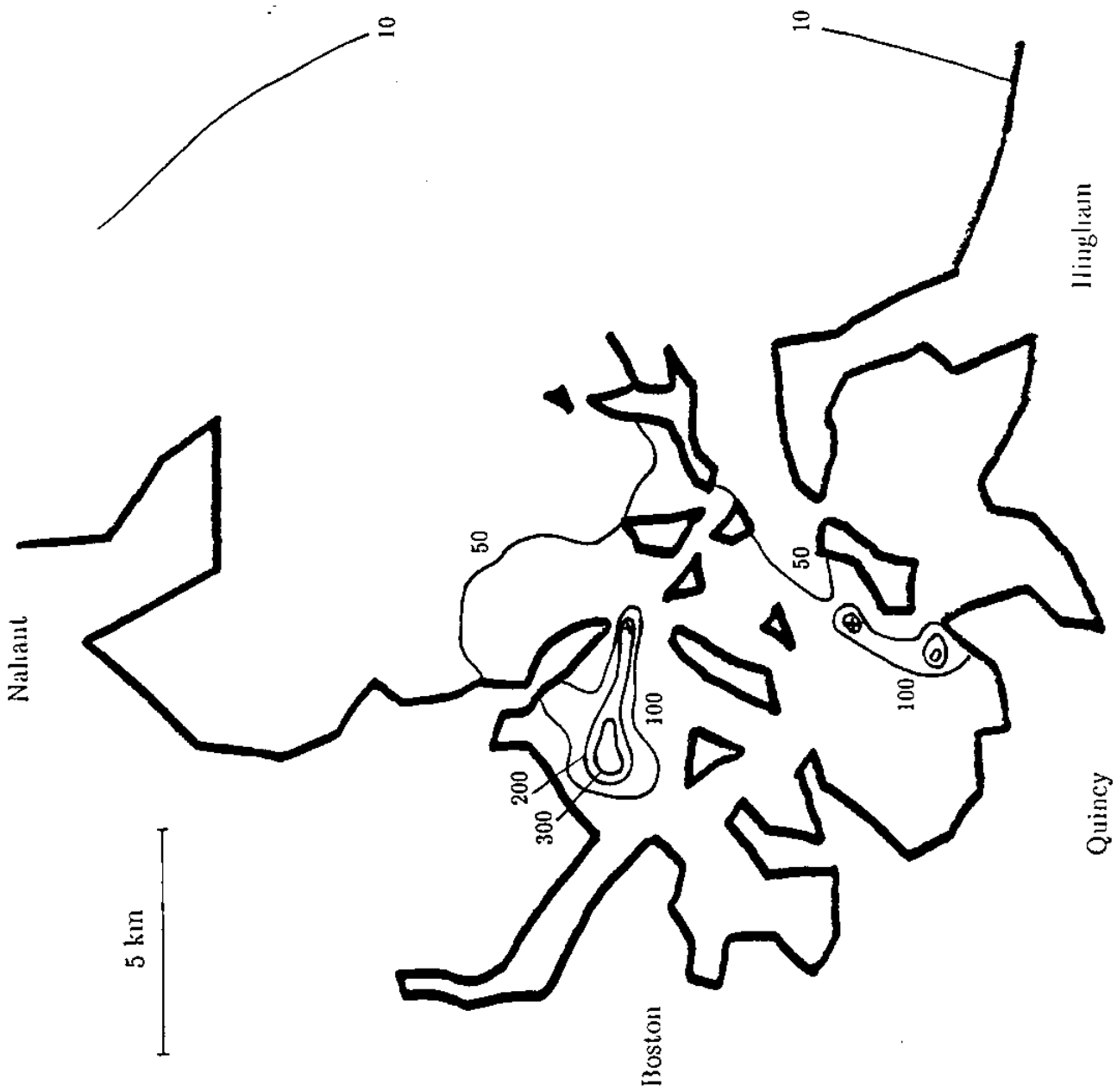


Figure 2.2b

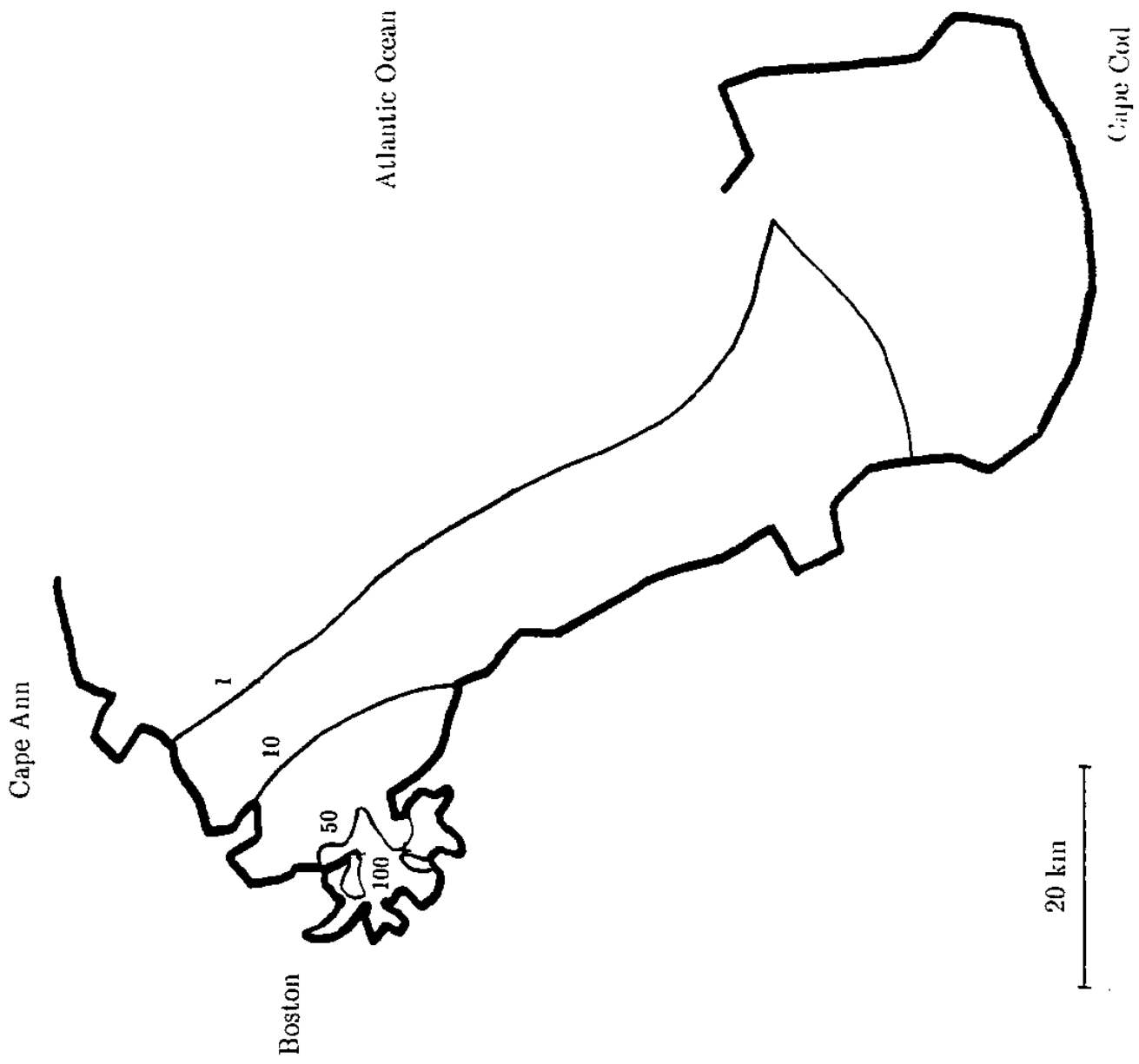


Figure 2.3a Simulated concentrations (ppt) for Run 2: Deer and Nut Is., tidal plus southerly drift, $k = 4 \text{ cm/hr}$



Figure 2.3b

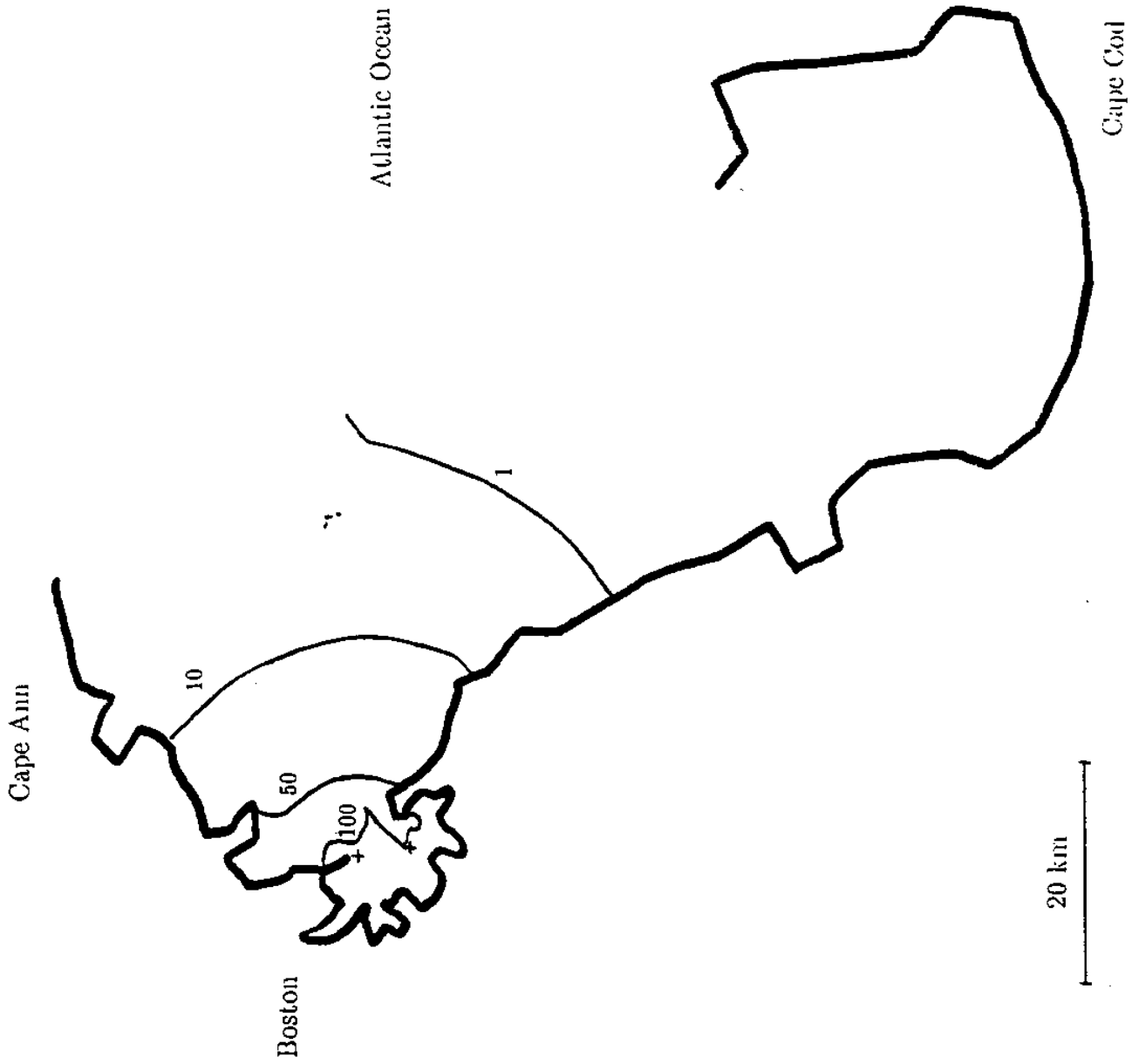


Figure 2.4a Simulated concentrations (ppt) for Run 7: Deer and Nut Is., tidal circulation only, $k = 1 \text{ cm/hr}$

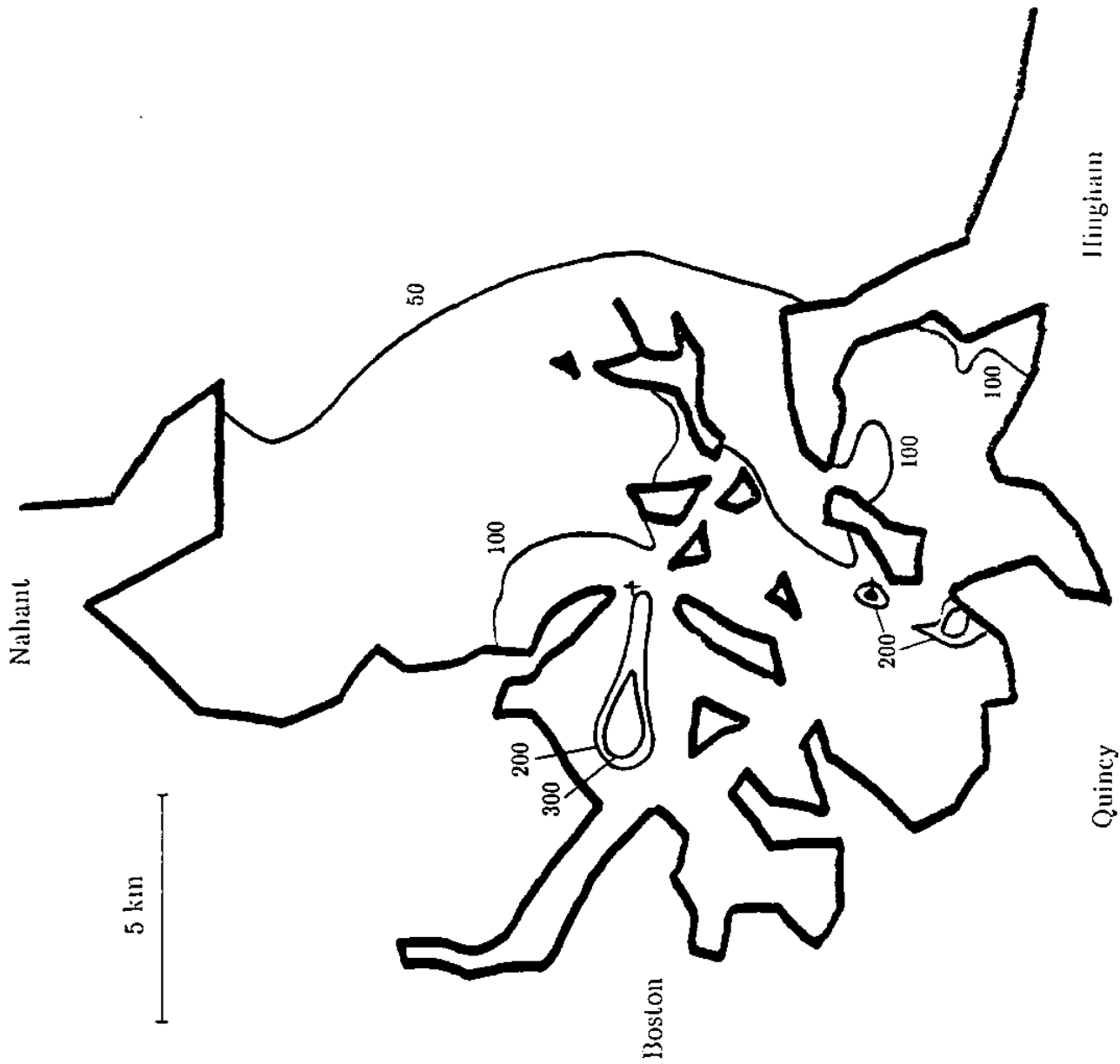


Figure 2.4b

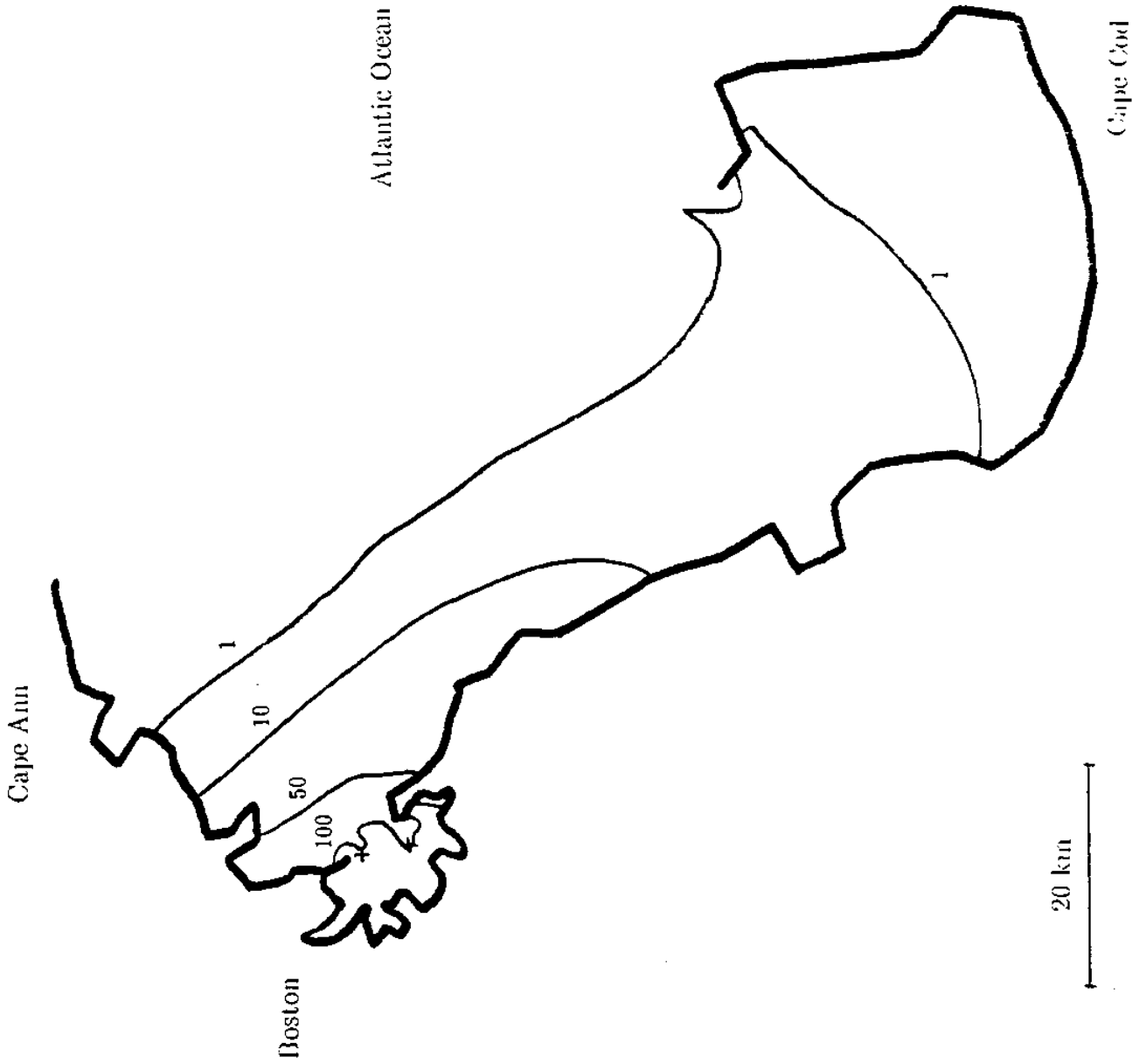


Figure 2.5a Simulated concentrations (ppt) for Run 10: Deer and Nut Is., tidal plus southerly drift, $k = 1 \text{ cm/hr}$

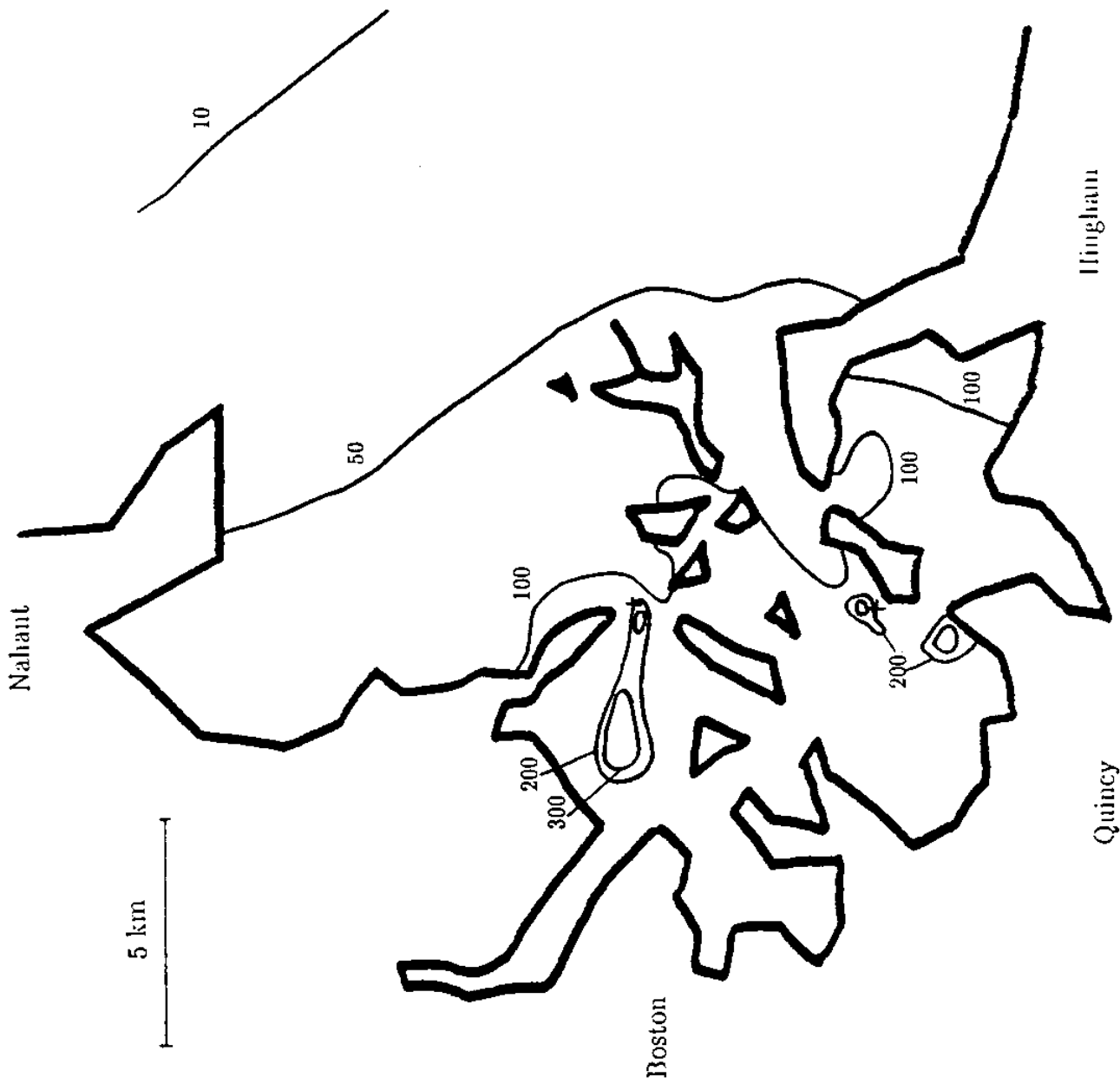


Figure 2.5b

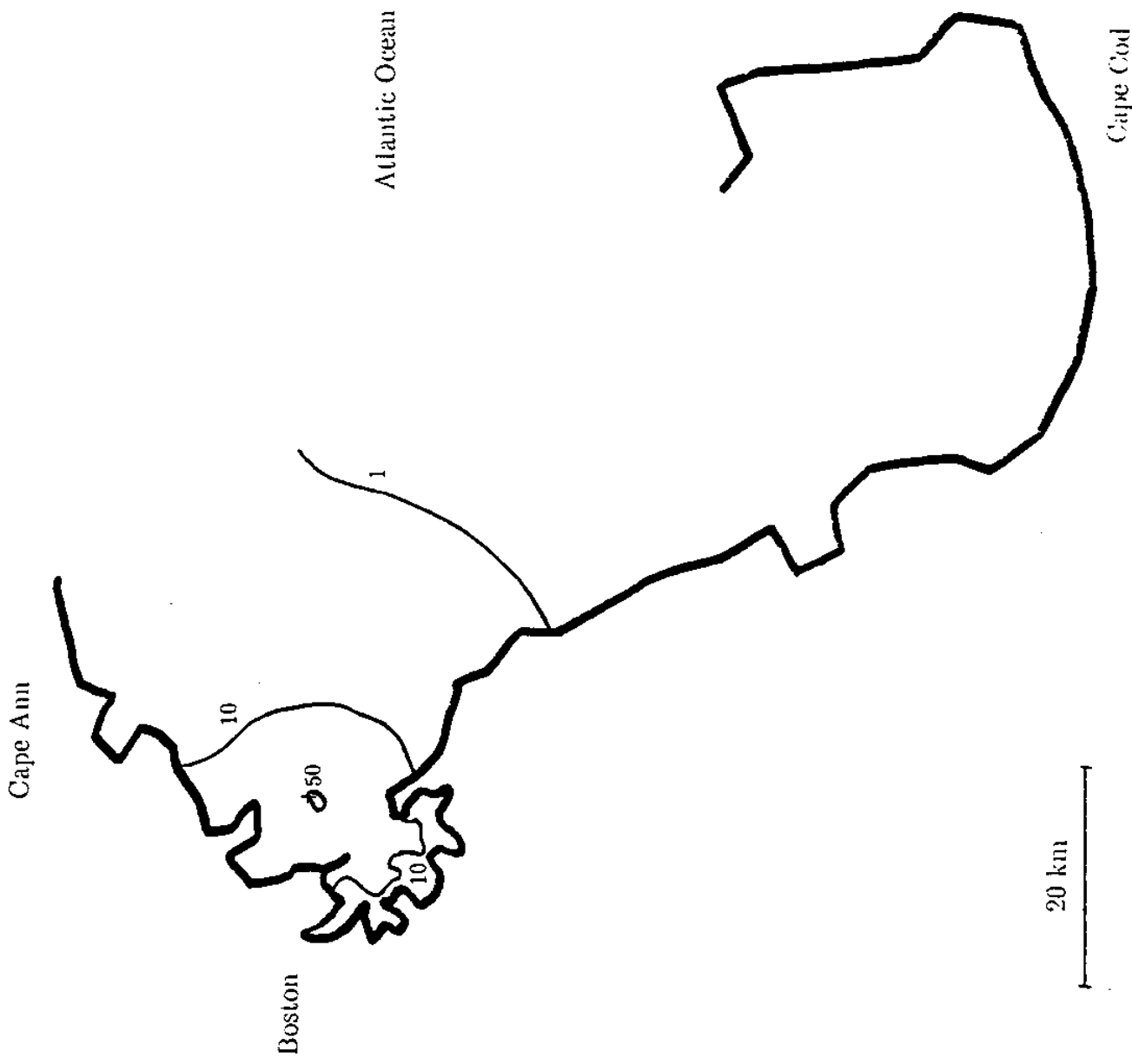


Figure 2.6a Simulated concentrations (ppt) for Run 5 Site 2, tidal circulation only, $k = 4 \text{ cm/hr}$

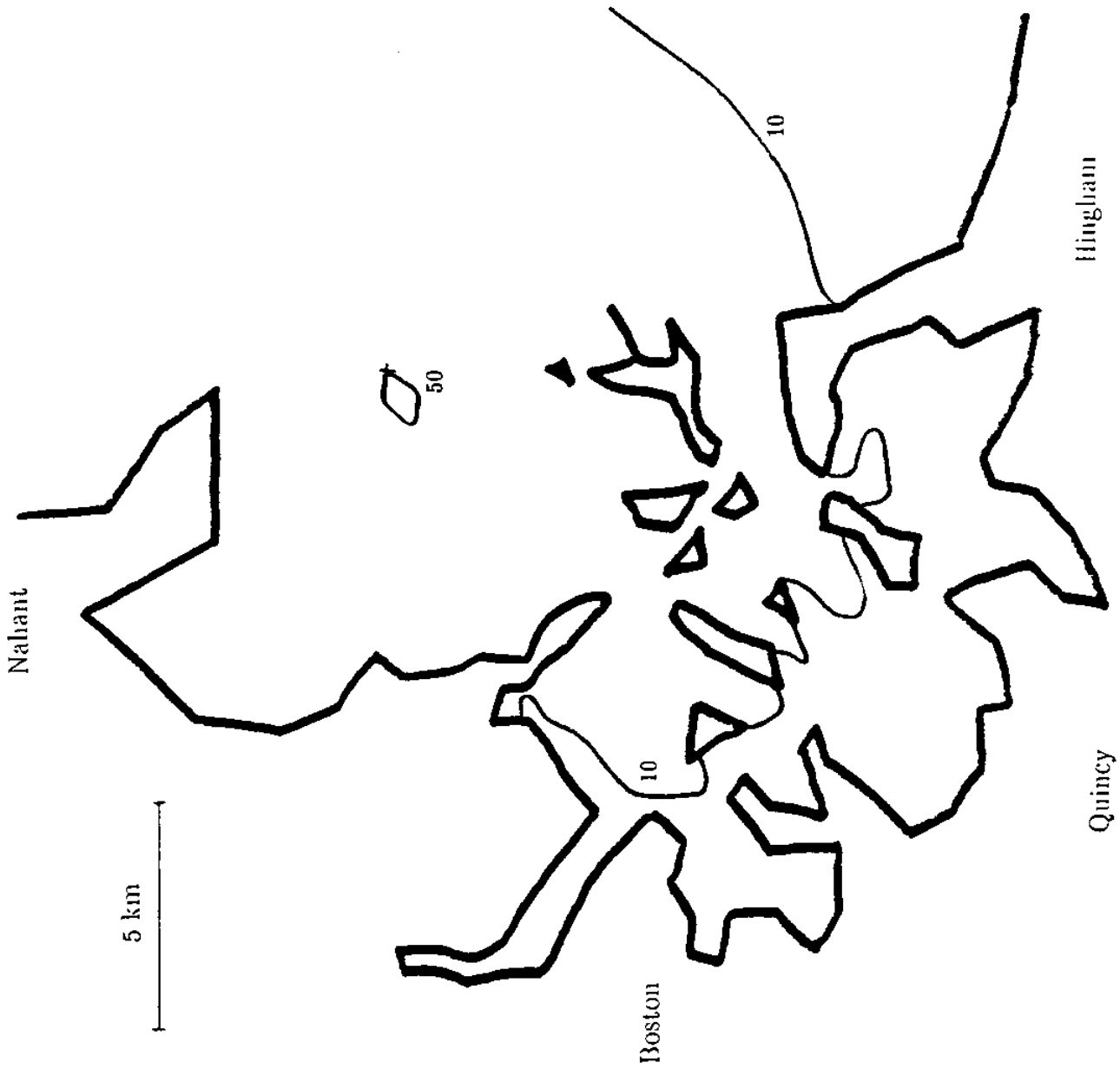


Figure 2.6b

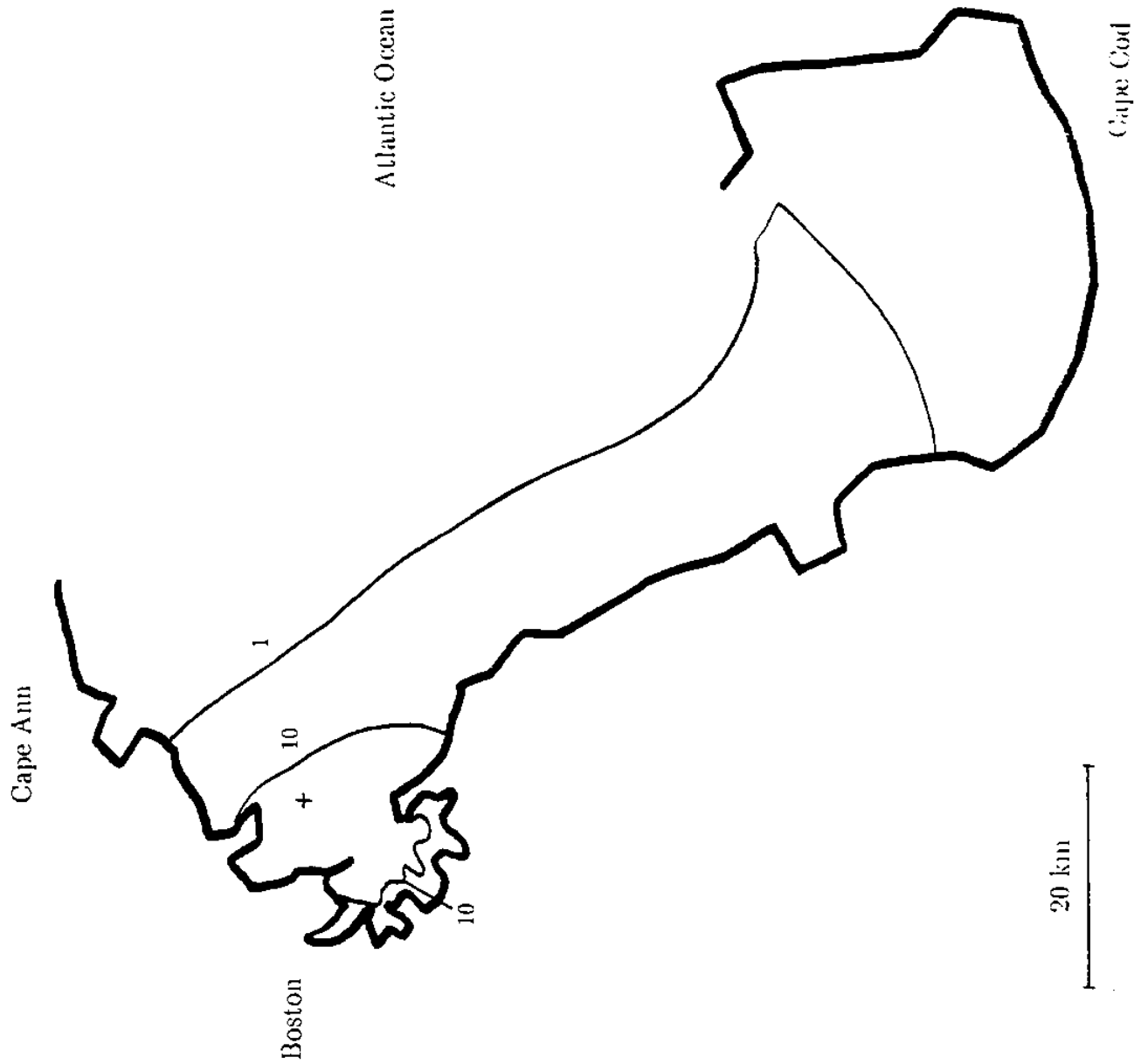


Figure 2.7a Simulated concentrations (ppt) for Run 3 Site 2, tidal circulation plus southerly drift, $k = 4 \text{ cm/hr}$

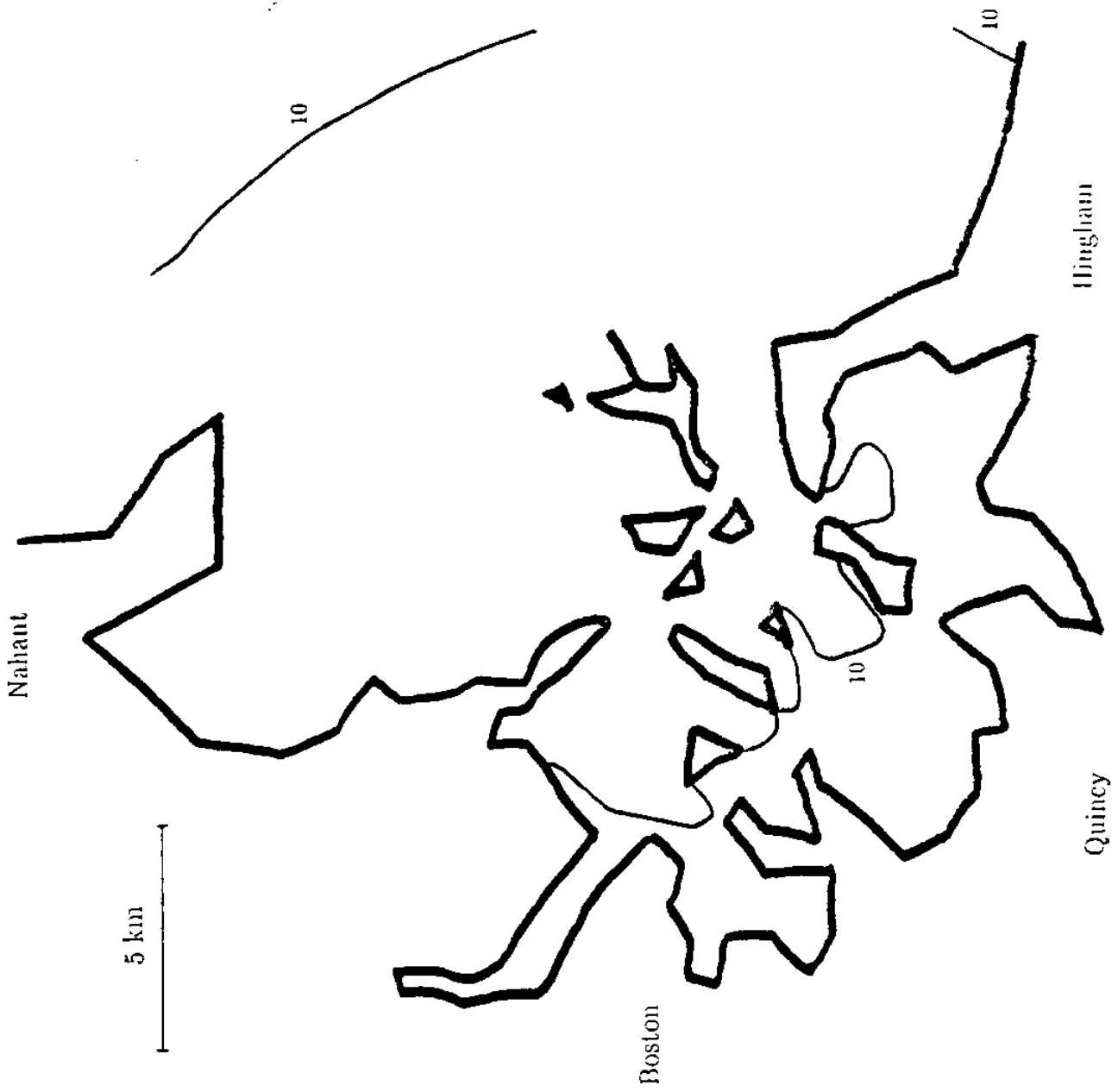


Figure 2.7b

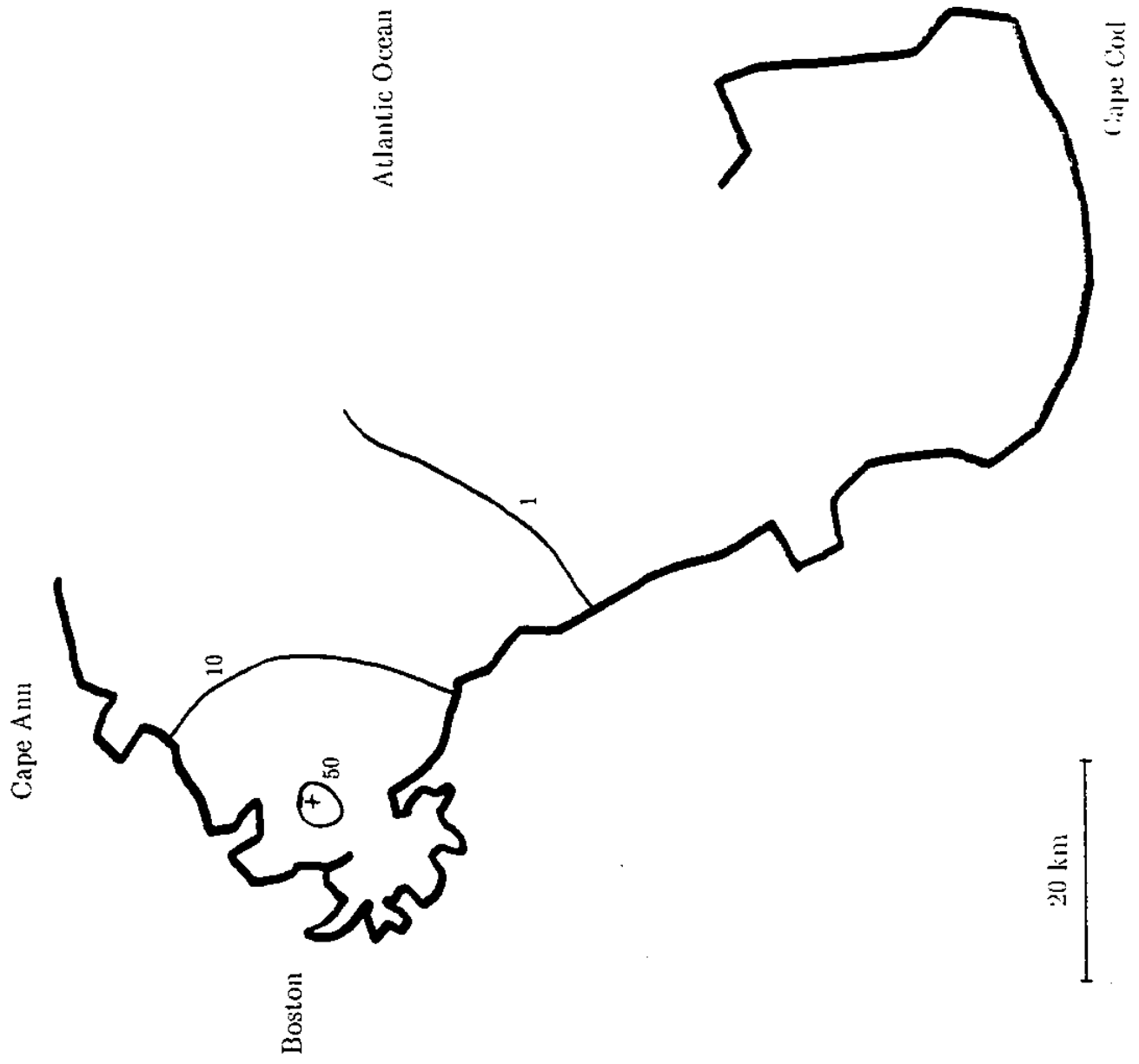


Figure 2.8a Simulated concentrations (ppt) for Run 8 Site 2, tidal circulation only, $k = 1 \text{ cm/hr}$

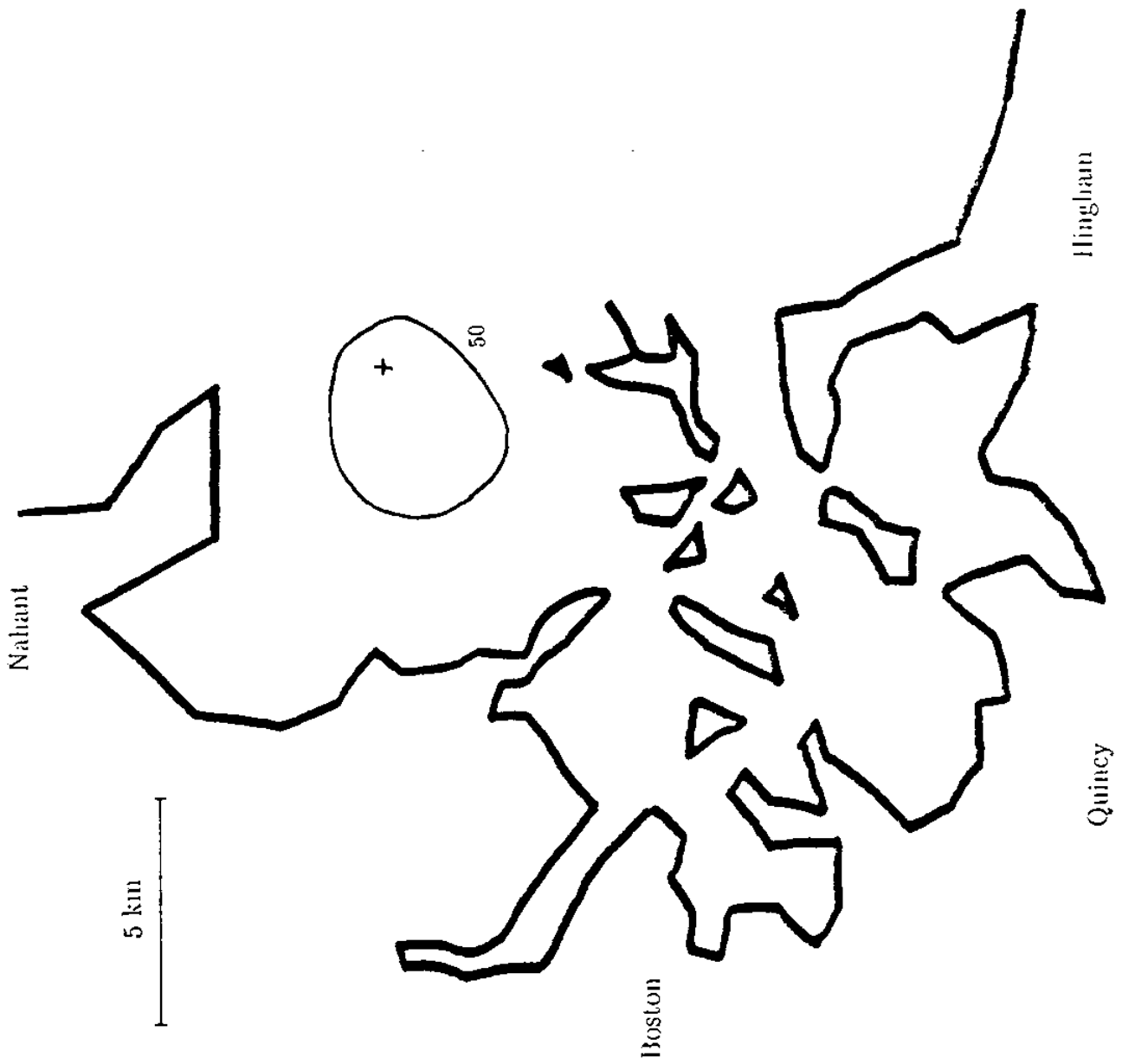


Figure 2.8b

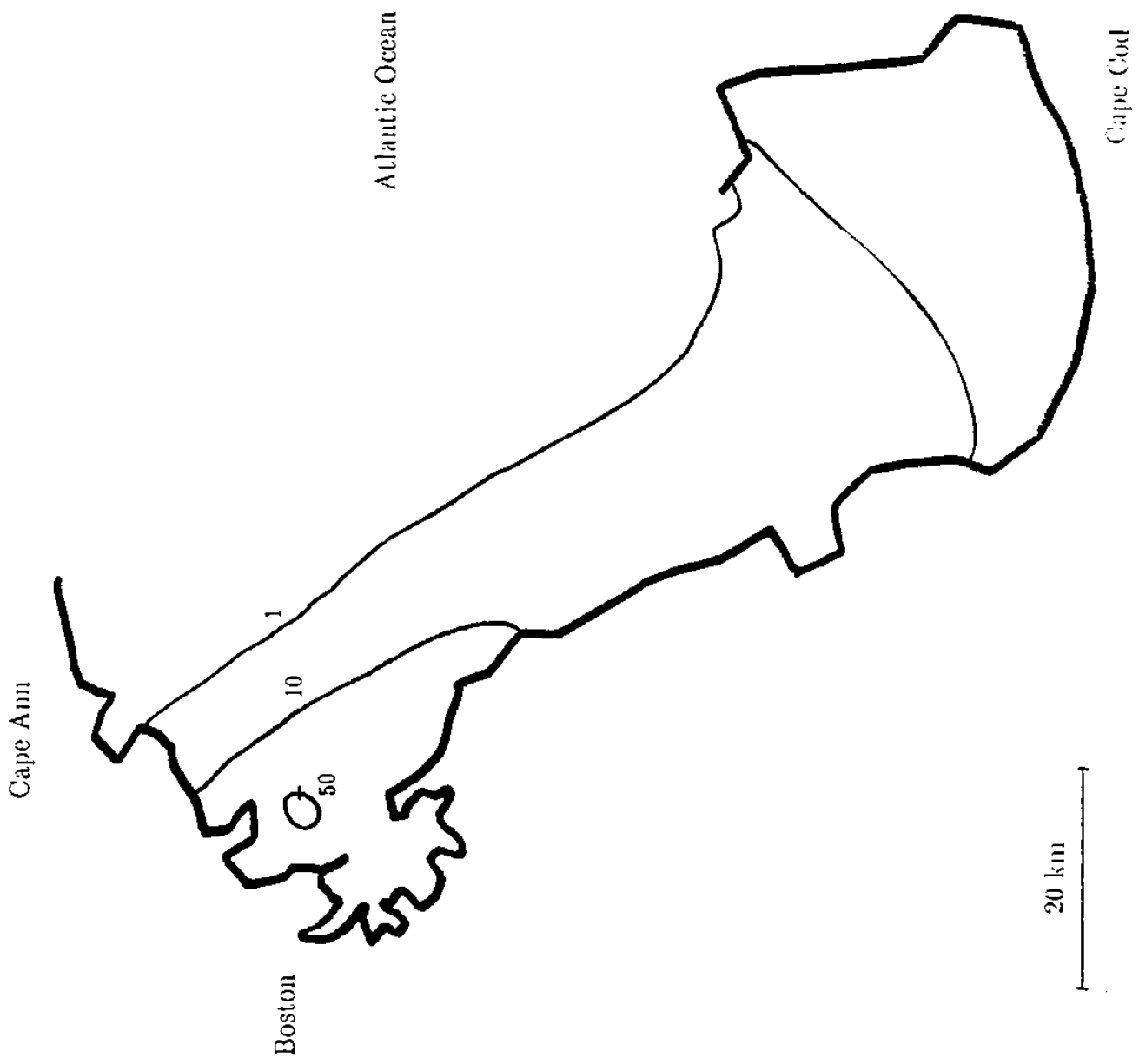


Figure 2.9a Simulated concentrations (ppt) for Run 11 Site 2, tidal circulation plus southerly drift, $k = 1 \text{ cm/hr}$

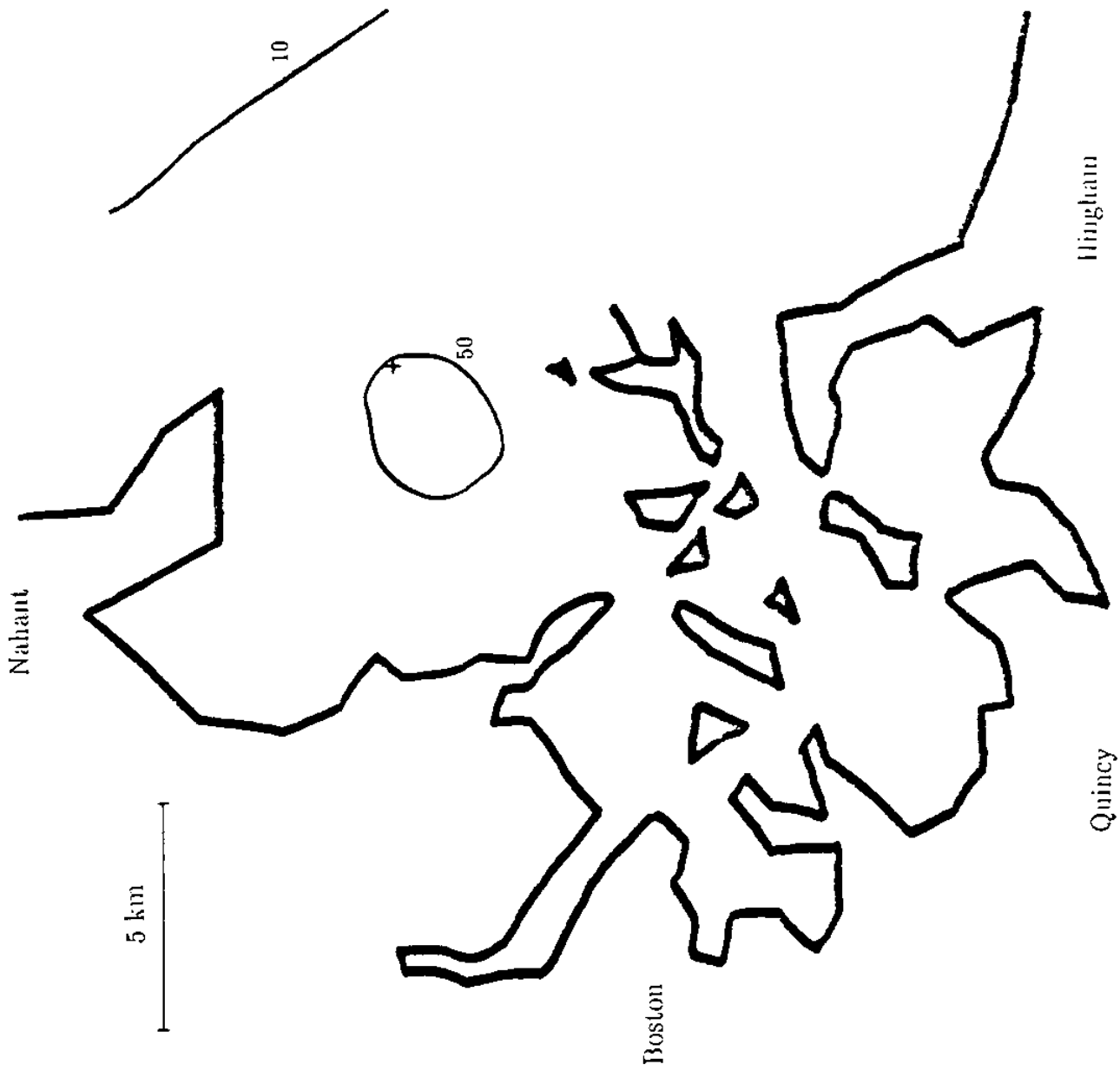


Figure 2.9b

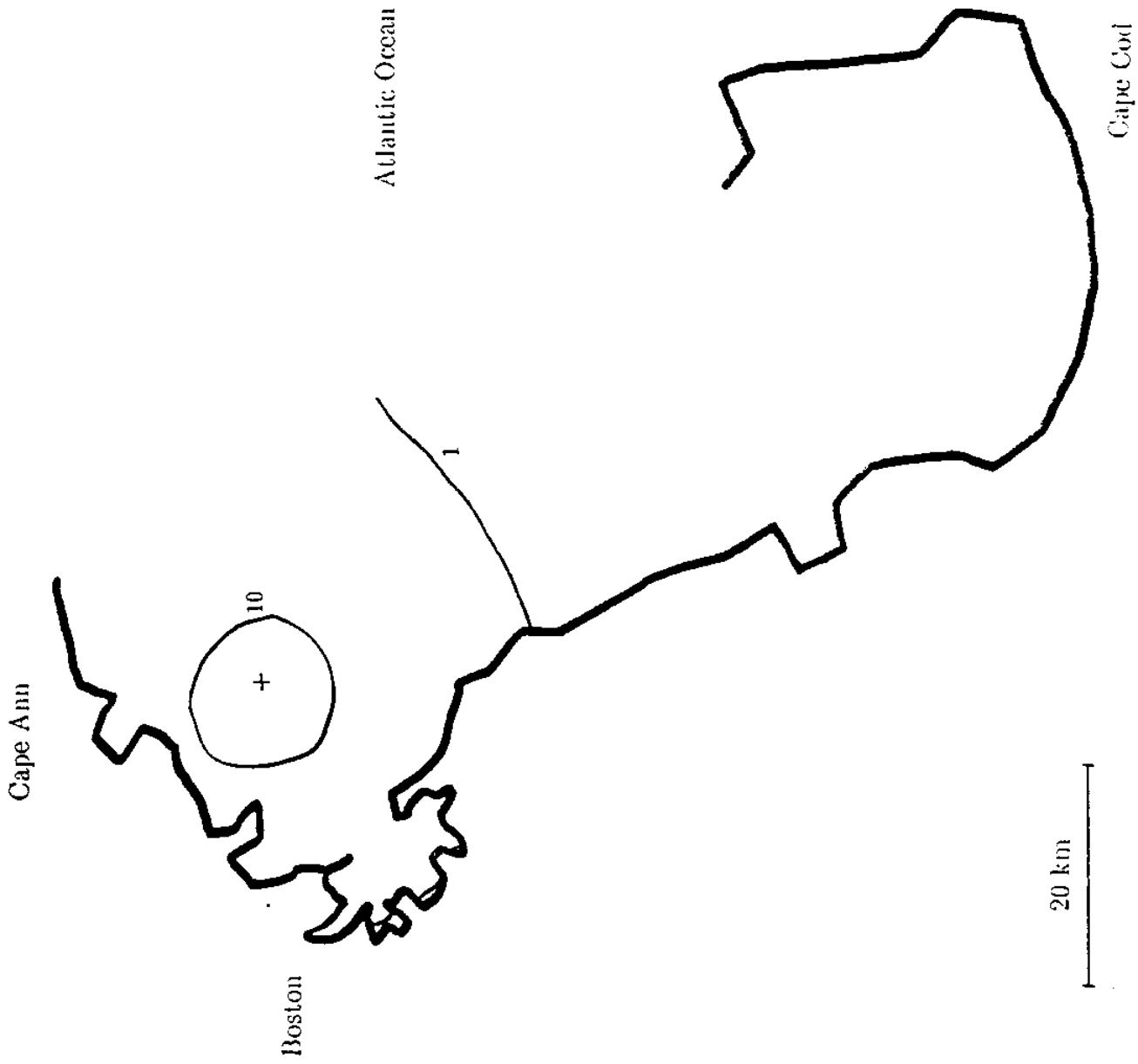


Figure 2.10a Simulated concentrations (ppt) for Run 6 Site 5, tidal circulation only, $k = 4$ cm/hr



Figure 2.10b

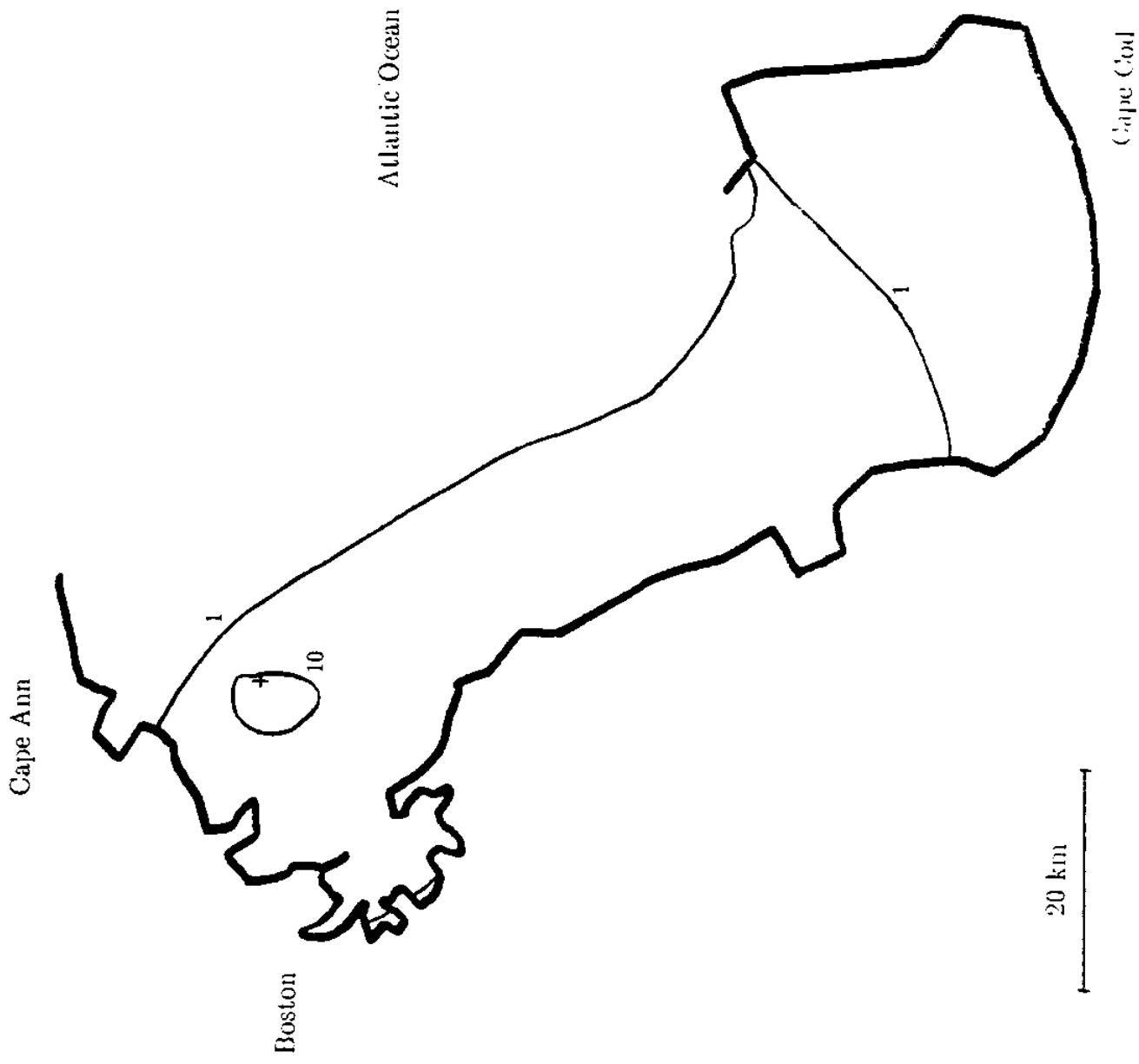


Figure 2.11a Simulated concentrations (ppt) for Run 4 Site 5, tidal circulation plus southerly drift, $k = 4 \text{ cm/hr}$



Figure 2.11b

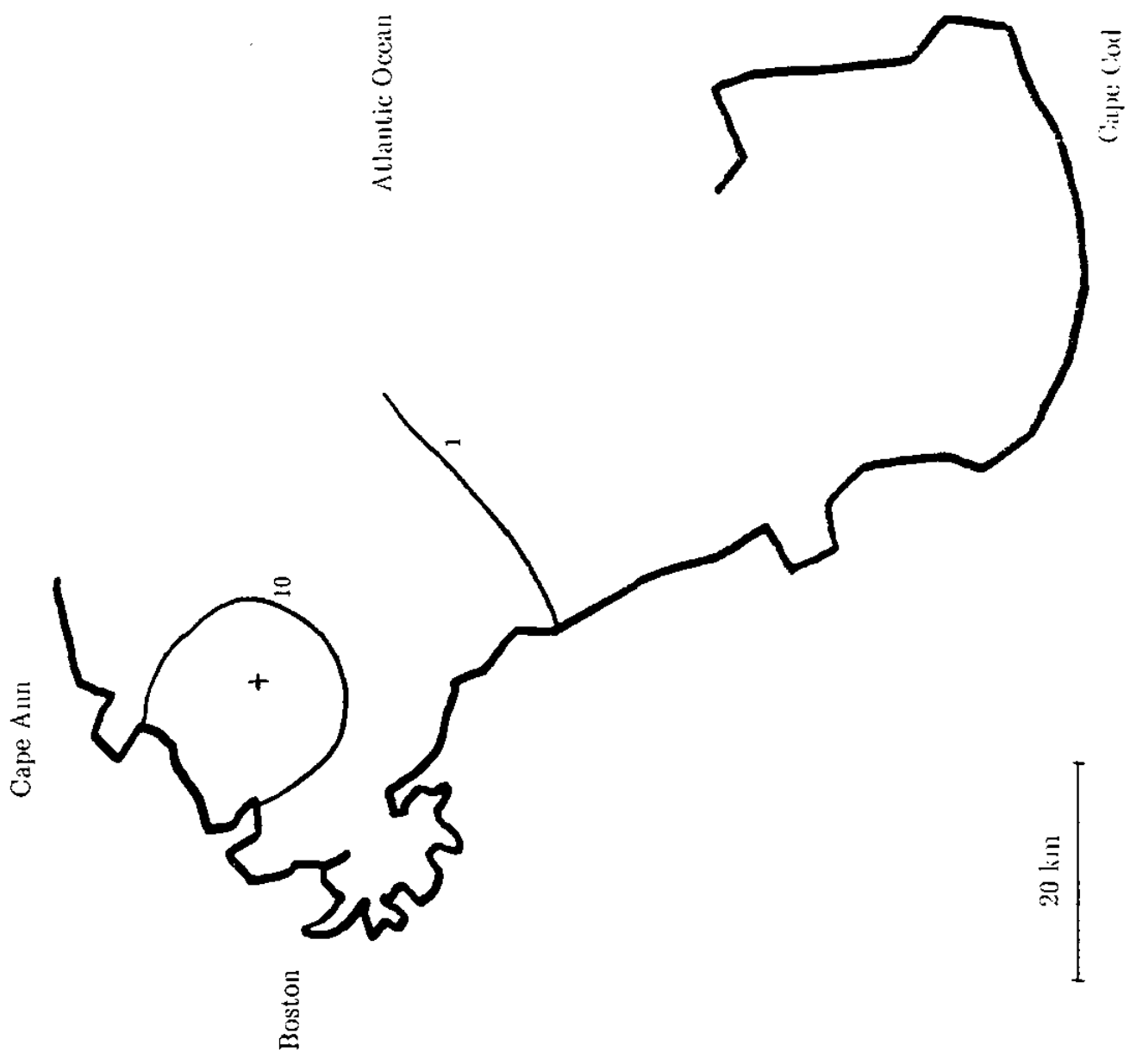


Figure 2.12a. Simulated concentrations (ppt) for Run 9 Site 5, tidal circulation only, $k = 1 \text{ cm/hr}$

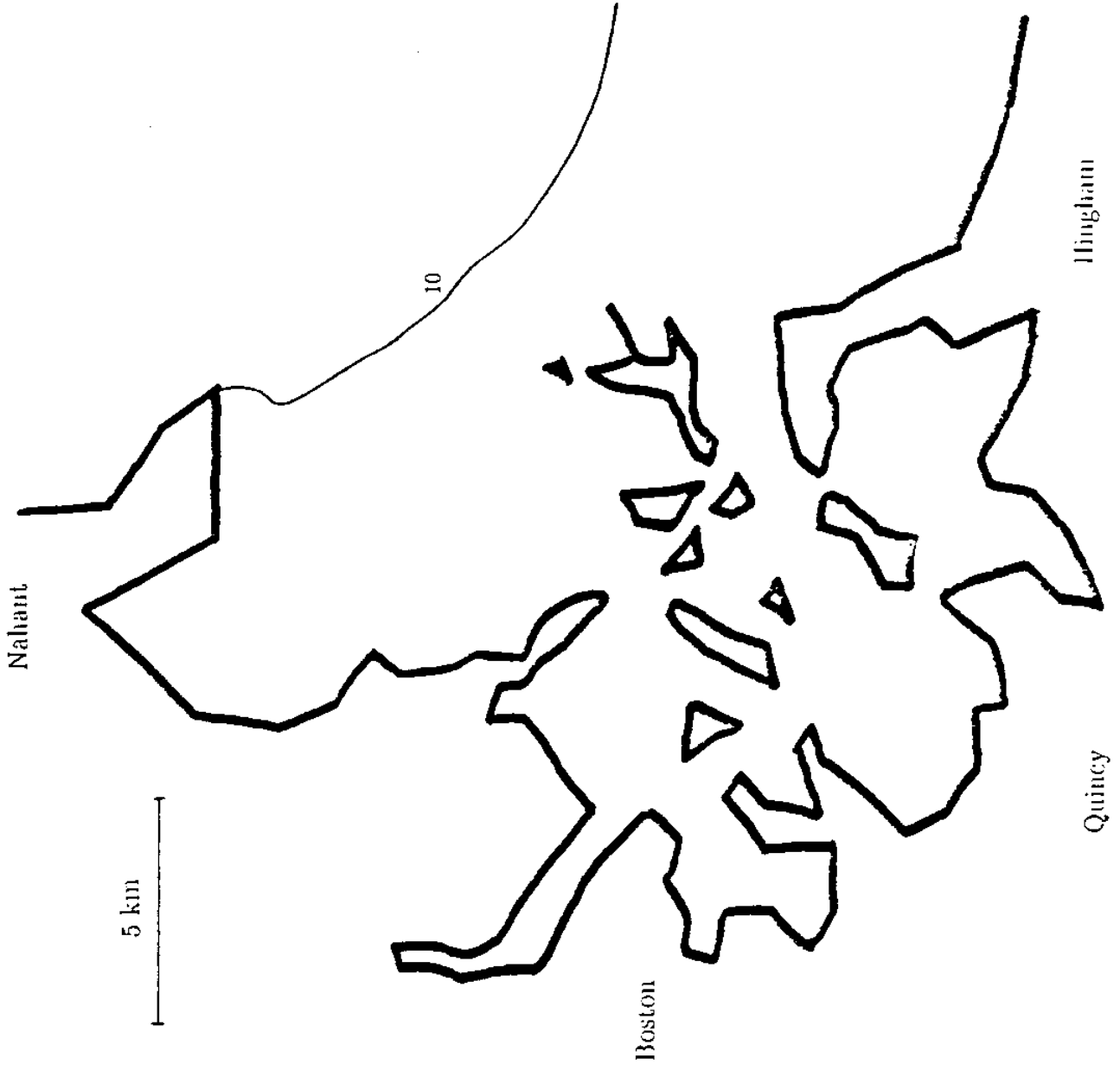


Figure 2.12b

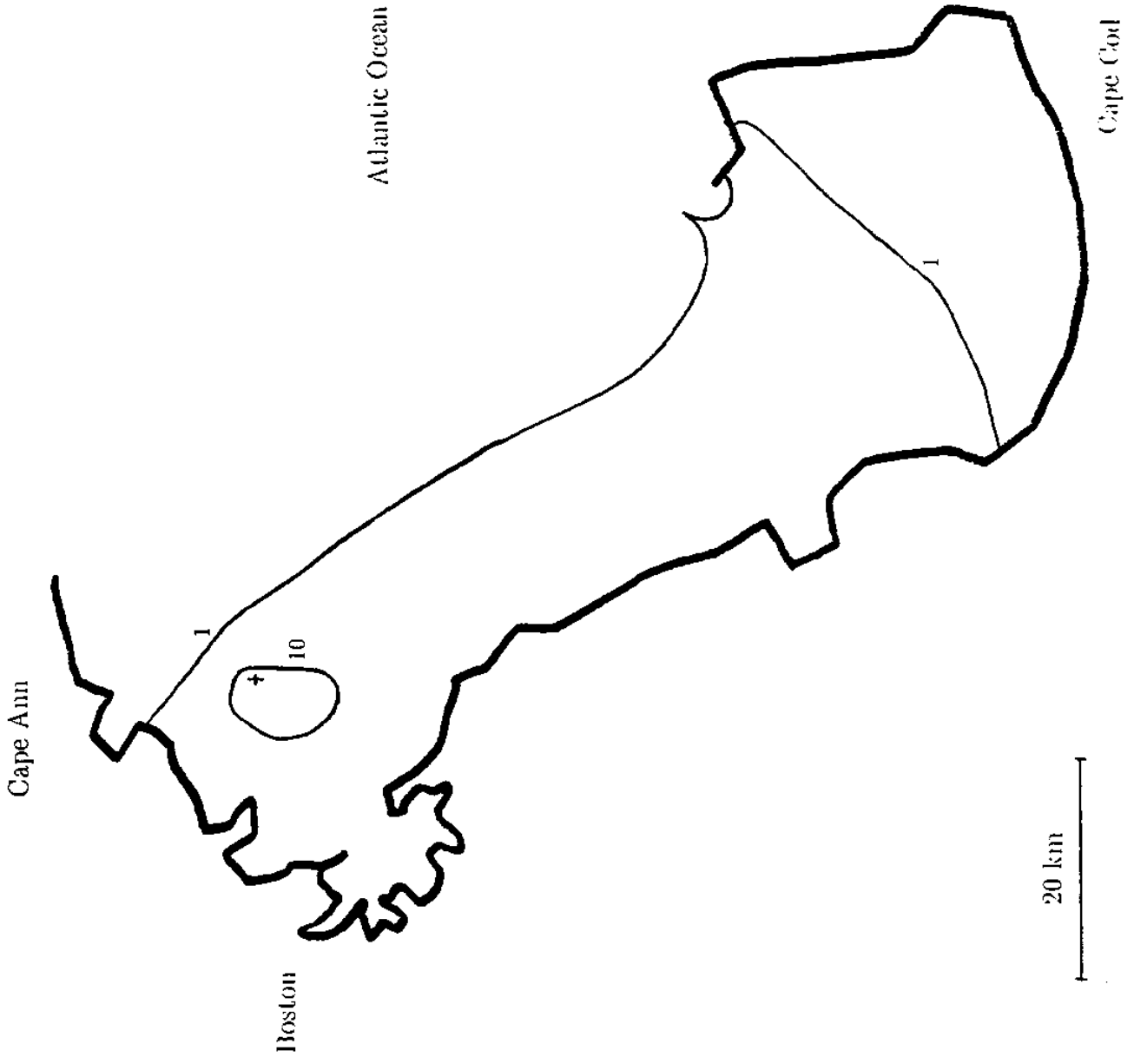


Figure 2.13a Simulated concentrations (ppt) for Run 12 Site 5, tidal circulation plus southerly drift, $k = 1 \text{ cm/hr}$

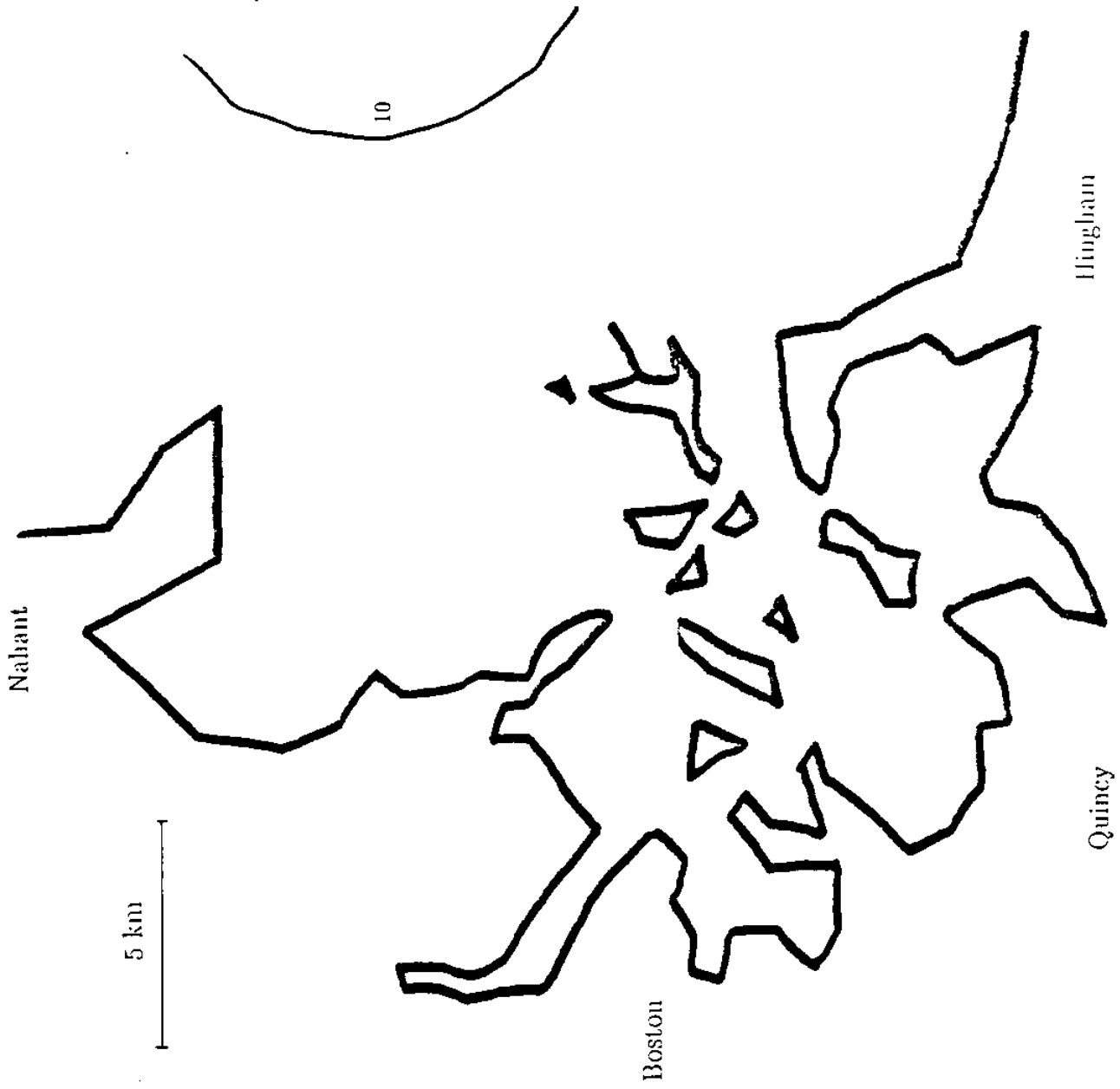


Figure 2.13b

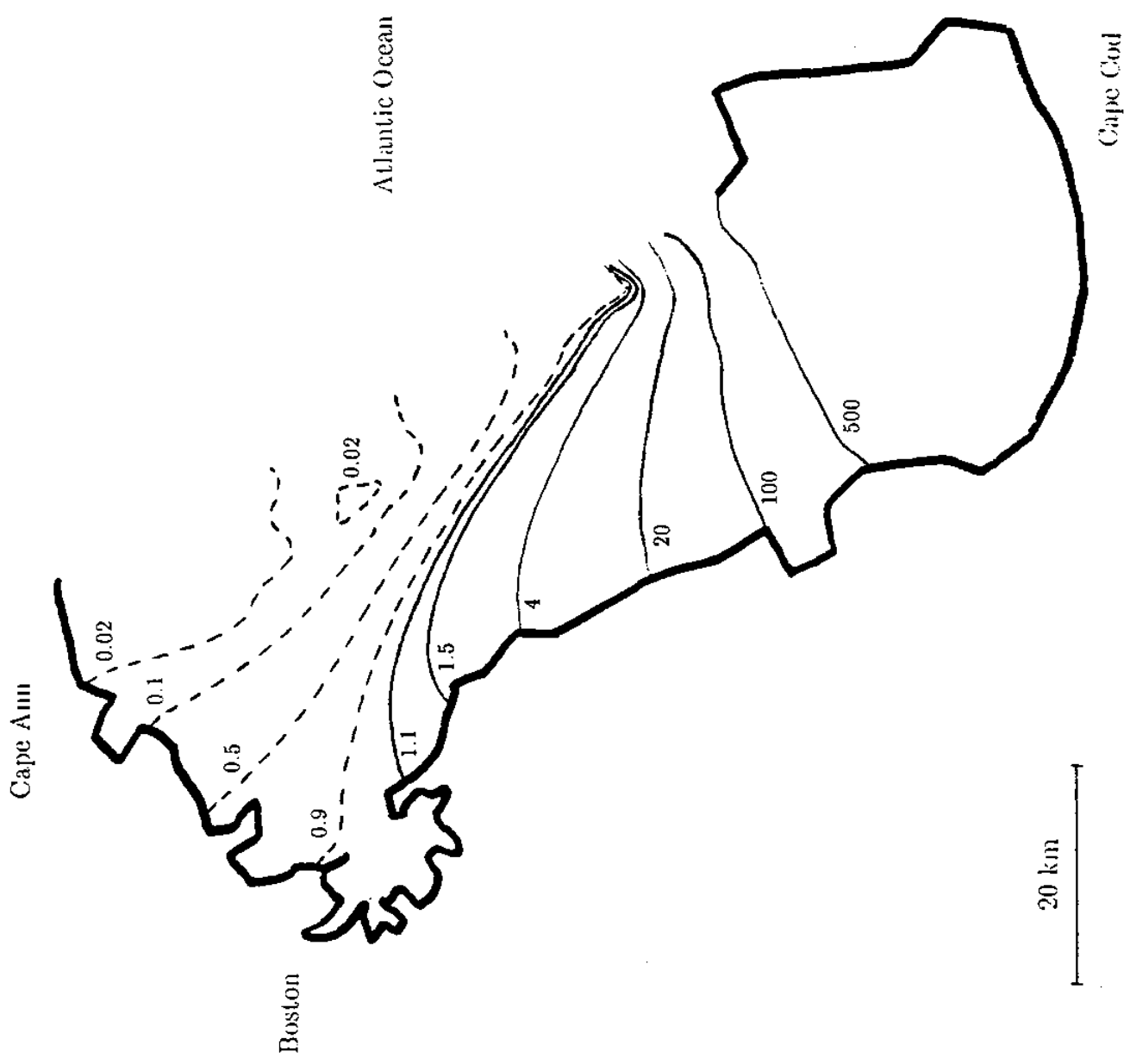


Figure 2.14a Sensitivity to steady drift. Ratio of concentration for Run 2 ($M_2 + \text{steady}$) to Run 1 (M_2 only).

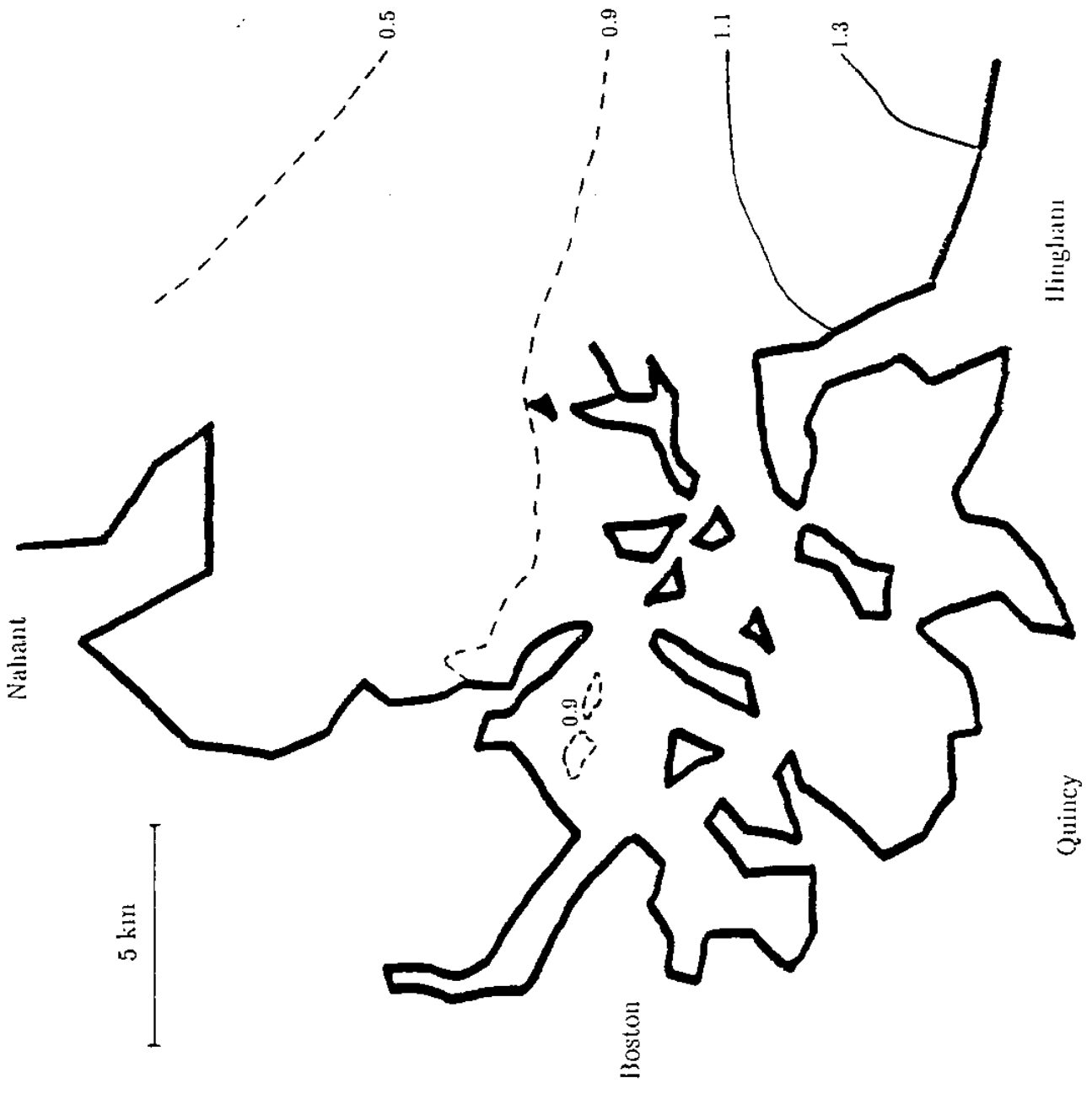


Figure 2.14b

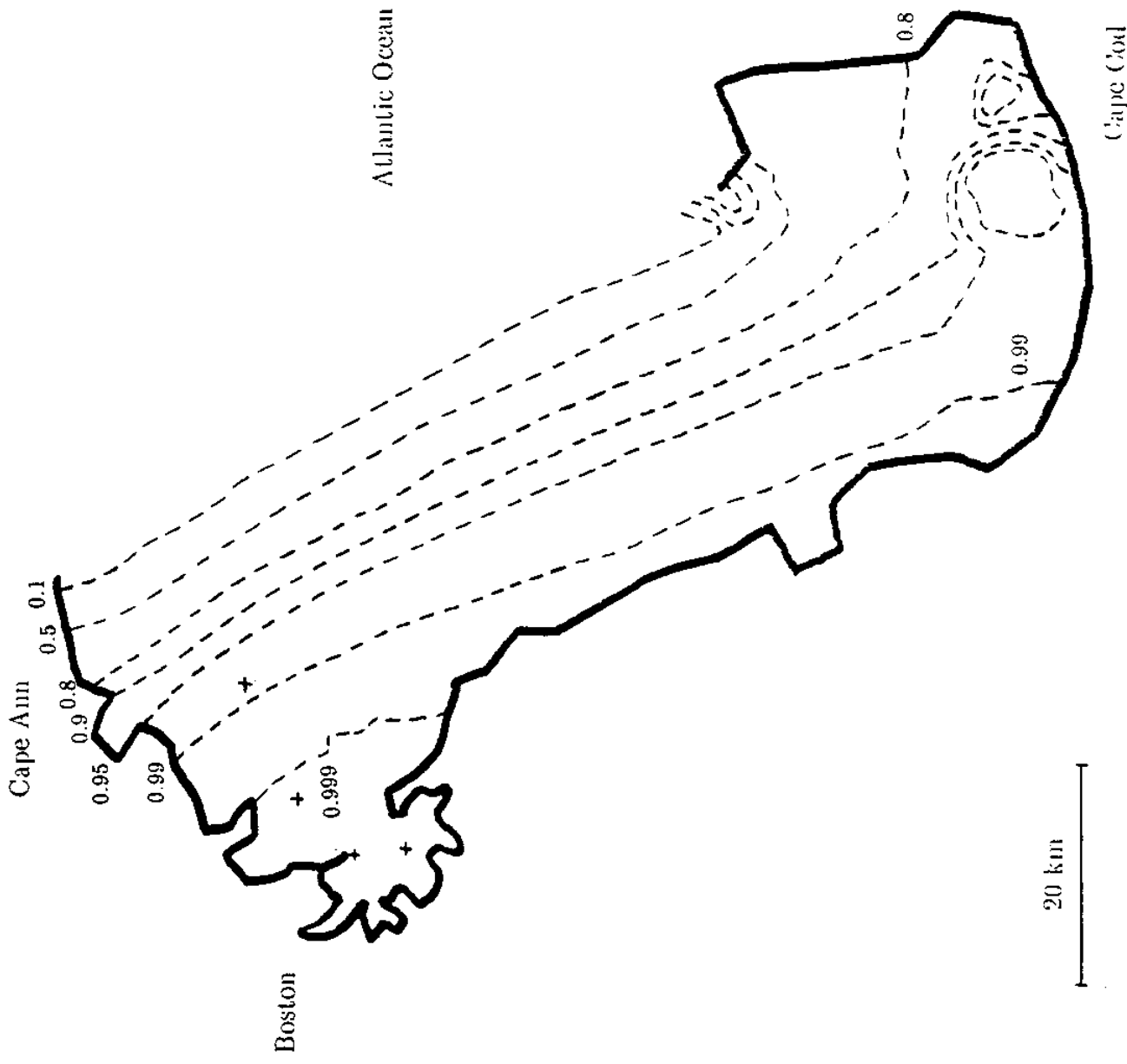


Figure 2.15 Sensitivity to open boundary condition. Ratio of concentration for Run 17 ($c = 0$) to Run 1 ($\partial c / \partial n = 0$)

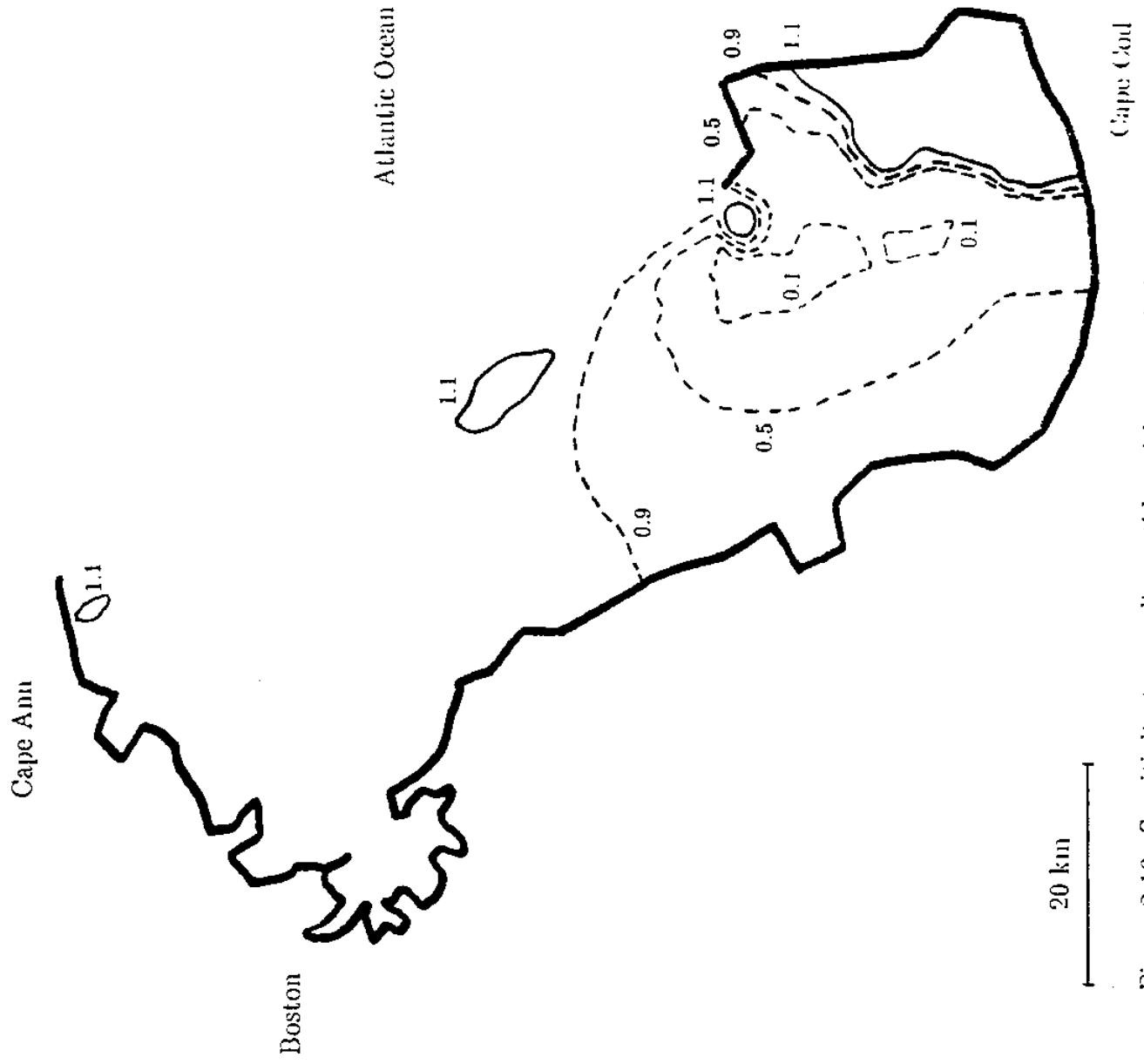


Figure 2.16a Sensitivity to non-linear tides with no net drift. Ratio of concentration for Run 25 (non-linear model) to Run 26 (linear model with iteration).

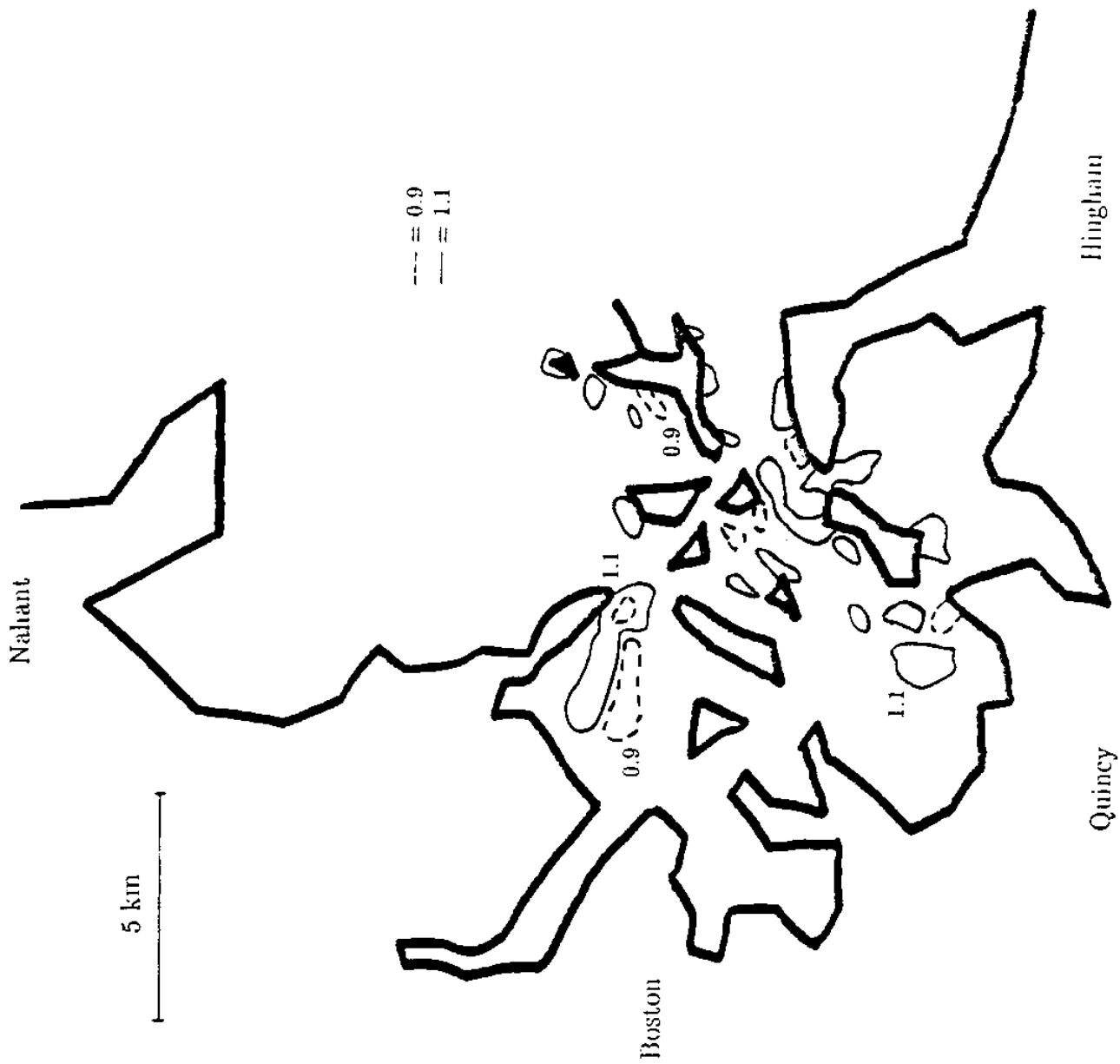


Figure 2.16b

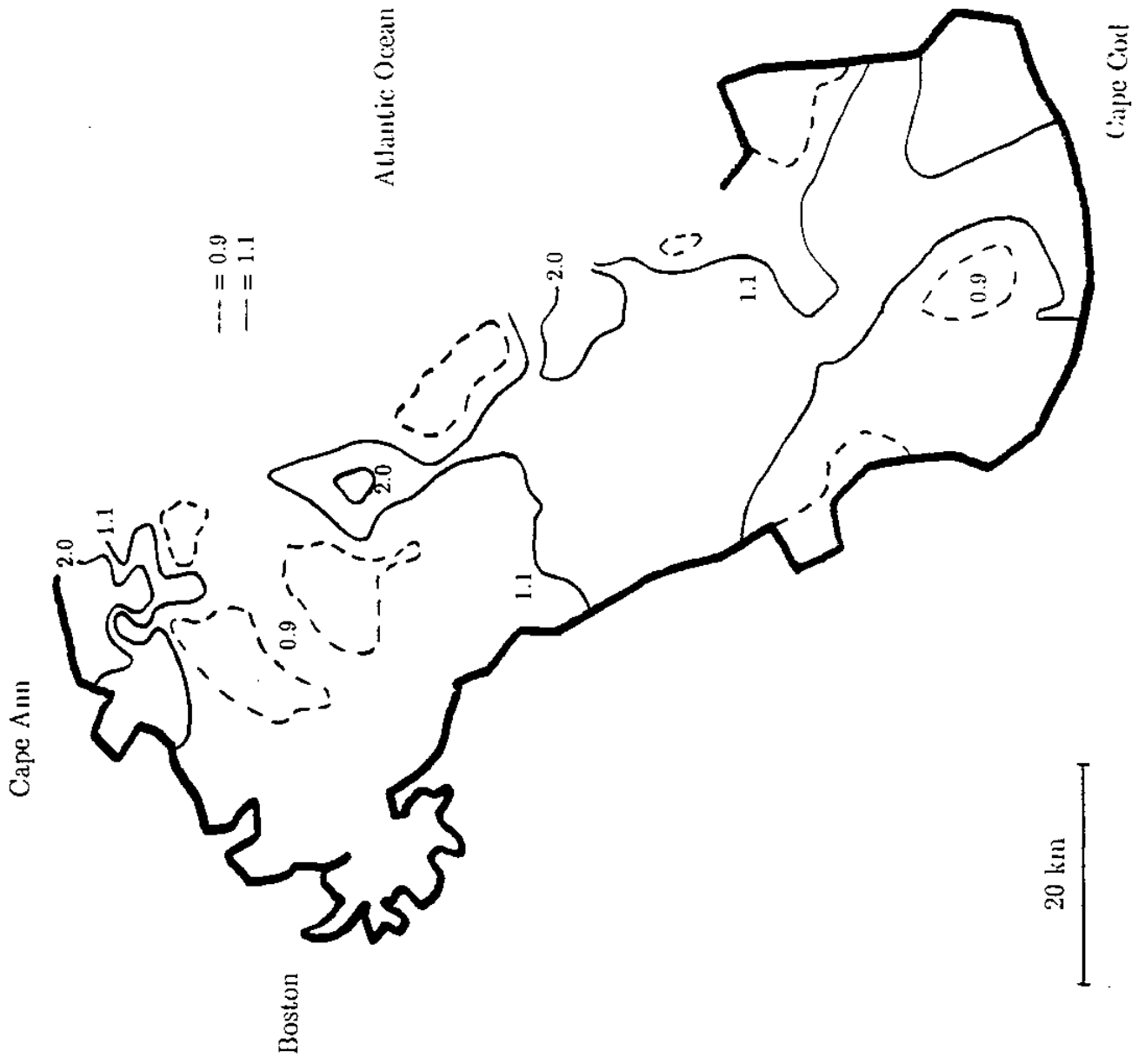


Figure 2.17a Sensitivity to non-linear tides with net drift. Ratio of concentration for Run 27 (non-linear model) to Run 28 (linear model with iteration)



Figure 2.17b

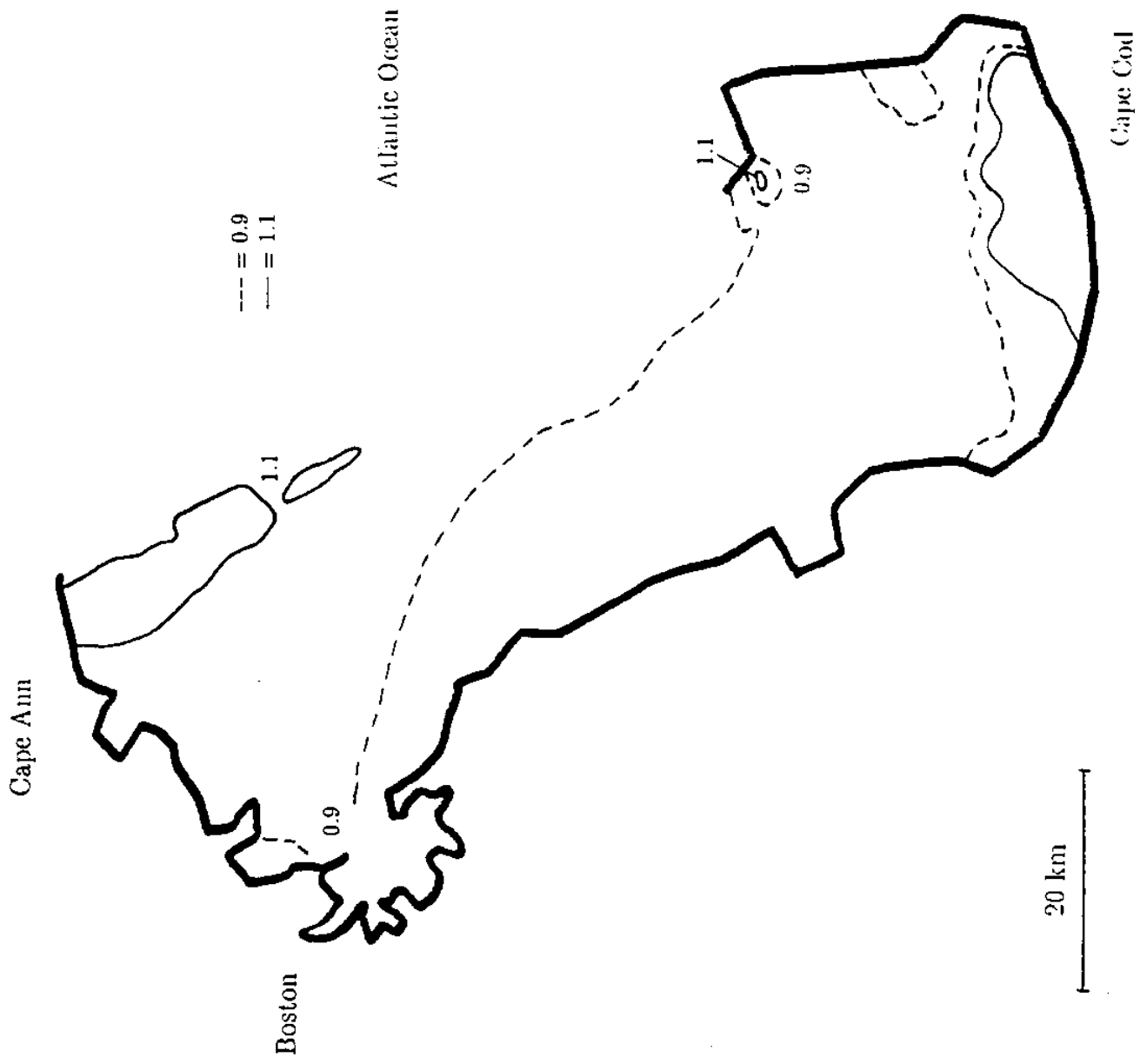


Figure 2.18a Sensitivity to tidal amplitude with no net drift. Ratio of concentration for Run 29 ($0.7 \times M_2$ tide) to Run 17 (M_2 tide)

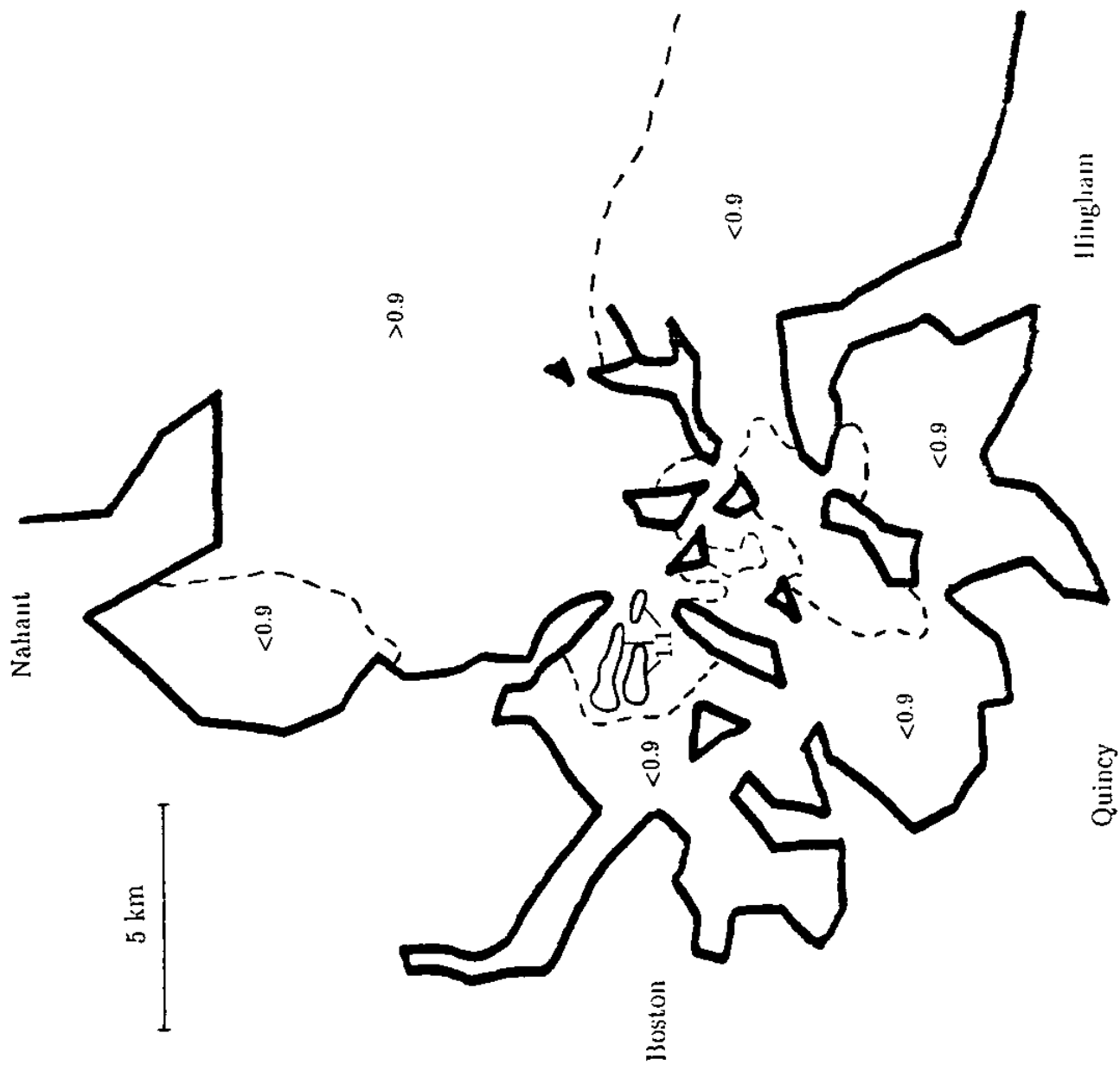


Figure 2.18b

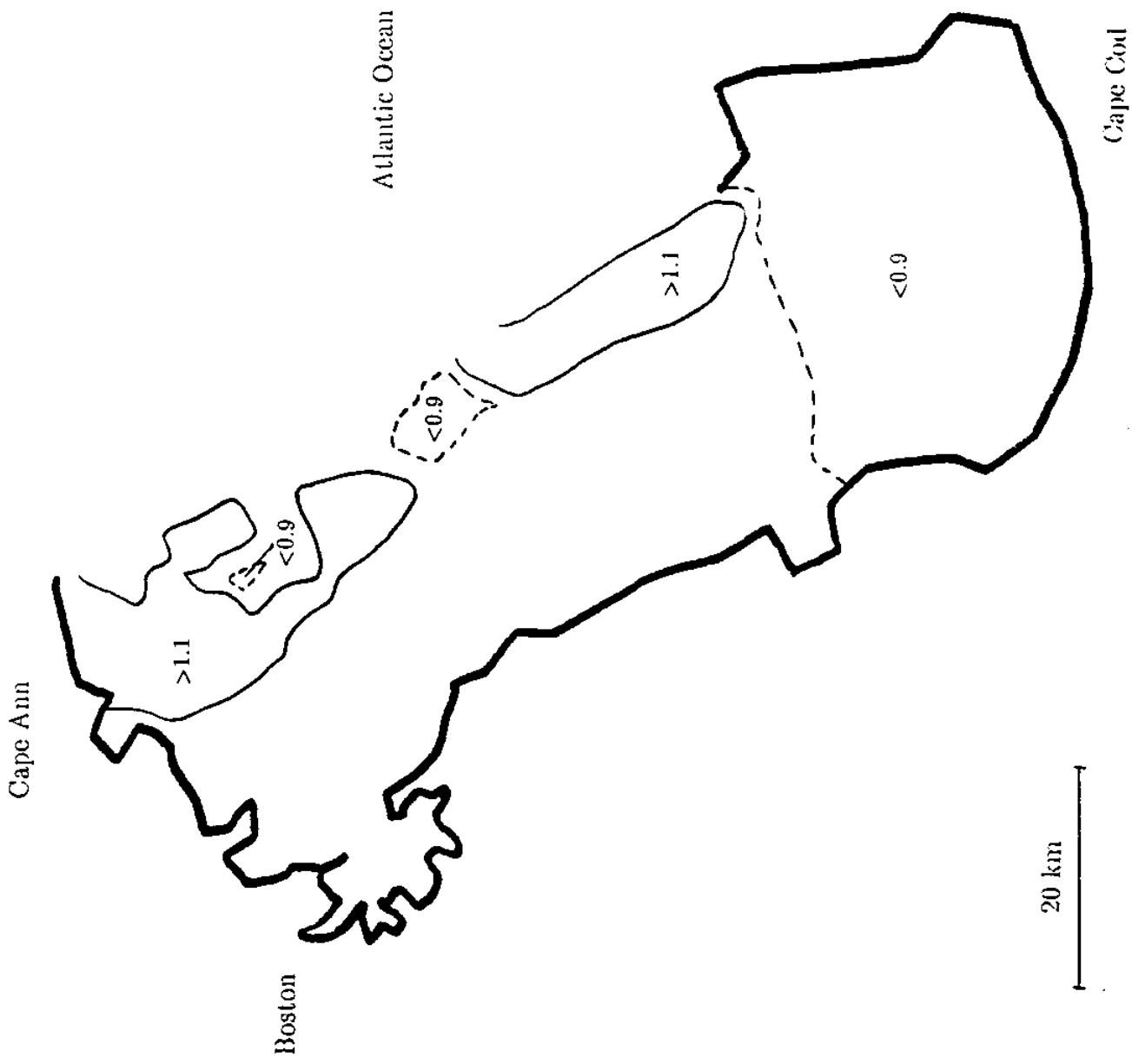


Figure 2.19a Sensitivity to tidal amplitude with net drift. Ratio of concentration for Run 30 ($0.7 \times M_2$ tide) to Run 34 (M_2 tide)



Figure 2.19b

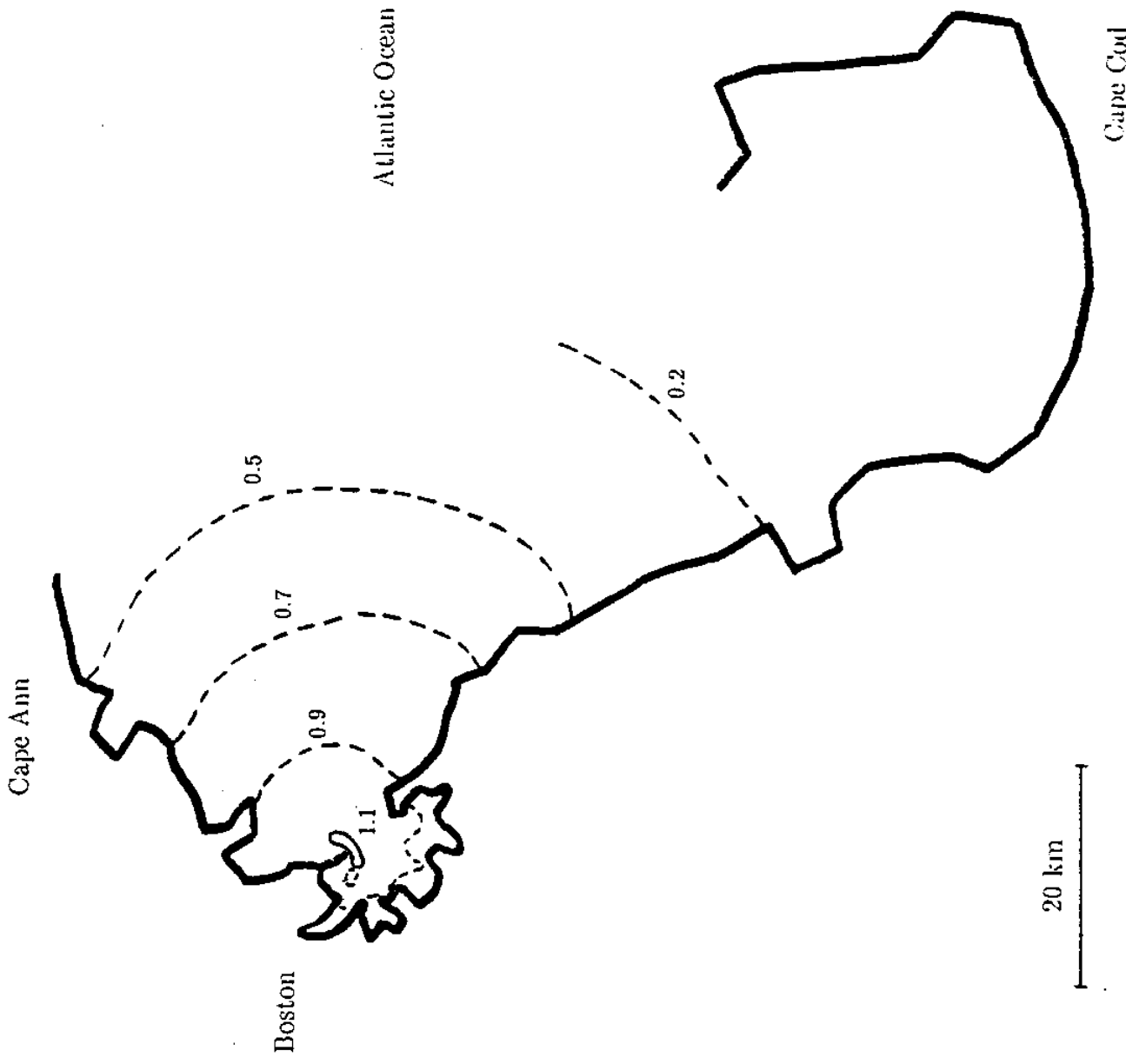


Figure 2.20a Sensitivity to dispersion coefficient. Ratio of concentration for Run 31 ($D = 49 \text{ m}^2/\text{s}$) to Run 17 ($D = 70 \text{ m}^2/\text{s}$)

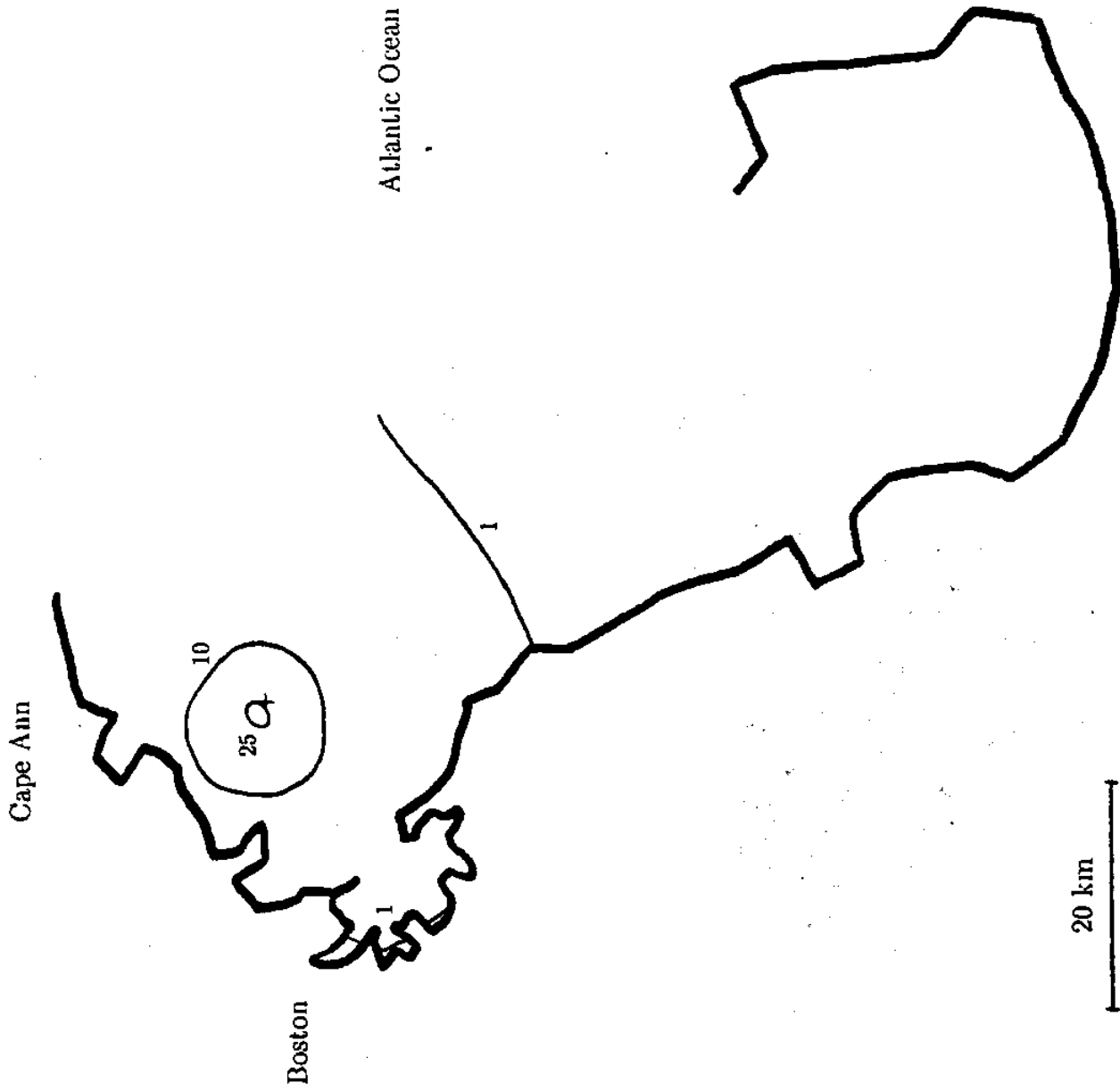


Figure 2.21 Sensitivity to near field representation. Concentration for Run 21 ($S = 2070|u| = 10$; $N = 3$; Site 5) to be compared with Run 6 (Figure 2.10a)

NEW GRID

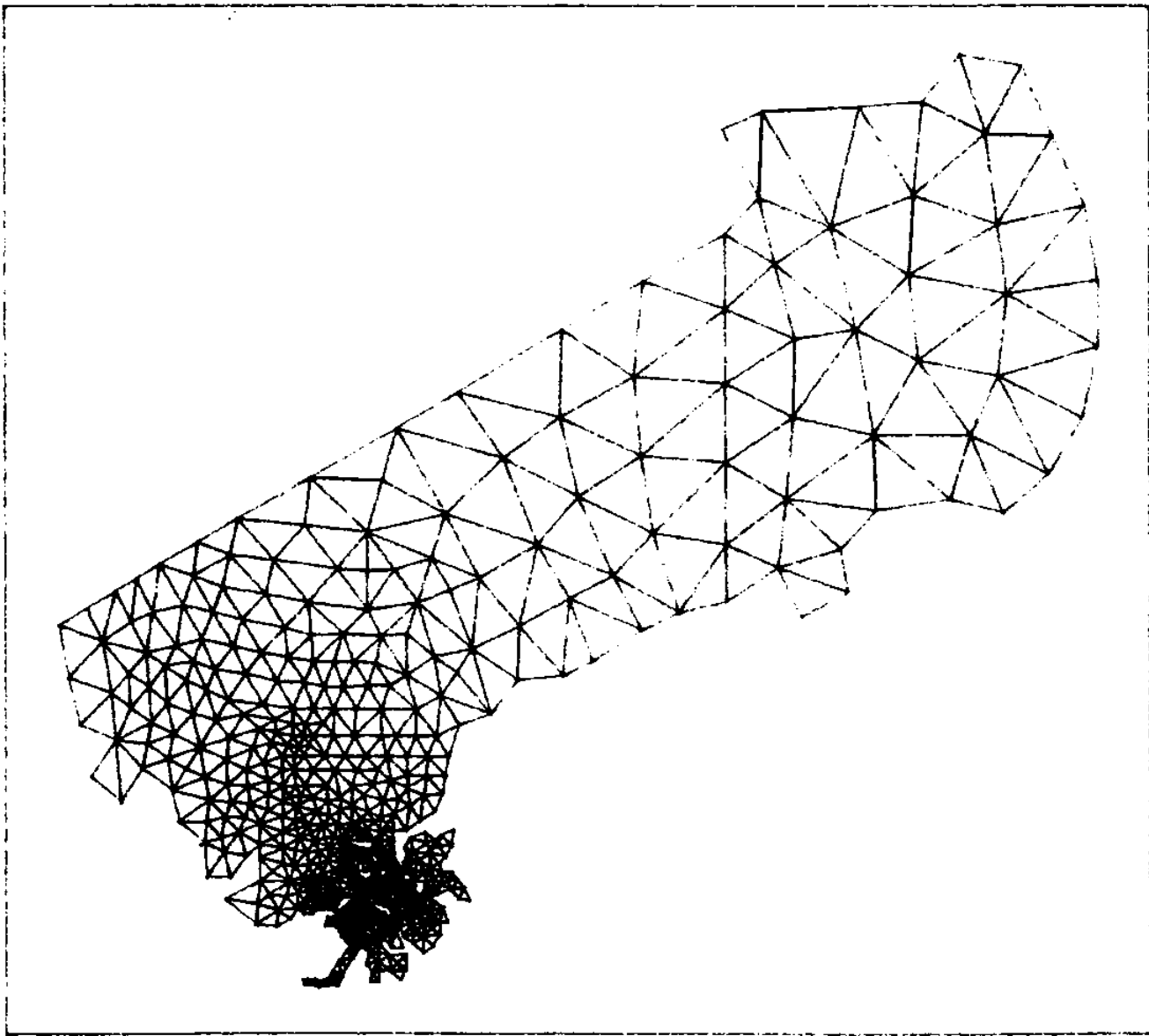


Figure 2.22 New grid; a) entire Massachusetts Bay

NEW GRID

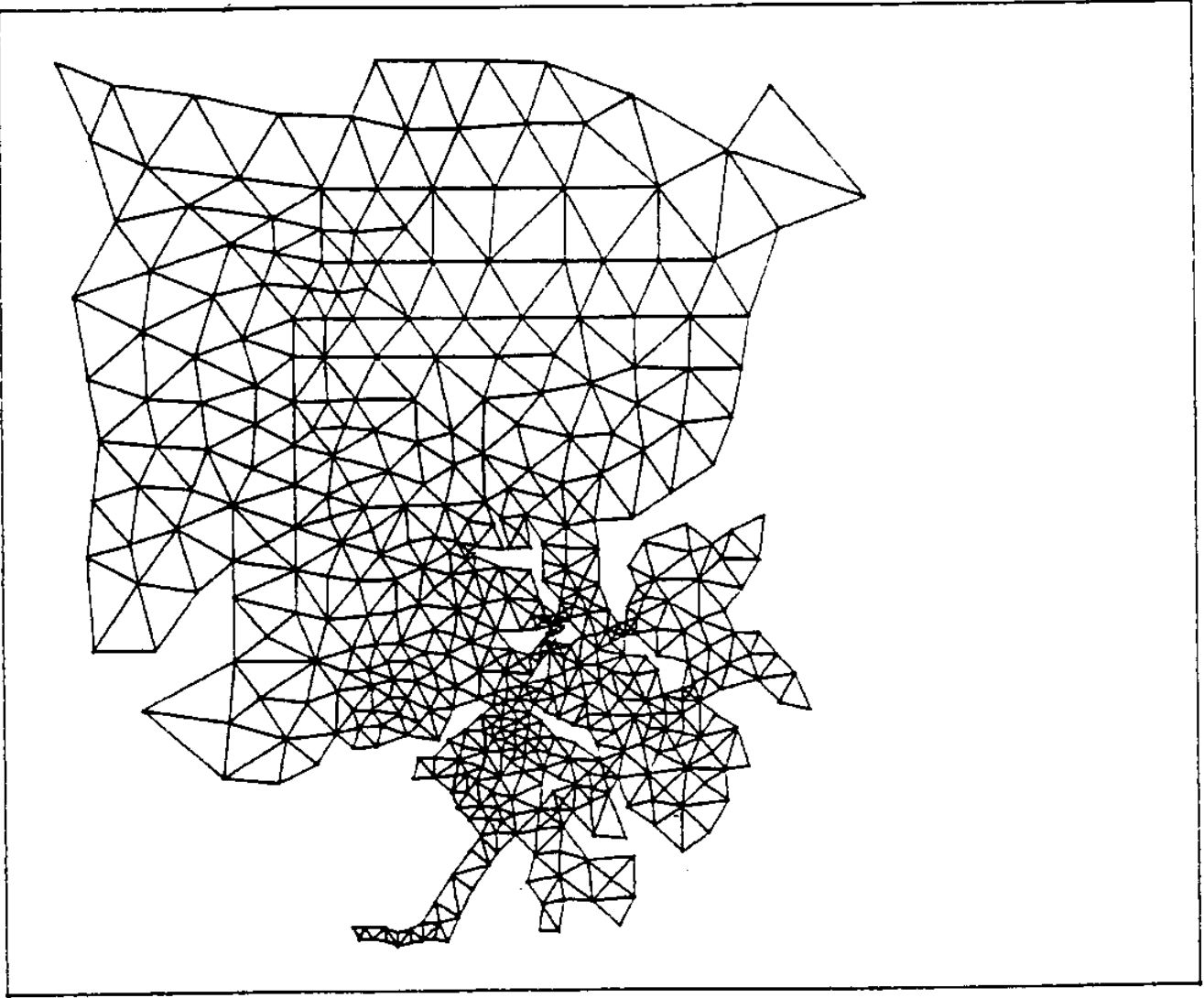


Figure 2.22b Detail of Boston Harbor and western Massachusetts Bay

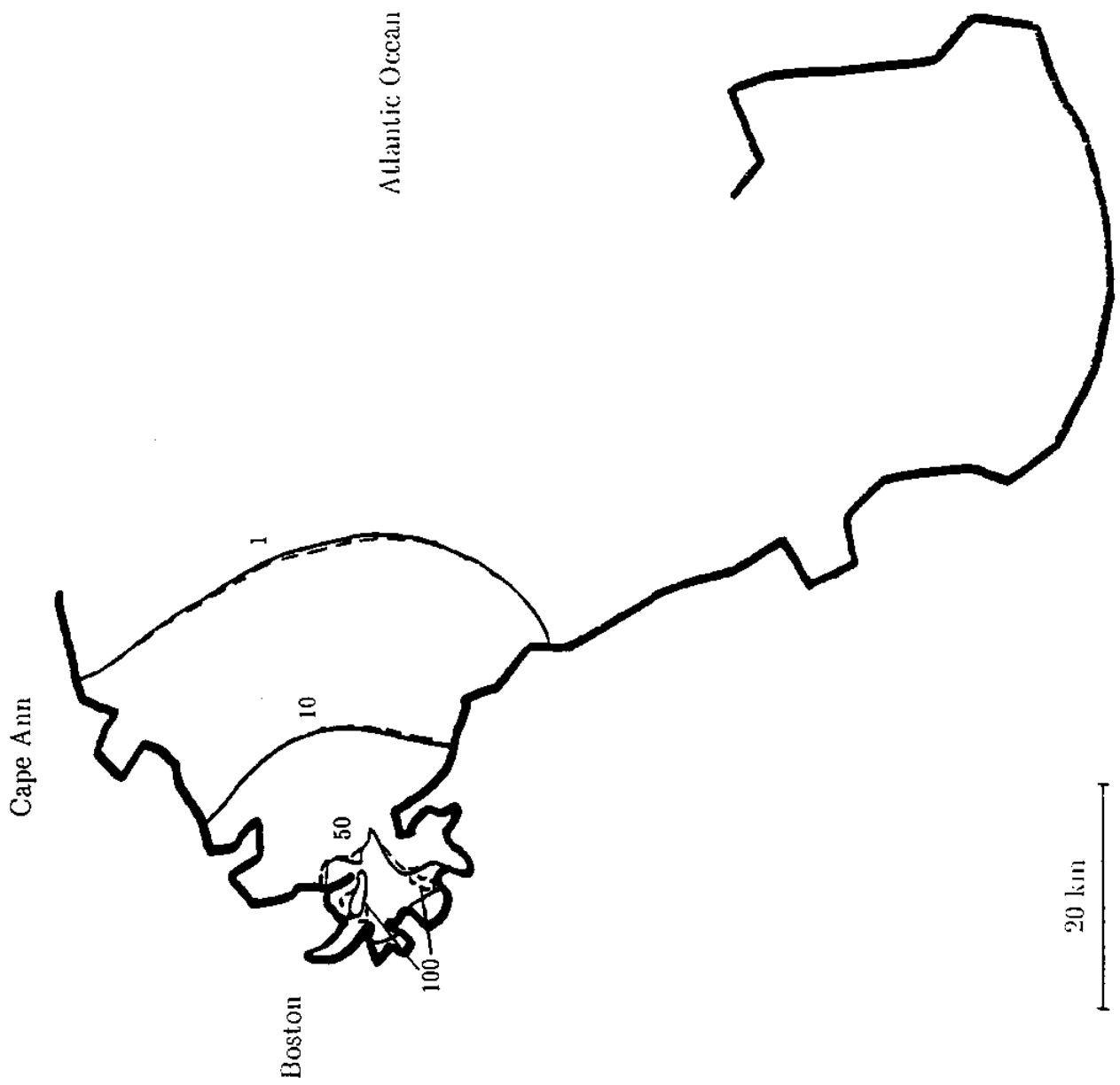


Figure 2.23 Sensitivity to grid. Concentration for Run 37 (new grid; Deer and Nut Island Sites) in solid lines compared with Run 17 (old grid; Deer and Nut Island sites) in dashed lines.

3. ANALYSIS OF CURRENT METER DATA AND RELATIONSHIP TO TEA PREDICTIONS

Moored current meters have been deployed at a number of locations in western Massachusetts Bay. For the period of approximately mid-March through mid-May 1987, measurements are available at stations 1, 3 upper, 3 lower, 5, 7, and 10, shown in Figure 3.1. These data will be discussed in the following as they relate to TEA simulations.

3.1 Tidal Components

A harmonic analysis program was used by CDM to compute 25 tidal harmonics, at frequencies of diurnal and higher, for current speeds (u and v components) and water surface elevation (from tide gauges located near Provincetown and Gloucester). Table 3.1 summarizes amplitudes of seven of the major tidal constituents for four records: water surface elevation near Gloucester and Provincetown and current speed at Stations 7 and 10. Note that Station 7 is one of the two outermost stations while Station 10 is one of the innermost stations. The rank order of the amplitude is included in parentheses.

A quick glance at this table confirms that the M_2 tide dominates throughout the region. In the outer (boundary) regions, the astronomical tides N_2 , S_2 , K_1 , and O_1 are second in importance whereas, nearer shore, the overtides of the M_2 tide (i.e., M_4 and M_6) attain more importance.

The dominance of the M_2 tide suggests that it is the best constituent to use for a visual comparison with computed tidal currents. Hence, Figures 3.2-3.6 show "measured" M_2 tidal ellipses computed from the harmonic analysis. Superimposed on these figures are simulated tidal ellipses at corresponding locations made with TEA using M_2 forcing on the open boundary. The five simulations are summarized in Table 3-2 and reflect use of different model modes (non-linear, linear with iteration, and linear), grids (old and

new), and friction factor C_F (.005 and .02). Characteristics of the measured and simulated ellipses are also summarized in Table 3-3.

In all simulations, the amplitude of the M_2 tide along the open boundary was assumed to vary linearly from a maximum of 1.30 m near Provincetown to a minimum of 1.25 m near Gloucester, in accordance with tide gauge measurements. These same tide gauge data showed a small phase difference (Gloucester leading Provincetown by about 10 minutes) though published tide tables imply significant variation in phase near the two points. At any rate, all simulations assumed a constant phase along the boundary. The non-linear runs included 9 frequencies: zero frequency, M_2 , M_4 , M_6 , M_{10} , M_{12} , M_{14} , and M_{16} .

The choice of C_F deserves some discussion. Based on information presented in Westerink et al. (1985), a representative value was thought to be about $C_F \approx 0.005$, which corresponds to a Manning's n of about 0.033 or a Darcy-Weisbach f of about 0.04.. However, calculations with the full non-linear model (including non-linear terms for bottom friction, convective acceleration, and finite amplitude) failed to converge with this value or with $C_F = 0.010$. And, in fact, solutions obtained with $C_F = 0.02$, while stable, exhibited some oscillation after 10 iterations. The non-linear model is known to be sensitive to a number of factors besides friction including the number of iterations and frequencies included and the value of an over-relaxation factor (Westerink et al., 1985). Hence convergence could likely improve with additional effort. Fortunately, based on results with the linear model using iteration, M_2 tides do not appear very sensitive to C_F .

Examining Figures 3.2-3.6 and Table 3-3, one clearly sees some variation among runs and between runs and data. However, predictions and measurements are generally within 20% regarding both speed and direction and show little sensitivity to bottom friction. Furthermore, there is no obvious improvement with the non-linear vs. the linear model either with iteration or without.

The relative insensitivity of simulated tides to the model (i.e., linear vs. non-linear) can also be seen in Figures 3.7 and 3.8 which show simulated current vectors using the non-linear model (again using 9 frequencies, with M_2 forcing and $C_F = 0.02$) and the linear model with iteration (M_2 only, $C_F = 0.02$) for phases of maximum ebb and high water slack referred to the M_2 cycle. Noting the differences in scale for the two phases, the simulated flow fields are quite similar except for some areas of the harbor and near the tip of Cape Cod. This observation, plus recognition that dispersion plays a prominent role in transport, explains the general lack of sensitivity to inclusion of the non-linear dynamics found in the ELA simulations presented in §2. In view of this insensitivity, it is suggested that future calculations use the linear model with iteration with a friction factor of $C_F = 0.005$. It is also suspected that improved agreement, if desired, could be obtained by refining bathymetry (especially near shoreline and harbor areas) and by resolving differences in tidal phase on the open boundary.

While the above discussion suggests that non-linearities are relatively unimportant in the simulation of concentrations, comparisons have also been made between measured and simulated M_4 and M_6 tides (the frequencies showing the strongest effect of non-linearity). Again, simulations were made using the non-linear model driven by only M_2 forcing. Table 3.4 summarizes simulated and measured amplitudes of the major axis of the tidal ellipse for M_2 , M_4 , and M_6 tides. Except for Station 1, the model generally underpredicts the magnitude of the overtides by a factor of about two. Limited model sensitivity suggests that the simulations of the overtides are sensitive to the number of frequencies included in the simulation, the number of iterations, and the bottom friction. Note that the model would not converge at lower (and more realistic) values of bottom friction and it is suspected that underprediction of the overtides is due in part to the relatively high values of C_F . Further effort is definitely warranted before the non-linear calculations could be

considered validated. However, in view of the insensitivity of computed concentrations to inclusion of non-linear terms, this was not a high priority.

3.2. Low Frequency Currents

Various analyses have been initiated by CDM and MIT with respect to low-frequency currents. Because existing data are limited to a 2-month period—and indeed a rather anomalous period characterized by large freshwater inflow—it is important that these efforts be continued and updated as more data become available.

Time series measurements for each station have been low-pass filtered by CDM to remove the tide. Visual comparison among recorded u and v components for different stations and amongst a similarly filtered time series of water surface elevation differences between Gloucester and Provincetown shows some correlation. Because of the non-uniform shoreline in relationship to the two u and v directions, a better visual comparison could be made if the current meter data were presented in terms of stick plots.

Table 3.5 and Figure 3.1 summarize RMS and 2-month mean current velocities for the various meters. While the data are limited (only 2 months) the following are of note. Average currents are small (none over 3 cm/s) and quite random spatially. (Among the six stations, net excursions can be found in each of the four quadrants of the Cartesian coordinate system.) Of possible significance, too, is the fact that the biggest difference in the onshore-offshore (u) component is between upper and lower meters at the same station (3). The net offshore flow for the upper meter and onshore flow for the lower meter could be the result of either wind-driven or density-driven circulation. RMS currents show more spatial consistency with an increase in RMS speed with distance offshore (i.e., lowest speeds at Stations 1 and 10; highest speeds at Stations 5 and 7).

These measured currents can provide initial guidance in determination of low frequency currents for use with TEA and ELA. Because the primary mechanism for generating low-frequency drift in TEA is through specifying boundary tilt, the objective is to determine realistic values for this tilt by comparing simulated with observed low-frequency currents. The observed currents discussed previously include RMS speeds (which include frequencies lower than about one day) and mean currents (which include frequencies lower than about 2 months). Considering that the time scales of weather systems are typically of order one week, it seems reasonable to expect simulated current speeds to fall between the mean and the RMS speeds.

Accordingly, two runs were made with TEA (linear mode with iteration) using a 10-cm south-to-north slope and values of $C_F = 0.005$ and 0.02 . As discussed previously, the former appears to be the more reasonable estimate. Steady current speeds ($\sqrt{u^2+v^2}$) for this run are compared in Table 3.6 with measured mean and RMS currents at various stations. Except for Station 1, simulated currents are well between the two extremes in measurements suggesting that a 10-cm tilt produces currents of the correct general magnitude.

Further study, however, is clearly warranted. In addition to examining more data, it is recommended to continue with the initial spectral analysis. In particular, it would be helpful to compare spectral plots of low-pass filtered currents, tidal elevation difference, and wind to determine, quantitatively, the correlation among the three as a function of frequency. The individual spectra will also help determine the dominant frequencies.

Table 3.1

Measured Amplitudes of Selected Tidal Harmonics

<u>Species</u>	<u>Tidal elevation (cm)</u>		<u>Current speed (cm/s)</u>	
	<u>Gloucester</u>	<u>P'town</u>	<u>Sta 7</u>	<u>Sta 10</u>
M ₂	125 (1)	130 (1)	8.9 (1)	40.0 (1)
N ₂	27 (2)	28 (2)	2.0 (3)	10.6 (2)
S ₂	20 (3)	21 (3)	2.0 (2)	6.2 (3)
K1	17 (4)	17 (4)	1.8 (4)	4.8 (5)
O1	13 (5)	14 (5)	0.6 (7)	2.8 (6)
M4	1.3 (13)	1.6 (14)	0.5 (8)	6.1 (4)
M6	1.1 (15)	3.0 (13)	0.5 (9)	2.5 (7)

Table 3.2

Summary of M₂ Tidal Simulations

<u>Simulation</u>	<u>Mode</u>	<u>Grid</u>	<u>C_f</u>
1	NL	old	0.02
2	Lin/It	old	0.02
3	Lin	old	0.005
4	Lin	new	0.005
5	Lin/It	old	0.005

Table 3.3

Simulated and Measured Characteristics of M₂ Tide

<u>Station</u>		<u>Meas</u>	<u>Sim1</u>	<u>Sim2</u>	<u>Sim3</u>	<u>Sim4</u>	<u>Sim5</u>
1	major axis ¹	6.8	11.1	11.7	12.7	14.4	10.3
	minor axis ¹	1.4	0.2	0.6	0.6	0.4	1.0
	orient ²	86	53	60	60	61	58
	sense ³	CW	CW	CW	CCW	CCW	CW
3	major axis	11.7	9.0	9.2	11.6	12.1	8.6
	minor axis	3.1	2.5	1.8	0.2	0.007	1.3
	orient	100	81	73	70	72	83
	sense	CCW	CCW	CCW	CCW	CW	CCW
5	major axis	12.0	10.9	10.9	13.4	12.7	10.4
	minor axis	0.5	1.9	1.4	2.9	3.0	2.6
	orient	96	92	90	78	80	92
	sense	CW	CW	CW	CW	CW	CW
7	major axis	8.9	10.9	10.9	11.7	12.0	10.8
	minor axis	1.0	1.1	1.2	2.3	2.7	2.0
	orient	88	100	100	92	90	101
	sense	CW	CW	CW	CW	CW	CW
10	major axis	40.0	46.1	44.4	53.5	54.0	44.2
	minor axis	1.1	0.6	0.3	0.6	0.4	1.1
	orient	92	84	83	83	83	84
	sense	CCW	CW	CW	CW	CW	CW

1 maximum, minimum tidal velocities, cm/s

2 orientation of ellipse, degrees CW from N

3 rotation of tidal currents

Table 3.4

Simulated* and Measured Major Axis Amplitudes (cm/s) of M_2 , M_4 , and M_6 Tides

<u>Station</u>	<u>M_2</u>			<u>M_4</u>			<u>M_6</u>		
	<u>Sim</u>	<u>Meas</u>	<u>Ratio</u>	<u>Sim</u>	<u>Meas</u>	<u>Ratio</u>	<u>Sim</u>	<u>Meas</u>	<u>Ratio</u>
1	11.1	6.8	1.64	0.67	0.56	1.19	0.35	0.14	2.53
3U	9.0	14.2	0.66	0.55	1.14	0.48	0.28	0.50	0.56
3L	9.0	11.7	0.77	0.55	1.56	0.35	0.28	0.55	0.51
5	10.9	12.0	0.90	0.31	1.18	0.26	0.25	0.51	0.49
7	10.9	8.9	1.23	0.26	0.50	0.52	0.18	0.48	0.37
10	46.1	40.0	1.15	4.64	6.06	0.77	3.28	2.54	1.29

*Simulation performed with non-linear model using $C_f = 0.020$ and M_2 forcing only

Table 3.5

Summary of Low Frequency Current Meter Data (cm/s)

<u>Station</u>	<u>Mean</u>			<u>RMS</u>		
	<u>U*</u>	<u>V*</u>	<u>$\sqrt{u^2+v^2}$</u>	<u>U_r</u>	<u>V_r</u>	<u>$\sqrt{u^2+v^2}$</u>
1	-1.0	-0.6	1.2	1.4	1.7	2.2
3U	1.1	-2.8	3.0	4.4	7.4	8.6
3L	-1.9	0.1	1.9	4.1	4.2	5.9
5	0.5	2.8	2.8	4.2	7.5	8.6
7	-0.5	1.0	1.1	7.4	8.9	11.6
10	-0.1	-0.0	0.1	3.7	2.1	4.3
Ave	-0.32	0.1	2.0	4.2	5.3	6.9

*U \equiv east; V \equiv north

Table 3.6

Amplitude of Simulated Steady Current Speeds (cm/s) Compared with Measurements

<u>Station</u>	<u>Simulated</u>	<u>Measured</u>	
		<u>Mean</u>	<u>RMS</u>
1	0.3	1.2	2.2
3 (ave of U and L)	2.8	2.0	7.2
5	5.7	2.8	8.6
7	3.9	1.1	11.6
10	0.6	0.1	4.3

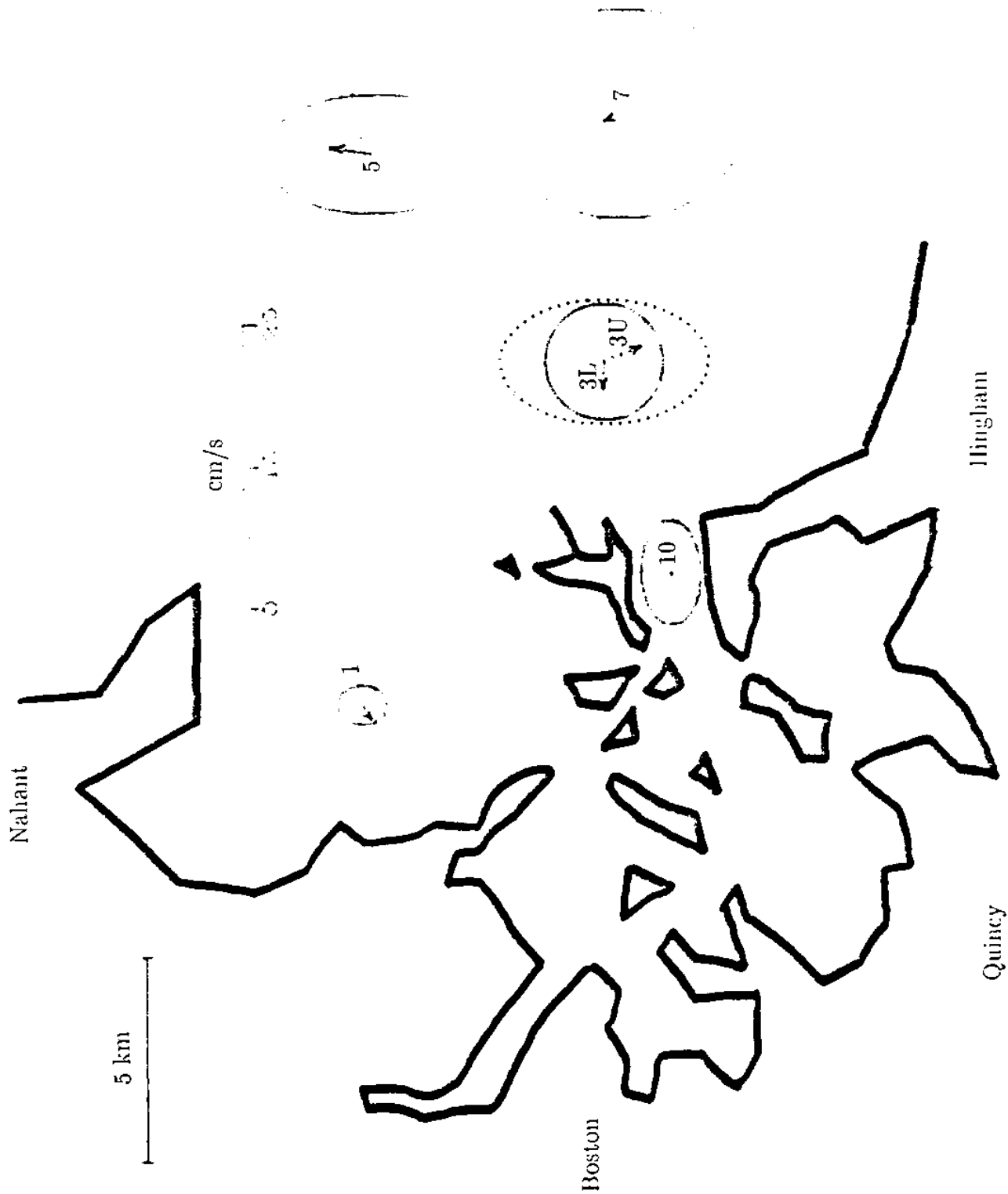


Figure 3.1 Current meter locations. Ellipses are based on RMS velocities from tidally filtered u and v components. Arrows denote two-month mean velocity.

M2 ELLIPSES FOR STATION 1

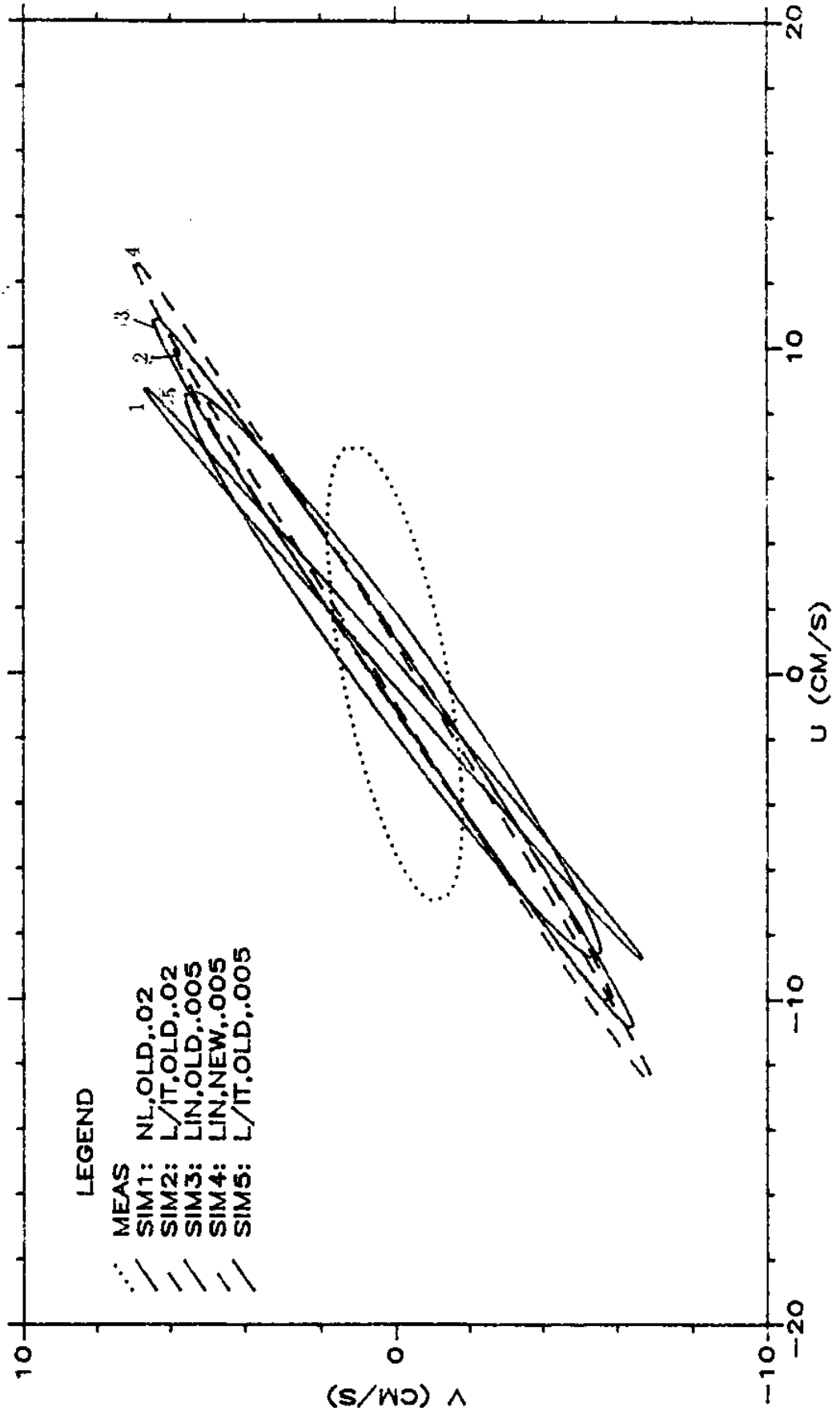


Figure 3.2 Measured and simulated M₂ tidal ellipses, Station 1

M2 ELLIPSES FOR STATION 3

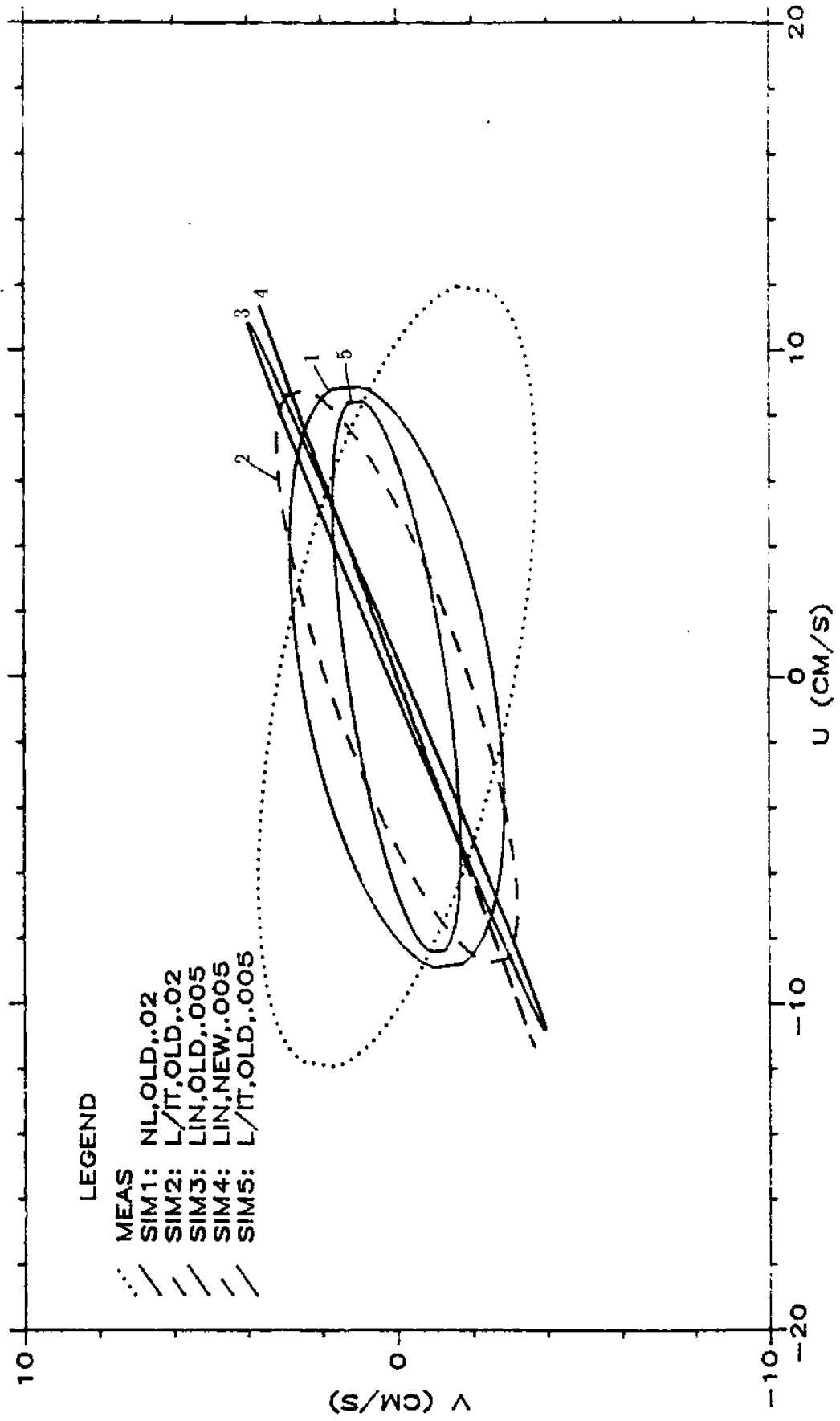


Figure 3.3 Measured and simulated M_2 tidal ellipses, Station 3

M2 ELLIPSES FOR STATION 5

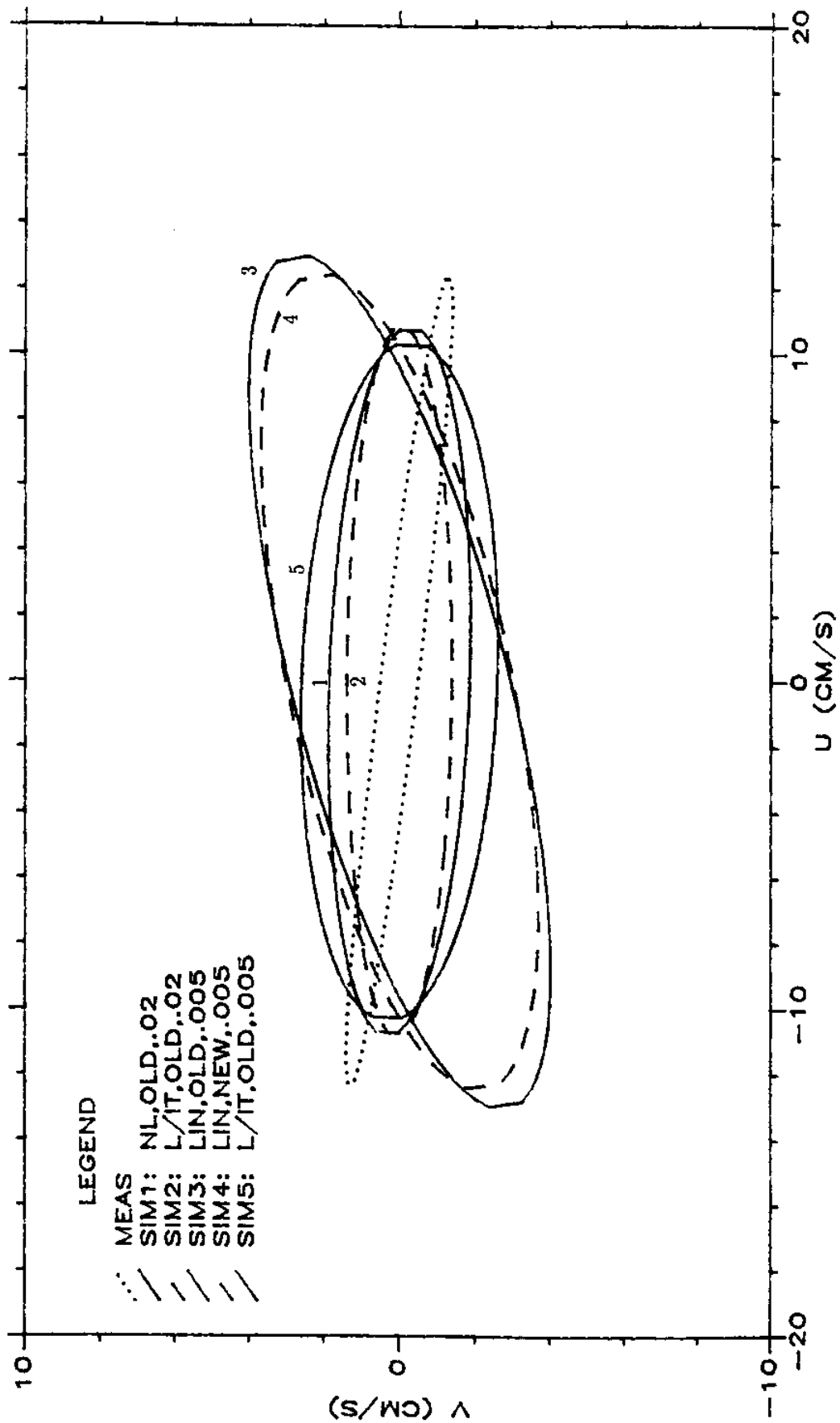


Figure 3.4 Measured and simulated M₂ tidal ellipses, Station 5

M2 ELLIPSES FOR STATION 7

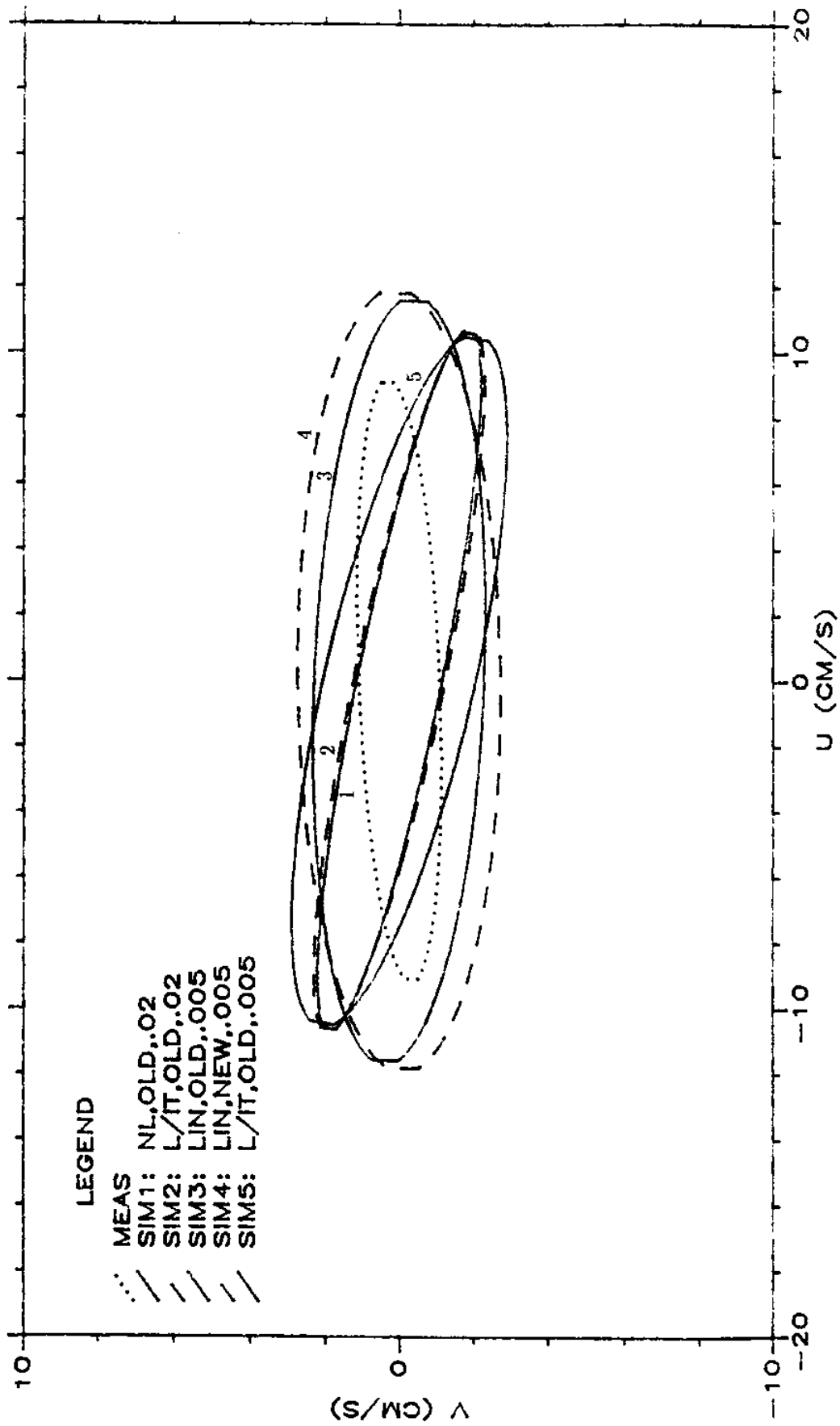


Figure 3.5 Measured and simulated M₂ tidal ellipses, Station 7

M2 ELLIPSES FOR STATION 10

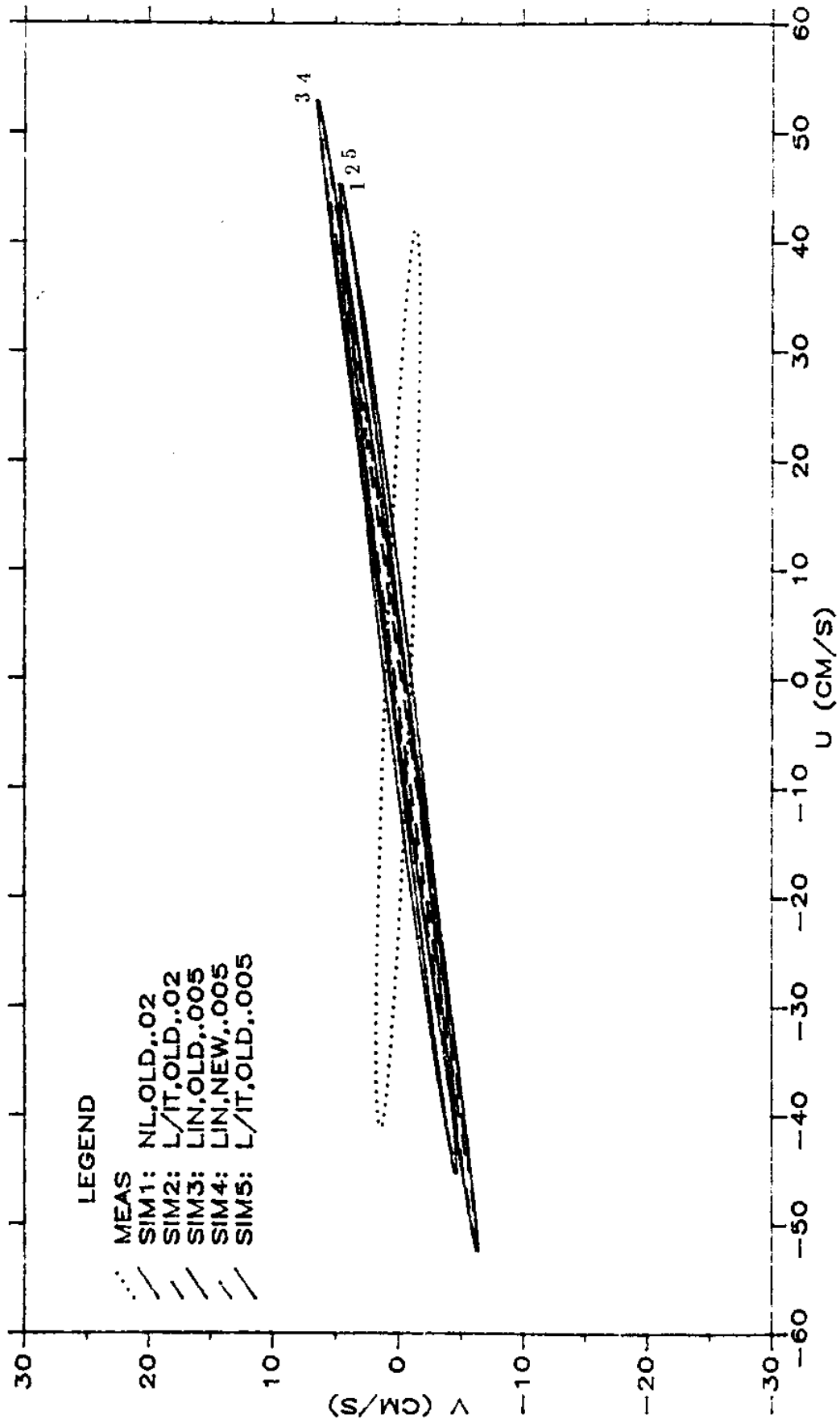


Figure 3.6 Measured and simulated M₂ tidal ellipses, Station 10

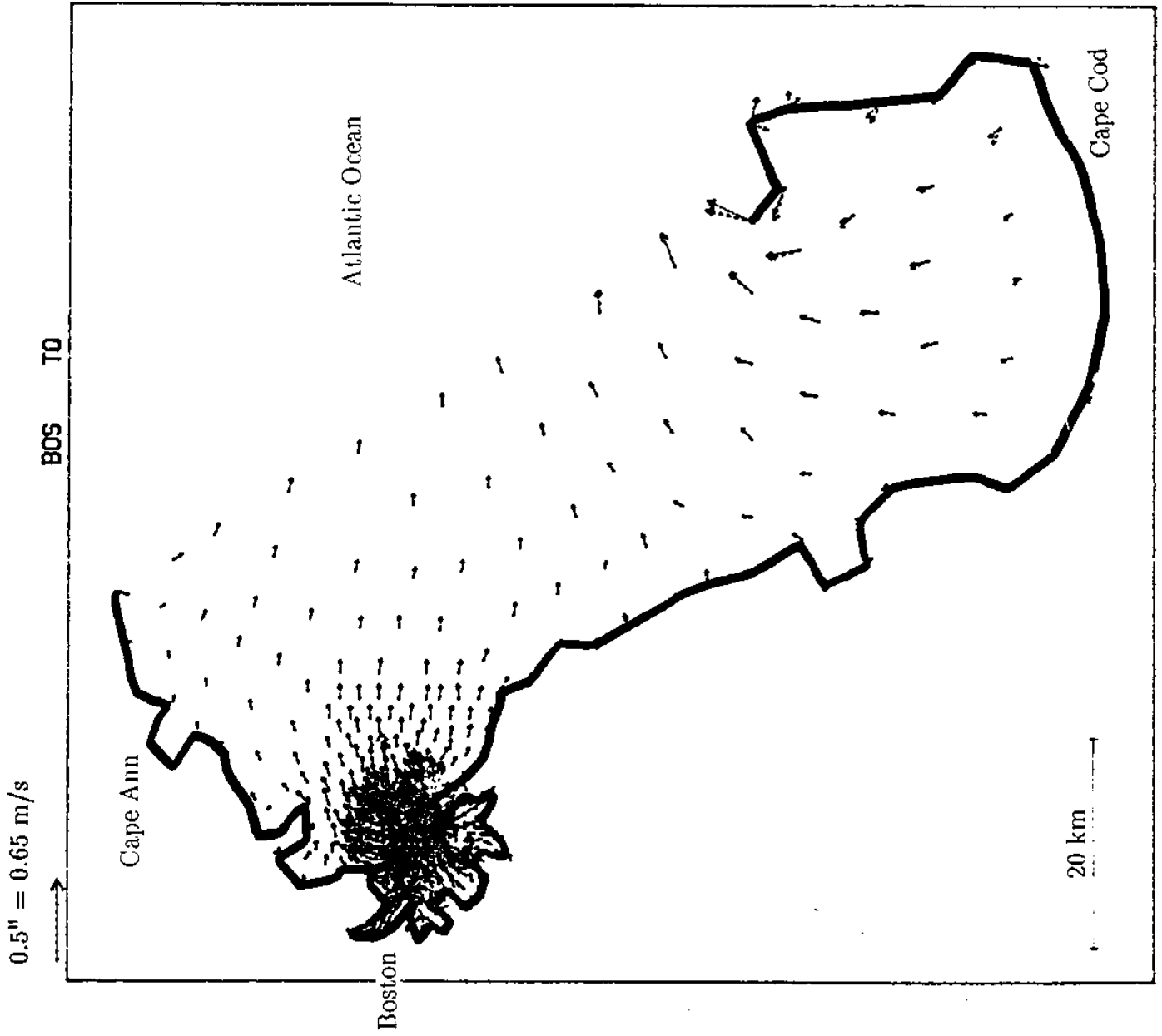


Figure 3.7a Comparison of simulated flow fields using non-linear model (dashed lines) and linear model with iteration (solid lines) for conditions of maximum ebb

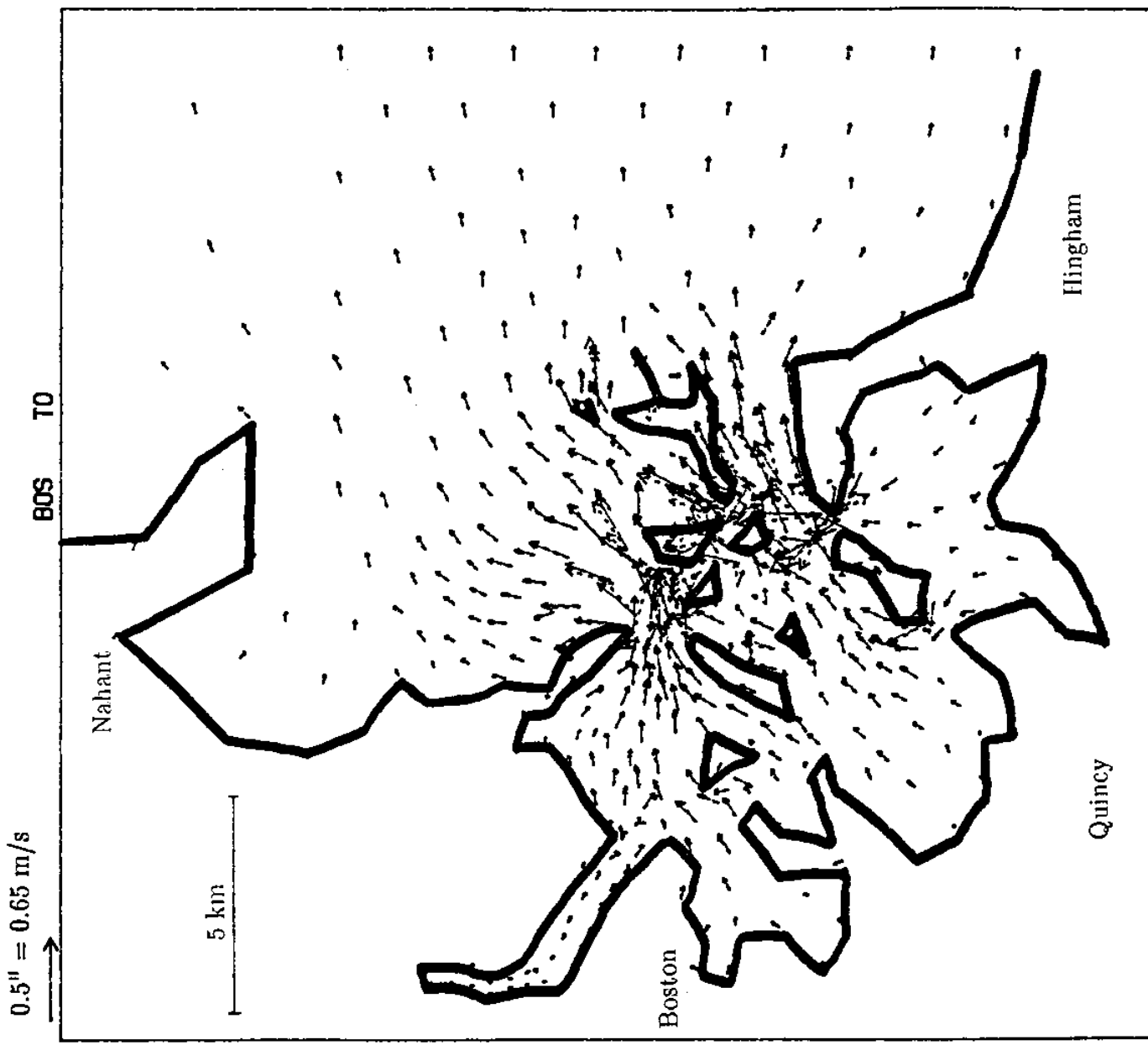


Figure 3.7b

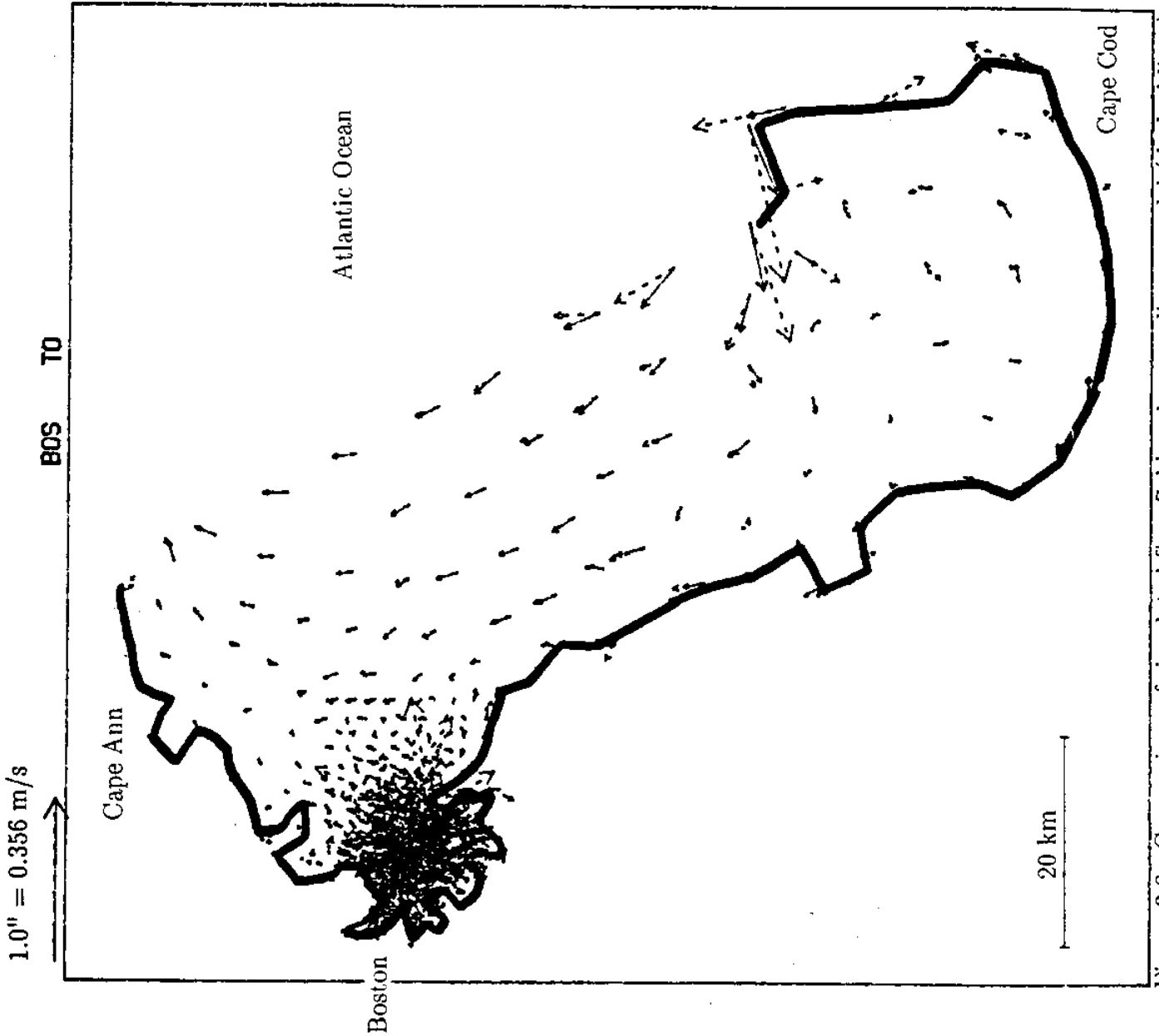


Figure 3.8a Comparison of simulated flow fields using non-linear model (dashed lines) and linear model with iteration (solid lines) for conditions of high water slack

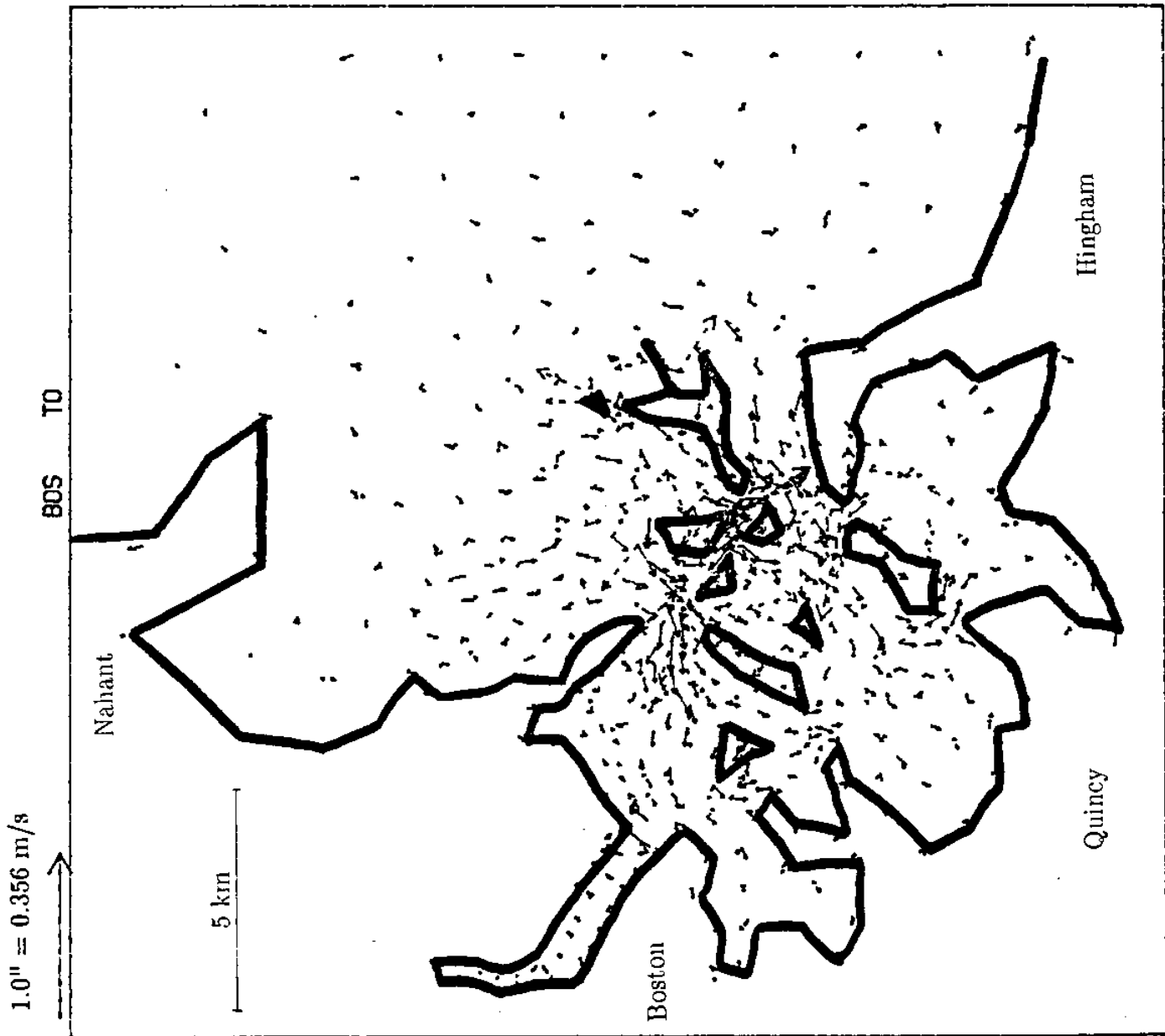


Figure 3.8b

4. HALOCARBON TRACER STUDY

4.1. Background

Volatile halogenated organic compounds (VHOC) can serve as continuous tracers of sewage effluent. These compounds include industrial solvents (e.g., CCl_4 , $\text{CCl}_2=\text{CCl}_2$, CH_3Cl_3 , $\text{CHCl}=\text{CCl}_2$) and haloforms formed by chlorination (CHCl_3 , CHCl_2Br , CHClBr_2 , and CHBr_3), and are found in the effluent at concentrations in the range of 1–10 ppb. Using gas chromatography, they can be detected in the receiving water down to concentrations in the range of 1–10 ppt allowing approximately a 1000-fold reduction in concentration to be detected. In order to obtain the same resolution in a continuous dye study one would require about 10 barrels of dye per day which would be both environmentally and economically prohibitive.

Their high detectability and zero cost are the major advantages of these tracers. Disadvantages include the fact that source loading from the treatment plants generally varies with time, extraneous sources may be present (industrial loading may enter the receiving water at sources other than the treatment plant(s) and other facilities such as CSO retention facilities, power plants, and other sewage treatment plants chlorinate their effluent), the compounds are not conservative (however, their major sink—volatilization—is reasonably well understood and the compounds exhibit little tendency to sorb to sediments) and data collection and analysis are rather tedious.

Kossik et al. (1986) conducted three VHOC tracer studies in the northern part of Boston Harbor—one each during October 1984, April 1985, and July 1985. Using a grid of somewhat smaller extent for ELA (than displayed in §2.1a), Kossik et al. (1986) compared simulated and measured concentration distribution, and determined calibrated values for the model coefficients (a constant dispersion coefficient D and a volatilization piston velocity k) by minimizing the mean square error between simulated and measured

concentrations. Somewhat different results were obtained for the solvents versus the haloforms and it was concluded that extraneous sources were present for the former. Using data for the two haloforms CHCl_2Br and CHClBr_2 , D was determined to be in the range of 50-100 m^2/s and k was determined to be in the range of 2 to 5 cm/hr .

4.2. Details of April 27, 1987, Survey

In order to increase the spatial coverage of the early surveys, a fourth survey was conducted, as described below. On April 27, 1987, a team of six individuals, using two boats, obtained samples at the 41 stations indicated on Figure 4.1a. Twenty-nine stations have a designation H for harbor while 12 have a designation B for bay. (Note that Stations H1-H6, H9, H28, and H29 correspond approximately to those of earlier surveys.) At most stations only a surface sample was collected but at six "bay" stations up to five samples in the vertical were obtained. (Based on previous surveys, concentrations within the harbor were expected to be generally well mixed while some stratification offshore could be expected.)

Samples in the harbor were collected between 0900 EDT and 1350 EDT covering an approximate $2\frac{1}{2}$ -hour period on either side of high tide which occurred in Boston Harbor at 1142 EDT. Samples in the bay were collected between 0915 EDT and 1615 EDT, or up to $4\frac{1}{2}$ hours after high tide. Unlike the previous three surveys, where measurements were generally collected within a 1-hour period before and after high tide (and hence could be considered reasonably synoptic), significant tidal drift was possible at some stations during this survey. To account for this, the horizontal location of each station has been "corrected" to an equivalent position at high slack thus creating an essentially synoptic picture. The correction has been made using the tracking algorithm of ELA based on observed semi-diurnal tides. The "corrected" locations are shown as stars in Figure 4.1b along with the original locations which are denoted by pluses. The scale of Figures 4.1a

and b are the same as that of Figure 2.22b showing the new grid and Figures 4.4a-4.10a which show measured and simulated concentrations (to be discussed later).

From April 15 through the morning of April 27, samples were collected from the effluent pipes at Deer and Nut Is. Samples were collected by treatment plant personnel, generally four times a day at 0300, 0900, 1500, and 2100 EDT. However, at Nut Is., after April 21, sample dates and times were apparently not recorded.

Procedures for collecting, extracting, and analyzing compounds were as described in Kossik et al. (1986) and so need not be described here.

4.3. Results

Effluent concentrations for eight compounds are reported in Tables 4.1 and 4.2 for the Deer and Nut Is. treatment plants, respectively. Table 4.1 also includes daily averaged treatment plant flow rate and mass loadings computed from daily averaged flow rate and daily averaged concentration. (Observed hourly variations in treatment plant flow rate were very small.) Corresponding calculations could not be made reliably at Nut Is., because of the missing logs. For Deer Is. the effluent concentrations are also plotted as a function of time in Figure 4.2a (for three solvents) and 4.2b (for two haloforms). Concentrations of the four Deer Is. haloforms are also plotted as a function of time of day in Figures 4.3a to 4.3d.

Water column concentrations for seven of the compounds are plotted on Figures 4.4a to 4.10a. (Reliable receiving water measurements could not be made for chloroform because of high background concentrations.) For the six "bay" stations with multiple-depth sampling, depth-average concentrations are presented while, for the remaining stations, surface values are used. Contours overlaying the measurements are for simulations which are discussed in §4.6. Note that on these plots, the "corrected" station location has been

used. Depth profiles for the six "bay" stations are plotted in part b of the corresponding figure.

4.4. Qualitative Observations

Before proceeding with model calibration, several preliminary calculations and comparison with primary data can be made. Table 4.3 summarizes statistics computed from the above data for the Deer Is. effluent data and concentrations in the northern harbor. Data for chloroform have again been omitted, and the data for bromoform should be considered separately for reasons discussed below.

Regarding the effluent data, weighted average loadings $\langle \dot{m} \rangle$ (representing the 13-day period prior to and including the day of the survey) were obtained for each constituent using an exponential filter

$$\langle \dot{m} \rangle = \frac{\sum_{i=0}^{n-1} \dot{m}(t-i\Delta t) e^{-\kappa i \Delta t}}{\sum_{i=0}^{N-1} e^{-\kappa i \Delta t}} \quad (4.1)$$

where $\dot{m}(t)$ and $\langle \dot{m} \rangle$ represent daily and filtered variables, $\Delta t = 1$ day, $N = 13$, and $\kappa = 0.1 \text{ d}^{-1}$. The purpose of the filter is to weight variables in accordance with their expected representation in the water column following loss due to volatilization. (Hence, recent loadings are weighted more heavily than past loadings.)

Included below the filtered values are corresponding means and standard deviations for Deer Is. effluent data from previous surveys (Kossik et al., 1986). These data suggest that for the solvents, effluent loadings for the current survey are somewhat higher, but within the range of past measurements, while for the haloforms, the present loadings are generally

two to three times lower. The fact that the effluent haloform measurements were higher for the previous surveys is likely due to bias in the way the previous data were sampled. Previous effluent sampling was conducted predominantly during morning hours (0800-1100). Examination of Table 4.1 shows significant daily variability with measurements for CHBr_2Cl and CHBr_3 , in particular, showing significantly higher values at 0900 than at other times of the day. Thus previous loading estimates for the haloforms are likely to be too high. Note that, because they could not reconcile calibrated parameters based on solvent and haloform measurements, Kossik et al. (1986) concluded that the loading estimates *for the solvents were too low* (i.e., that there were extraneous sources). Accounting for the above factor would significantly reduce the discrepancy in the previous calibrations. In an attempt to better understand the diurnal variability of effluent concentrations, a 48-hour survey was made from August 3 to 5, 1987, in which Deer Is. effluent was sampled once an hour. Presentation of results, including analysis of correlating factors, will be presented in a later report.

Regarding water column measurements, average concentrations $\overline{c_F}$ in the northern portion of the harbor (inshore of Deer Is. and roughly north of Long Is.) are summarized in Table 4.3 for each constituent. The specific stations used to compute the averages are listed in a footnote to the table. It can be noted that concentrations of both solvents and haloforms are comparable in magnitude with those of previous studies.

The ratio of effluent loading to average harbor concentration, $\frac{\langle \dot{m} \rangle}{c_F}$, is proportional to removal rate (reflecting both hydrodynamic flushing and volatilization) and is listed in Table 4.3. The reciprocal of removal rate can be converted to a residence time by multiplying by the appropriate harbor volume. Residence times for the Deer Is. effluent discharge in the northern harbor are listed in Table 4.3 and, omitting data for bromoform, range from 6.5 to 11.7 days with an average of 9.1 days. (These calculations are based on a

high tide volume of $391 \times 10^6 \text{ m}^3$ corresponding to segments VI-X and C4-C6 defined by Ketchum et al. (1951); residence times calculated without segments C4-C6 (Dorchester Bay) range from 5.7 to 10.3 days.) The consistency among constituents is encouraging and is better, in general, than found in previous surveys. (Residence times for the same constituents have been computed for previous survey data and their ranges are also listed in Table 4.3; observed variability in these data are felt to be due in large part to the absence of sufficient sampling of effluent data prior to the survey to properly define $\langle \bar{r} \rangle$.)

Considering the April 1987 survey in which measurements of $\langle \bar{r} \rangle$ were much better resolved, it is possible that the computed variations in residence times among compounds is due to true physiochemical differences in the rates of volatilization among the compounds. Indeed, the ordering of residence times among compounds listed in Table 4.3 is highly correlated with the ordering of residence times reported for similar compounds by Helz and Hsu (1978) for laboratory experiments with stirred reactors. These data are also displayed in Table 4.3. Note that because mixing in a stirred reactor is not the same as tidal mixing in Boston Harbor, the ordering of residence times, rather than the actual magnitudes, should be compared. These data will be examined further in a attempt to better understand volatilization, but such an examination is beyond the scope of the present study.

The computed residence time for bromoform (148 days) is clearly anomalous. While bromoform is the least volatile compound listed (as confirmed by the data of Helz and Hsu, 1978, in Table 4.3), the computed time is far greater than would be expected based on hydrodynamic flushing alone, thus leading one to suspect an extraneous source(s). The receiving water data of Figure 4.8a, and to an even greater degree data from previous surveys, show an increasing gradient of bromoform concentration moving toward shore, a graphical indication of other (shoreline) sources.

The most obvious candidate is chlorination of condenser cooling water at coastal power plants. Because it is seawater which is being chlorinated, bromoform is the predominant (>95%) haloform to be formed, although small quantities of CHBr_2Cl (<5%) may also be formed (Helz and Hsu, 1978; Battelle, 1982). Boston Edison operates two large power stations on Boston Harbor: Mystic Station in Everett with generating capacity from Units 4, 5, 6, and 7 totaling about 1000 MWe and New Boston, in South Boston, with capacity from Units 1 and 2 totaling about 700 MWe. Standard practice is to chlorinate each unit for two hours per day.

Although no measurements were taken specifically at the Boston Edison plants, bromoform loading can be estimated from data collected at the Redondo Generating Station in Southern California where effluent concentrations of CHBr_3 were found in the range of 3 to 13 ppb (Battelle, 1982). If this same range were to apply to the Boston Edison stations, then the daily average loading would fall in the range of 1 to 4 Kg/d. The factor of order 5 difference in this estimate and the observed bromoform loading rate of 0.57 Kg/d for Deer Is. is sufficient to explain the exaggerated residence time for bromoform shown in Table 4.3. On the other hand, if the production of CHBr_2Cl by power plant chlorination is estimated as 3% of that of CHBr_3 , then an estimated 0.03 to 0.12 Kg/d of CHBr_2Cl is being formed. This amounts to 2 to 10% of the loading observed for Deer Is., which is small compared with variability in the Deer Is. measurements and compared with other extraneous sources discussed below.

Outside the harbor, concentrations generally decrease with distance, as expected, except for Station B11 where locally higher concentrations were found for all constituents. Vertical profiles indicate substantial variation with depth. It should be emphasized that this survey was conducted within several weeks of record rainfall. Hydrographic surveys by the USGS indicate significant horizontal as well as vertical variation in salinity and hence

density which provides a plausible explanation of the observed vertical variation in concentration: sewage effluent, containing VHOC, is being trapped at different vertical elevations, according to its density after mixing, in comparison with the highly variable ambient density. In retrospect, it is unfortunate that salinity and temperature were not measured along with VHOC.

The exceptional rainfall could also contribute some extraneous loading of VHOC via local and remote (i.e., Merrimack R.) sources. We have no handle on VHOC concentration in the Merrimack R., but we were able to survey local authorities who chlorinate effluent. (Note that most municipal treatment plants are required to chlorinate from April 1 through mid-October.) Table 4.4 summarizes weighted average flow rates (obtained with the exponential filter defined by Eq. 4.1) for the SESD, Lynn, Swampscott, and Hull treatment plants, and the Chas. River Estuary Facility (a CSO) along with corresponding data for Deer and Nut Is. While no data are available for concentrations, the flow rates from these sources represent approximately 15% of the combined Deer and Nut Is. flow. To the extent that extraneous sources are present for one or more of the constituents, the measured effluent concentrations and loadings should be viewed as lower bounds.

4.5. Model Calibration

Procedures similar to those described in Kossik et al. (1986) were used to formally calibrate model parameters—a constant dispersion coefficient D and a constant volatilization rate k —based on the April 27, 1987, data.

Briefly, TEA was run in linear mode (without iteration) using the new grid with M_2 forcing and no low frequency currents—conditions which are consistent with the long-term observations presented in §3. A set of 19 runs was then made with ELA where D varied between 5 and 100 m^2/s , k varied between 0.5 and 10.0 cm/hr , and a constant mass loading

\dot{m} was used for each treatment plant. (\dot{m} was chosen proportional to flow rate.) Note that for runs with lower values of k , calculations had to be run for as much as 1000 time steps. (Using a Δt of 3.1 hr, this is approximately 130 days.) Simulated concentrations at high tide were interpolated to each of the 41 sampling stations in the harbor and bay, and a multi-variate linear regression program was used to fit bi-quadratic equations of the form

$$c_{ij} = \dot{m}_j \left[a_{i1} + \frac{a_{i2}}{D} + \frac{a_{i3}}{k} + \frac{a_{i4}}{Dk} + \frac{a_{i5}}{D^2} + \frac{a_{i6}}{k^2} + \frac{a_{i7}}{D^2k} + \frac{a_{i8}}{Dk^2} + \frac{a_{i9}}{D^2k^2} \right] \quad (4.2)$$

where c_{ij} is the simulated concentration at location i ($i = 1$ to 41) for compound j , and a_{i1} to a_{i9} are fitting parameters. Note that Eq. (4.2) applies to any compound j as long as the appropriate value of \dot{m}_j is used. However, because the relative magnitude of \dot{m} for the two treatment plants is not exactly the same for all compounds, this procedure involves some error. Because Deer Is. is the larger plant, results are scaled to the mass loadings computed at Deer Is.

Having described the simulated concentration at each station i as a continuous function of the input parameters (D , k , and \dot{m}), the error E between the simulated concentrations $c_{i,j}$ and the measured concentration for a given compound j , $c_{i,j}^m$, can be computed as a function of D and k as

$$E_{ij}(D,k) = c_{ij}^m - C_{ij}(D,k) \quad (4.3)$$

Equal weighting was given to 37 sampling stations (omitting Stations H1, H3, H4, and B11 because of suspected extraneous sources or proximity to the Deer Is. plume) in defining a normalized root mean square error for each compound

$$E_j^{\text{RMS}} = \frac{\left[\frac{1}{37} \sum_{i=1}^{37} E_{ij}^2 \right]^{\frac{1}{2}}}{\overline{c_{ij}^m}} \quad (4.4)$$

where $\overline{c_{ij}^m}$ is the average concentration for compound j , defined so that E_j^{RMS} will be non-dimensional. Calibration consisted of seeking parameter values D and k that minimized E_j^{RMS} , whether individually, or averaged over different compounds j .

Data for CH_3CCl_3 , TCE, TetraCE, CHBrCl_2 , and CHBr_2Cl were used in the optimization. CHCl_3 and CHBr_3 were omitted for reasons stated previously and CCl_4 was not used because of its generally lower concentrations. Table 4.5 summarizes the optimal combinations of k and D for each of the five compounds taken individually. These data suggest $0.7 < k < 1.4$ cm/hr and $31 < D < 103$ m²/s.

Despite the variation in optimal parameter values, the contour plots of E_j^{RMS} vs. D and k were quite similar among compounds. Coupled with the reasonable consistency in computed residence times among compounds (Table 4.3), and the fact that D should be identical for all compounds while k should not vary significantly among compounds (Kossik et al., 1986), suggested that the errors be averaged. Thus an average error was computed based on the five compounds, CH_3CCl_3 , TCE, TetraCE, CHBrCl_2 , and CHBr_2Cl ,

$$E_T^{\text{RMS}} = \frac{1}{5} \sum_{j=1}^5 E_j^{\text{RMS}} \quad (4.5)$$

Figure 4.11 shows a contour plot of E_T^{RMS} vs D and k . As shown in Table 4.5, the optimal values of k and D obtained in this manner are 1.22 cm/hr and 45 m²/s, respectively.

Because ELA will be applied to a range of both volatile and non-volatile compounds, we are more interested in D than k . Unfortunately, the error contours appear more sensitive

to k than to D . For example, while the minimum value of E (0.418) occurs at $k = 1.22$ cm/hr and $D = 45$ m²/s, the contour of $E = 0.420$ extends from a k of approximately 1.0 to 1.3 cm/hr while D varies from approximately $D = 35$ to 80 m²/s. The contour of $E = 0.450$ extends from approximately $k = 0.7$ to 2.0 cm/hr while D varies from approximately 17 to greater than 105 m²/s. Similar lack of sensitivity is observed if compounds are considered individually or if they are grouped in sub-sets.

4.6. Discussion

Based on the above analysis, best-fit values of $k = 1.2$ cm/hr and $D = 45$ m²/s are identified, and Figures 4.4a through 4.9a show concentration contours computed with these parameters overlaying measurements. Computed contours are shown for CCl₄ even though the data were not used in calibrating, but contours are not shown for CHBr₃ because of suspected extraneous sources. Also note that data from all 41 measurement stations are displayed, although only data from 37 stations were used in the calibration.

It is noted that the value of D is at the low end, but still consistent with the range of 50–100 m²/s determined by Kossik (1986) while the value of $k = 1.2$ cm/hr is significantly below the range of 2–5 cm/hr found previously. In the case of k , the lower value for the present survey is most likely due to the 2–3 fold decrease in the estimate of haloform loading allowed by the more thorough effluent sampling in the recent survey.

Some sensitivity was performed to identify the effect of uncertainty in \dot{m} on the calibrated values of D and k . In general, increasing \dot{m} during optimization increased both D and k . (Heuristically, if more mass is being input to the model, the optimization is forced to use higher values of D and k in order to decrease simulated concentrations to effect agreement with measurements.) To the extent that total mass loadings to the system may be underestimated (due to the existence of extraneous sources), the calibrated

values of k and D can be viewed as a lower bound. On the other hand, if extraneous mass is being introduced away from the two treatment plants, the optimization may be overestimating the value of D in order to increase the spatial distribution—an effect in the opposite direction. These opposing influences, coupled with the mild sensitivity of computed error contours to D and the calculated variation in D with varying tidal amplitude all underscore the uncertainty of the dispersion process.

Table 4.1

Deer Is. Effluent Samples

<u>Date/Time</u>	<u>Q</u> (m ³ /s)	<u>CHCl₃</u> (ppb)	<u>CH₃CCl₃</u> (ppb)	<u>CCl₄</u> (ppb)	<u>TCE</u> (ppb)	<u>CHBrCl₂</u> (ppb)	<u>CHBr₂Cl</u> (ppb)	<u>TetraCE</u> (ppb)	<u>CHBr₃</u> (ppb)
4.15.87 1500		2.02	3.19	0.10	4.91	0.64	0.53	6.96	0.47
2100		4.38	12.90	0.13	8.36	0.68	0.43	8.98	+ ³
daily ave.	17.0		(11.8) ¹	(.18)	(9.75)	(.97)	(.70)	(11.7)	(0.42)
4.16.87 0300		3.52	6.98	0.19	7.15	0.87	0.62	9.14	+
0900		1.91	5.11	0.17	6.37	0.76	1.04	4.93	0.95
1500		2.54	5.12	0.11	5.89	0.76	0.49	8.65	+
2100		3.34	26.72	0.21	5.81	0.71	0.60	6.47	+
daily ave.	17.7		(12.8)	(.26)	(9.6)	(1.18)	(.93)	(11.1)	(0.48)
4.17.87 0300		3.02	8.95	0.16	5.81	0.76	0.44	9.04	+
0900		1.90	7.42	0.17	5.72	0.78	1.13	4.90	1.13
1500		4.07	7.43	0.08	7.94	0.88	0.48	12.59	+
2100		4.33	10.08	- ²	5.44	0.31	+	6.90	-
daily ave.	17.8		(13.0)	(.17)	(9.5)	(1.05)	(.83)	(12.8)	(0.55)
4.18.87 0300		5.21	8.81	0.14	7.19	0.74	0.32	8.54	+
0900		2.69	6.23	0.14	6.99	1.10	1.87	5.62	2.04
1500		3.68	4.88	0.13	7.77	0.82	0.38	7.38	+
2100		4.59	4.65	0.14	8.72	1.24	1.13	7.41	0.60
daily ave.	17.7		(9.4)	(.21)	(11.8)	(1.52)	(1.41)	(11.1)	(1.09)
4.19.87 0300		2.92	4.47	0.12	9.02	0.65	0.48	9.93	+
0900		2.60	4.67	0.16	8.97	1.12	2.15	9.15	2.91
1500		2.86	3.52	1.13	7.72	0.94	0.60	5.75	+
2100		3.20	3.25	0.14	7.14	1.10	1.11	9.08	0.74
daily ave.	16.8		(5.8)	(.20)	(11.9)	(1.38)	(1.57)	(12.3)	(1.40)
4.20.87 0300		2.79	2.75	0.11	6.38	0.96	0.48	4.70	+
0900		2.35	3.25	0.08	7.46	1.07	1.65	4.48	1.67
1500		4.30	14.37	0.07	8.45	0.35	+	15.80	+
2100		5.48	16.73	0.25	9.44	0.81	0.21	15.30	+
daily ave.	15.8		(12.7)	(.18)	(10.8)	(1.09)	(.83)	(13.8)	(0.67)
4.21.87 0300		4.89	9.74	0.12	7.41	0.99	0.36	7.85	+
0900		2.59	12.71	0.13	9.22	0.93	0.97	6.12	0.61
1500		4.93	13.97	0.14	8.85	0.88	0.40	10.40	+
2100		6.60	10.67	0.14	7.64	0.79	0.28	11.26	+
daily ave.	15.6		(15.9)	(.18)	(11.2)	(1.21)	(.67)	(12.0)	(0.31)
4.22.87 0300		6.54	8.46	0.38	10.64	1.50	1.00	8.98	0.53
1500		3.80	15.12	0.15	7.75	1.13	1.06	18.58	0.50
2100		14.24	28.82	0.14	14.56	1.50	0.70	21.70	+
daily ave.	15.3		(23.1)	(.29)	(14.5)	(1.82)	(1.22)	(21.7)	(0.37)

Table 4.1 (cont'd)

Date/Time	Q (m ³ /s)	CHCl ₃ (ppb)	CH ₂ CCl ₃ (ppb)	CCl ₄ (ppb)	TCE (ppb)	CHBrCl ₂ (ppb)	CHBr ₂ Cl (ppb)	TetraCE (ppb)	CHBr ₃ (ppb)
4.23.87 0300		17.95	29.39	0.17	21.40	2.06	1.46	28.73	+
1500		8.63	33.29	0.10	16.79	1.18	0.96	20.31	+
2100		15.71	26.90	0.24	19.12	1.71	0.58	17.92	+
daily ave.	15.2		(39.2)	(.21)	(25.1)	(2.17)	(1.31)	(13.6)	(0.13)
4.24.87 0300		1.16	3.02	0.05	2.02	+	+	6.82	+
0700		14.68	39.8	0.96	28.65	3.46	1.75	28.10	0.47
1500		7.81	15.59	0.27	13.08	1.12	0.90	14.67	+
2100		13.50	19.29	0.10	17.35	1.15	0.24	16.17	+
daily ave.	14.9		(20)	(.45)	(19.7)	(1.88)	(.96)	(21.2)	(0.24)
4.25.87 0300		10.60	28.25	0.14	19.07	1.03	0.38	20.20	+
0900		3.85	7.21	0.20	9.64	1.30	0.91	9.76	+
1500		4.70	8.74	0.22	10.33	1.31	1.24	13.48	0.75
daily ave.	15.0		(19.0)	(.25)	(16.7)	(1.56)	(1.08)	(18.6)	(0.41)
4.26.87 0900		4.12	5.68	0.18	10.67	1.53	1.51	9.34	0.80
1500		3.28	4.79	0.24	7.90	1.18	1.46	6.70	0.90
2100		5.56	4.18	0.21	7.44	1.21	0.51	7.29	+
daily ave.	14.9		(6.28)	(.27)	(11.2)	(1.69)	(1.54)	(9.4)	(0.77)
4.27.87 0300		4.74	4.25	0.24	7.55	1.49	1.32	7.50	0.68
0900		3.42	4.07	0.15	8.05	1.44	1.32	5.84	0.52
daily ave.	14.8		(5.35)	(.26)	(10.0)	(1.88)	(1.88)	(8.59)	(0.77)
filt <ṁ>			15.1	.24	13.8	1.64	1.24	13.8	0.57 ⁴
$\frac{\dot{m}_{DI}}{\langle Q \rangle_{DI}} \frac{\langle Q_{NI} \rangle}{\dot{m}_{NI}}$			2.2	1.8	3.3	0.3	1.0	1.1	
c ₀ for Q ₀ = 15.7m ³ /s			11.4	.18	10.2	1.21	0.91	10.2	

1 values in parentheses are daily average mass loading in kg/d

2 - denotes concentration less than threshold of 0.05 ppb

3 + denotes concentration less than threshold of 0.2 ppb

4 assumes concentrations denoted by + are 0.1 ppb

Table 4.2

Nut Is. Effluent Samples

<u>Date/Time</u>	<u>Q</u> (m ³ /s)	<u>CHCl₃</u> (ppb)	<u>CH₂CCl₃</u> (ppb)	<u>CCl₄</u> (ppb)	<u>TCE</u> (ppb)	<u>CHBrCl₂</u> (ppb)	<u>CHBr₂Cl</u> (ppb)	<u>TetraCE</u> (ppb)	<u>CHBr₃</u> (ppb)
4.16.87 0900		2.44	3.46	0.06	2.59	1.05	0.87	6.52	0.43
1500		1.67	2.69	0.06	1.77	0.55	0.35	4.83	+ ²
2100		1.82	2.67	0.05	1.84	0.82	0.73	4.37	0.31
daily ave.	10.3								
4.17.87 0300		1.46	2.20	- ¹	1.43	0.65	0.58	3.71	0.22
0900		1.54	2.91	0.07	2.13	0.76	0.72	5.40	0.33
1500		2.82	3.92	0.09	2.61	0.97	0.66	7.46	+
daily ave.	9.8								
4.18.87 0300		4.55	4.36	0.09	2.70	0.96	0.48	9.80	+
0900		2.74	3.98	0.11	3.51	1.00	0.78	8.09	+
1500		3.21	3.76	0.10	2.86	0.70	0.28	8.00	+
2100		2.36	2.29	0.07	2.06	0.68	0.36	6.52	+
daily ave.	9.6								
4.19.87 0300		3.20	6.42	0.10	4.27	1.63	0.80	12.79	+
0900		2.12	3.82	0.06	3.33	0.97	0.80	6.91	0.36
1500		2.94	3.26	0.10	2.51	0.99	0.53	5.61	+
2100		2.50	3.53	0.09	2.82	0.67	0.29	5.78	+
daily ave.	9.3								
4.20.87 0300		3.03	3.45	0.10	2.62	1.49	0.56	5.64	+
0900		3.01	4.38	0.12	3.38	1.41	1.19	6.69	0.48
1500?		2.67	4.37	0.11	3.31	1.39	1.15	6.55	0.42
2100?		2.24	8.06	0.08	2.94	0.88	0.59	6.72	+
daily ave.	8.8								
4.21.87 0300?		3.35	3.93	0.07	2.91	1.53	0.56	6.93	0.35
0900?		3.59	3.98	0.10	2.71	2.10	1.15	6.60	0.48
4.22.87 0300?		2.87	3.95	0.11	2.85	1.99	1.59	8.04	0.48
0900?		4.22	8.12	0.11	2.90	1.63	0.69	13.35	0.28
<4.24.87 1500		7.87	7.17	0.25	5.23	3.01	1.27	11.90	0.72
<4.24.87 1500		6.01	10.24	0.16	4.62	1.39	0.70	45.00	+
<4.24.87 1500		7.39	9.04	0.17	5.49	3.92	2.00	16.99	0.94
<4.27.87 0900		4.89	8.12	0.15	4.89	1.46	0.44	11.03	+
<4.27.87 0900		3.46	6.37	0.09	3.38	2.39	1.73	8.22	0.46
?		3.86	5.91	0.10	3.15	2.53	2.28	8.76	0.93
?		3.50	5.46	0.13	3.24	2.80	1.13	7.85	0.40
?		3.28	4.94	0.10	2.63	1.87	0.99	6.45	0.34
?		3.74	5.83	0.08	3.01	2.38	2.04	8.29	0.61
?		3.45	5.90	0.09	3.01	1.76	1.49	8.56	0.43
?		4.12	7.66	0.15	4.49	3.00	1.97	25.94	+

1 - denotes concentration less than threshold of 0.05 ppb

2 + denotes concentration less than threshold of 0.2 ppb

Table 4.3

Average Loadings at Deer Is. and Residence Times for Northern Boston Harbor

	<u>CH₂CCl₃</u>	<u>TCE</u>	<u>CHBrCl₂</u>	<u>CHBr₂Cl</u>	<u>TetraCE</u>	<u>CCl₄</u>	<u>CHBr₃</u>	<u>Ave</u>
mass loading < \dot{m} >, (Kg/d) ¹	15.1	13.8	1.64	1.24	13.8	0.24	0.57	
ave loading 8-84 to 9-85 ² (std dev)	11.0 (6.6)	7.9 (4.4)	4.2 (2.0)	3.4 (2.3)	12.3 (7.7)	-- --	1.4 (1.4)	
ave harbor conc \bar{c}_F (ppt)	249 ³	246 ³	34.5 ⁴	36.8 ⁴	327 ³	7.0 ⁵	215 ³	
< \dot{m} >/ \bar{c}_F	0.061	0.056	0.048	0.034	0.042	0.034	0.0027	
Res time, t_{res} , (d) ⁶	6.5	7.1	8.3	11.7	9.5	11.7	148	9.1 ⁸
Range in res time from prev. surveys (d)	5.0-18.9	6.4-16.5	2.1-6.3	1.7-4.2	5.2-15.8	--	16.0-51	6.8 ⁸
Exp res time ⁹ (d)	3.6	3.6	4.7	6.1	4.1	4.0	10.2	

1 Computed from daily average data of Table 4.1 using Eq. 4.1

2 Ave of 18 daily values measured between Aug. 84 and Sept. 85 from Kossik et al. (1986)

3 Computed from measurements at Stations H2-H7, H28, H29

4 Computed from measurements at Stations H1-H7, H28, H29

5 Computed from measurements at Stations H1-H3, H5-H7, H28, H29

6 $t_{res} \approx 0.40 \frac{\bar{c}_F}{\langle \dot{m} \rangle}$ based on high tide volume in northern basin of $391 \times 10^6 \text{m}^3$.

This volume includes segments VI-X and C4-C6 defined by Ketchum et al. (1951)

7 Range computed for surveys of Oct. 30, 1984, April 25, 1985, and July 2, 1985

8 Omits data for CHBr₃

9 Extrapolation from laboratory data in a stirred reactor (Helz and Hsu, 1978), assuming 10 m depth

Table 4.4

Filtered Flow Rates* for Other Sources Contributing Chlorinated Effluent
to Mass Bay

<u>Facility</u>	<u><Q></u>
Deer Is	360 mgd
Nut Is	198
SESD	43.9
Lynn	35.3
Swampscott	3.4
Hull	1.6
Chas R Est Facility	0.6

*weighted average flow rates from April 13-27, 1987, computed with exponential filter (Eq. 4.1) using $K = 0.1 \text{ d}^{-1}$, $N = 15$, and $\Delta t = 1 \text{ day}$

Table 4.5

Summary of Calibrated Values of
Volatilization Piston Velocity k
and Dispersion Coefficient D

	$\frac{k}{(\text{cm/hr})}$	$\frac{D}{(\text{m}^2/\text{s})}$
CHBrCl_2	1.22	33
CHBr_2Cl	0.68	57
$\text{CHCl}=\text{CCl}_2$	1.04	103
CH_3CCl_3	1.40	59
$\text{CCl}_2=\text{CCl}_2$	1.04	31
All 5 together	1.22	45

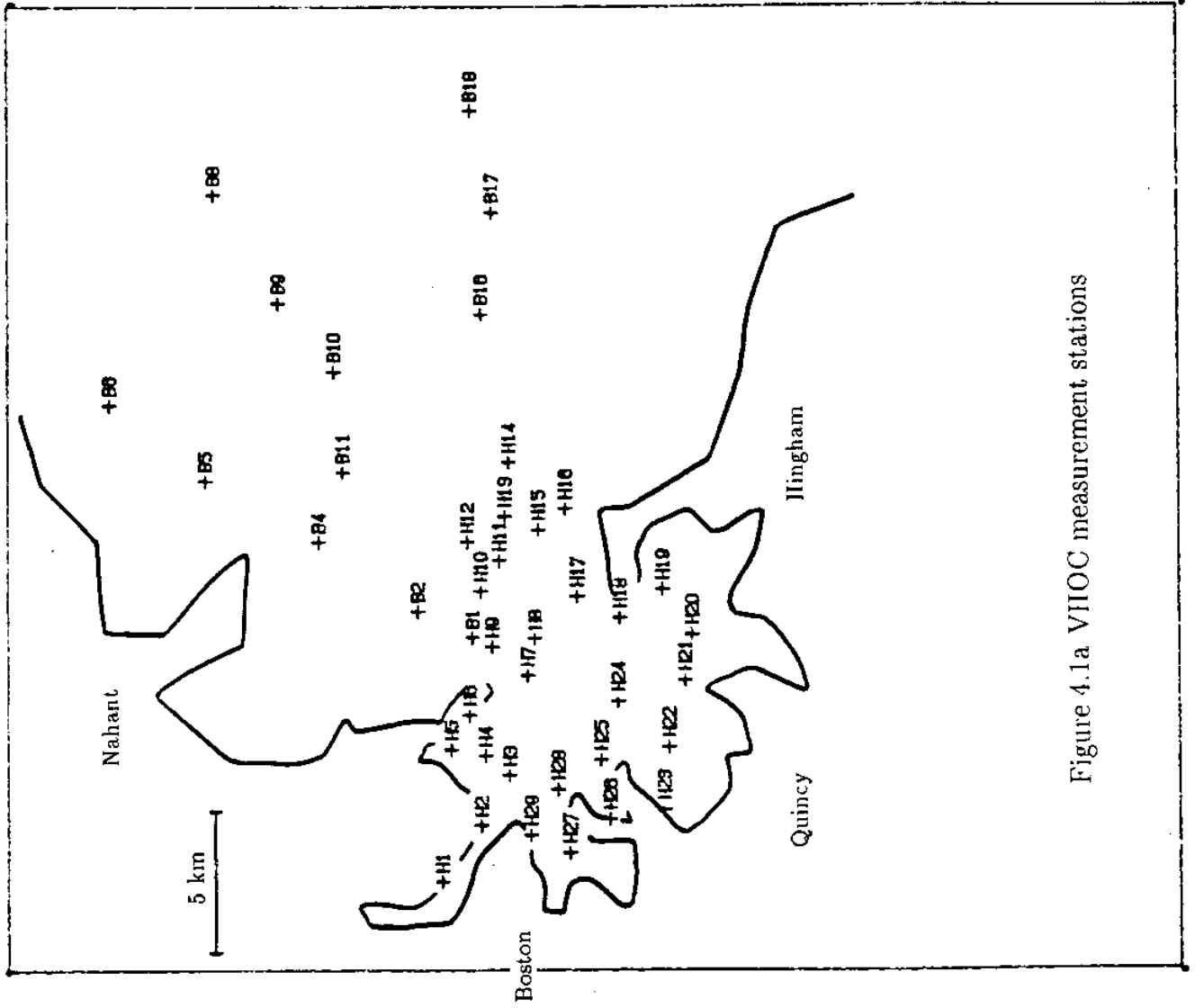


Figure 4.1a VIIOC measurement stations

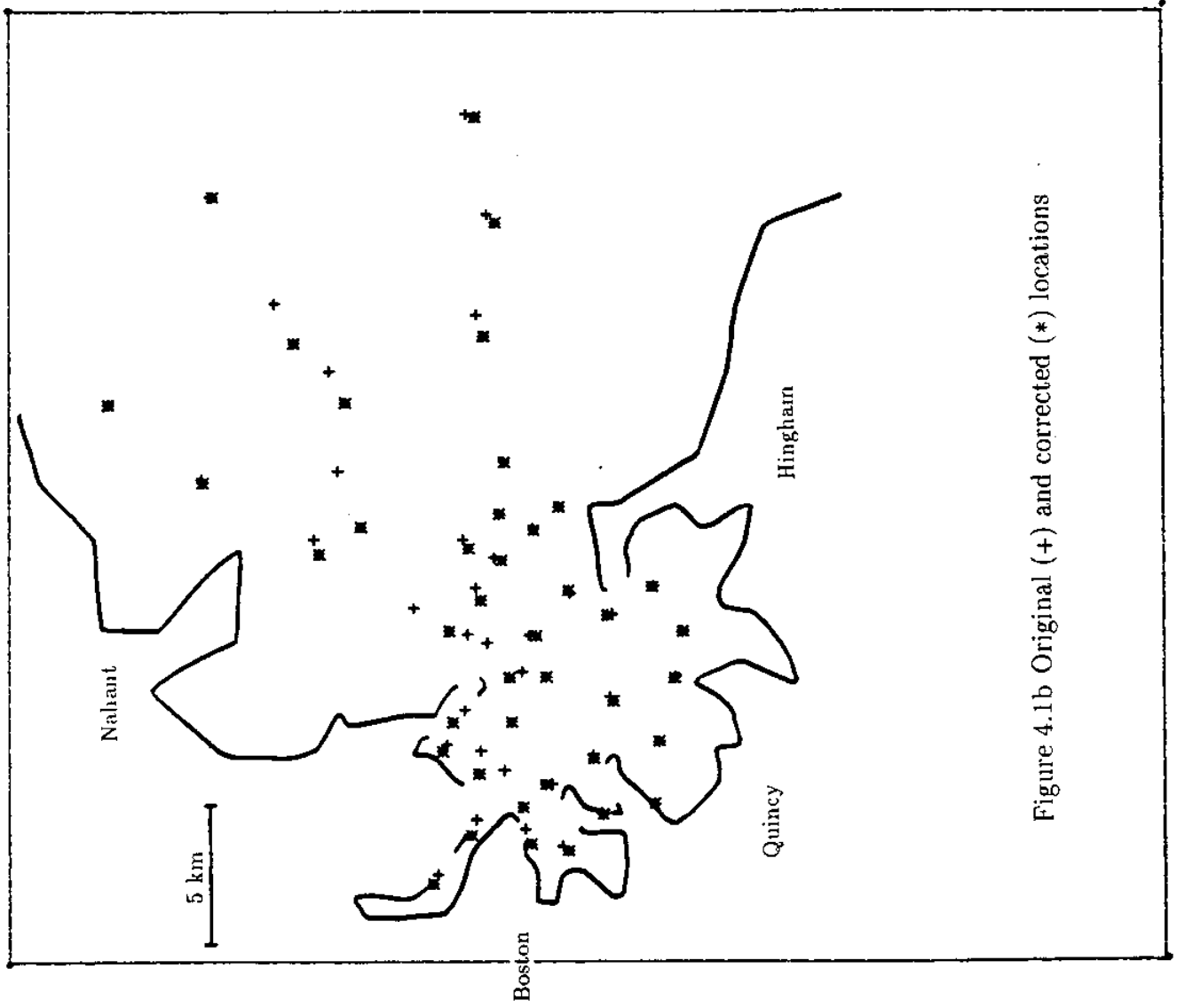


Figure 4.1b Original (+) and corrected (*) locations

Deer Island Treatment Plant

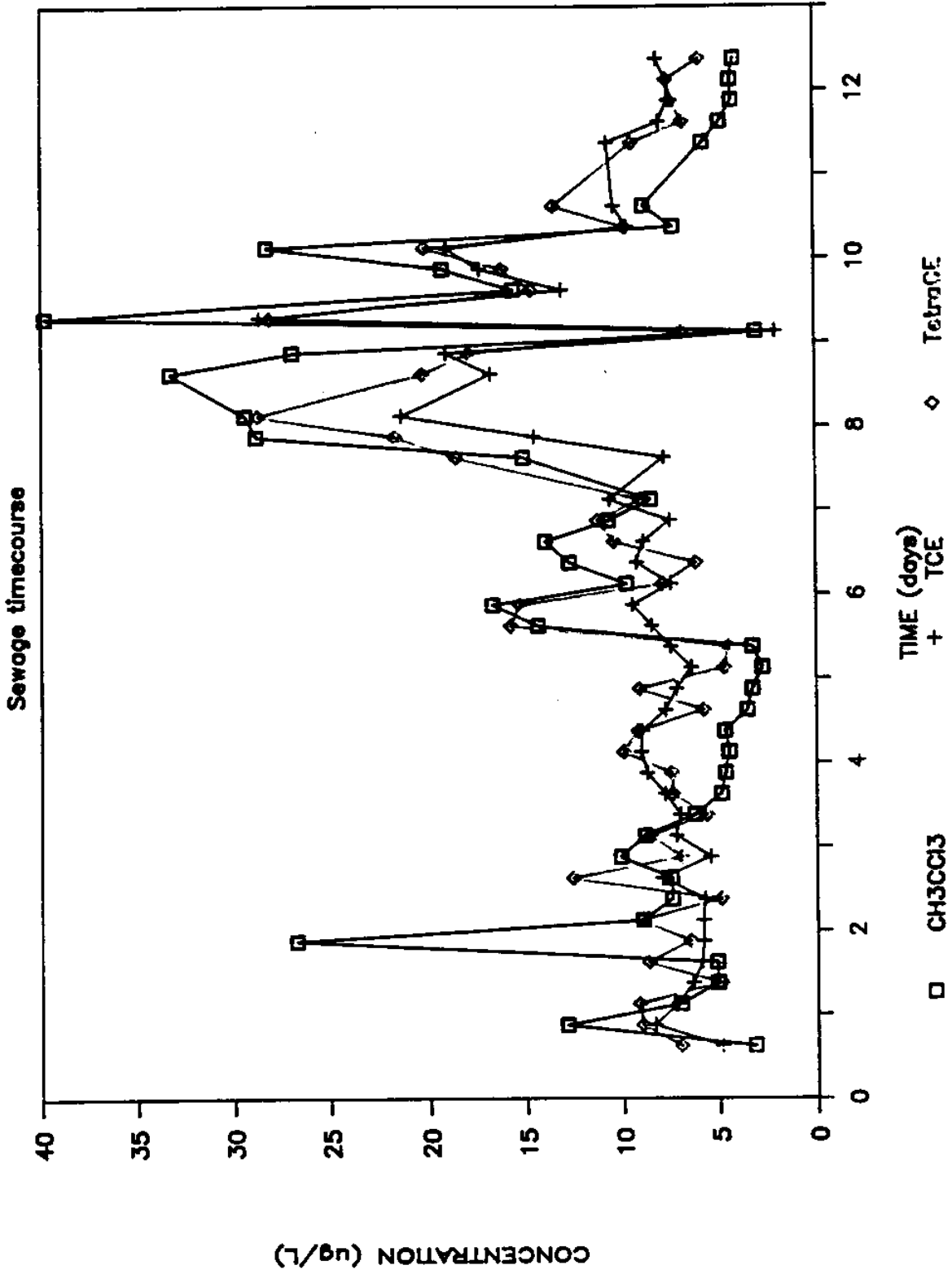


Figure 4.2 Deer Island effluent concentrations as a function of time. Day 0 is April 15, 1987, Day 12 is April 27, 1987. a) Data for CH₃CCl₃, CHCl₂=CCl₂, and CCl₂=CCl₂

Deer Island Treatment Plant

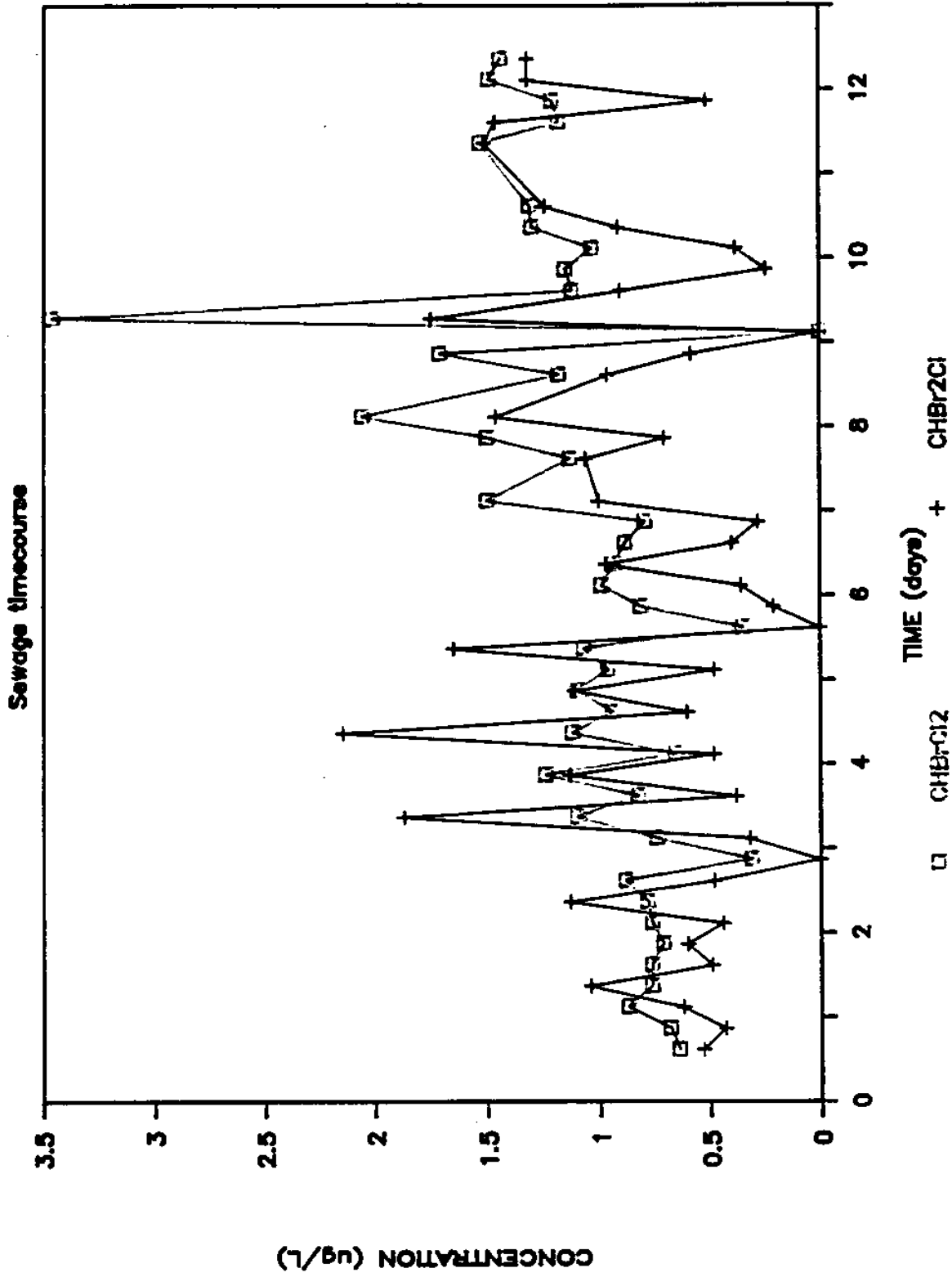


Figure 4.2b Data for CHBrCl₂ and CHBr₂Cl

Haloform variations

Deer Island Treatment Plant

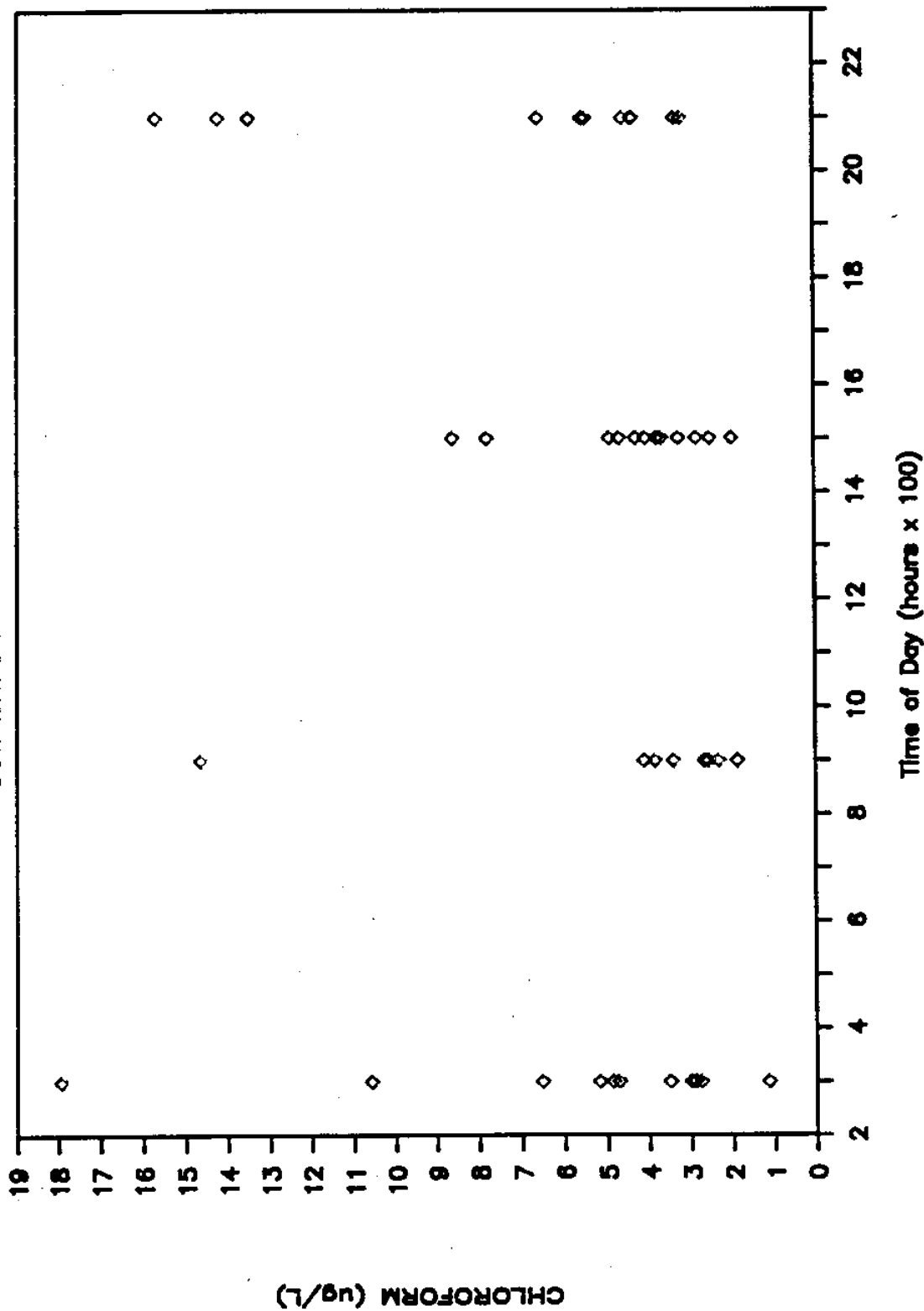


Figure 4.3 Deer Island haloform concentrations plotted as a function of time of day.
a) Data for CHCl_3

Haloform variations

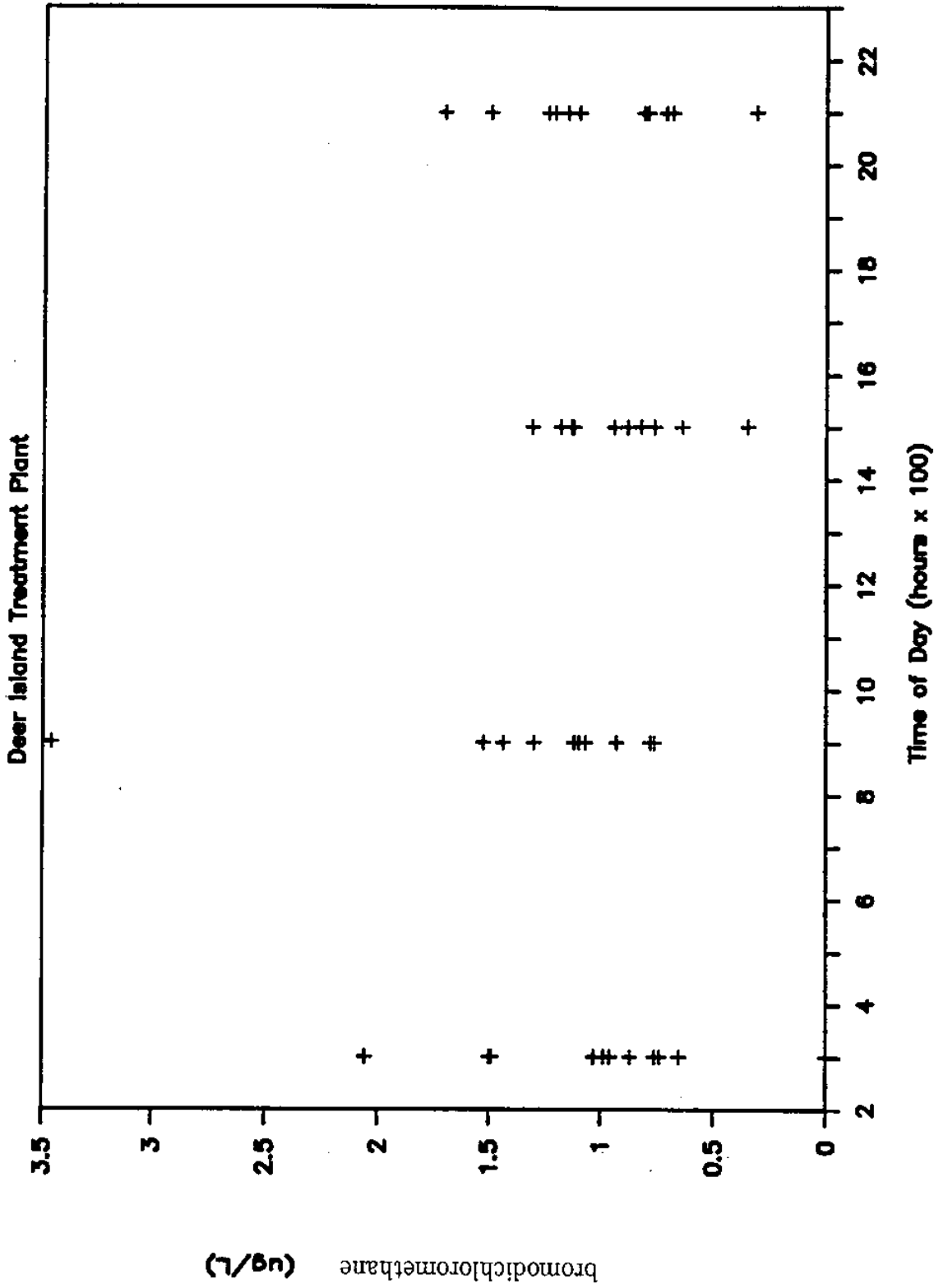


Figure 4.3b Data for CHBrCl₂

Haloform variations

Deer Island Treatment Plant

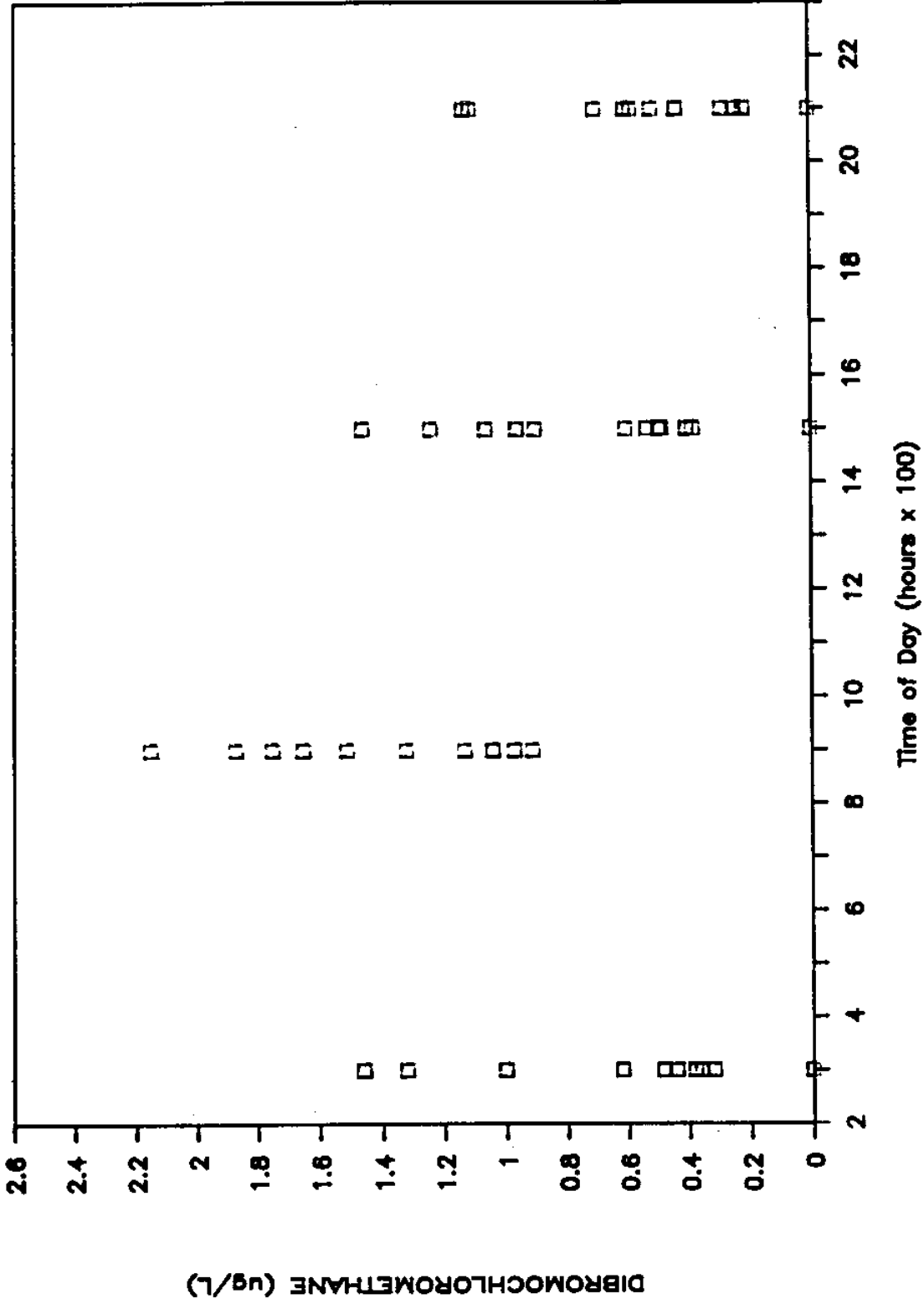


Figure 4.3c Data for CHBr₂Cl

Haloform variations

Deer Island Treatment Plant

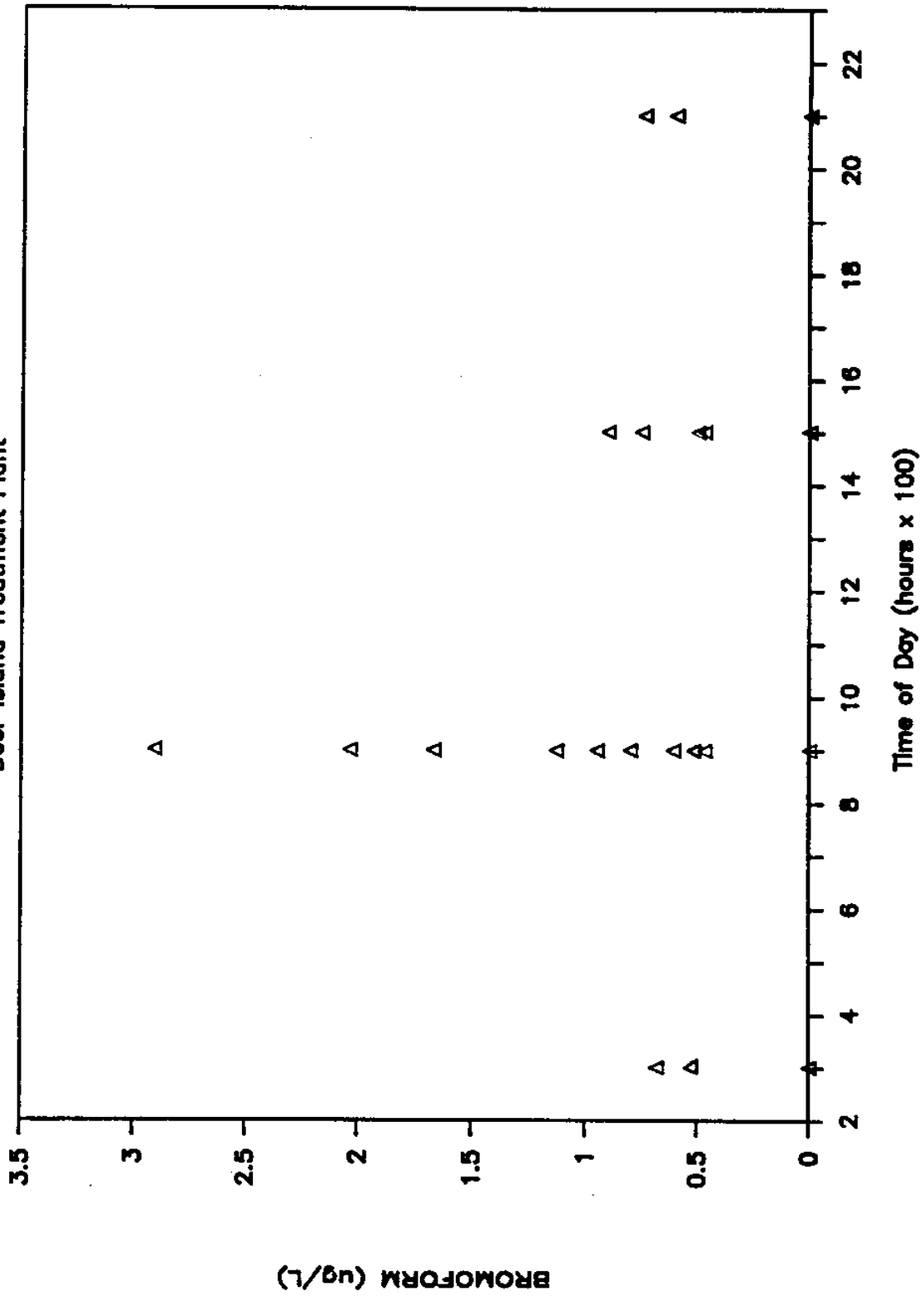


Figure 4.3d Data for CHBr₃

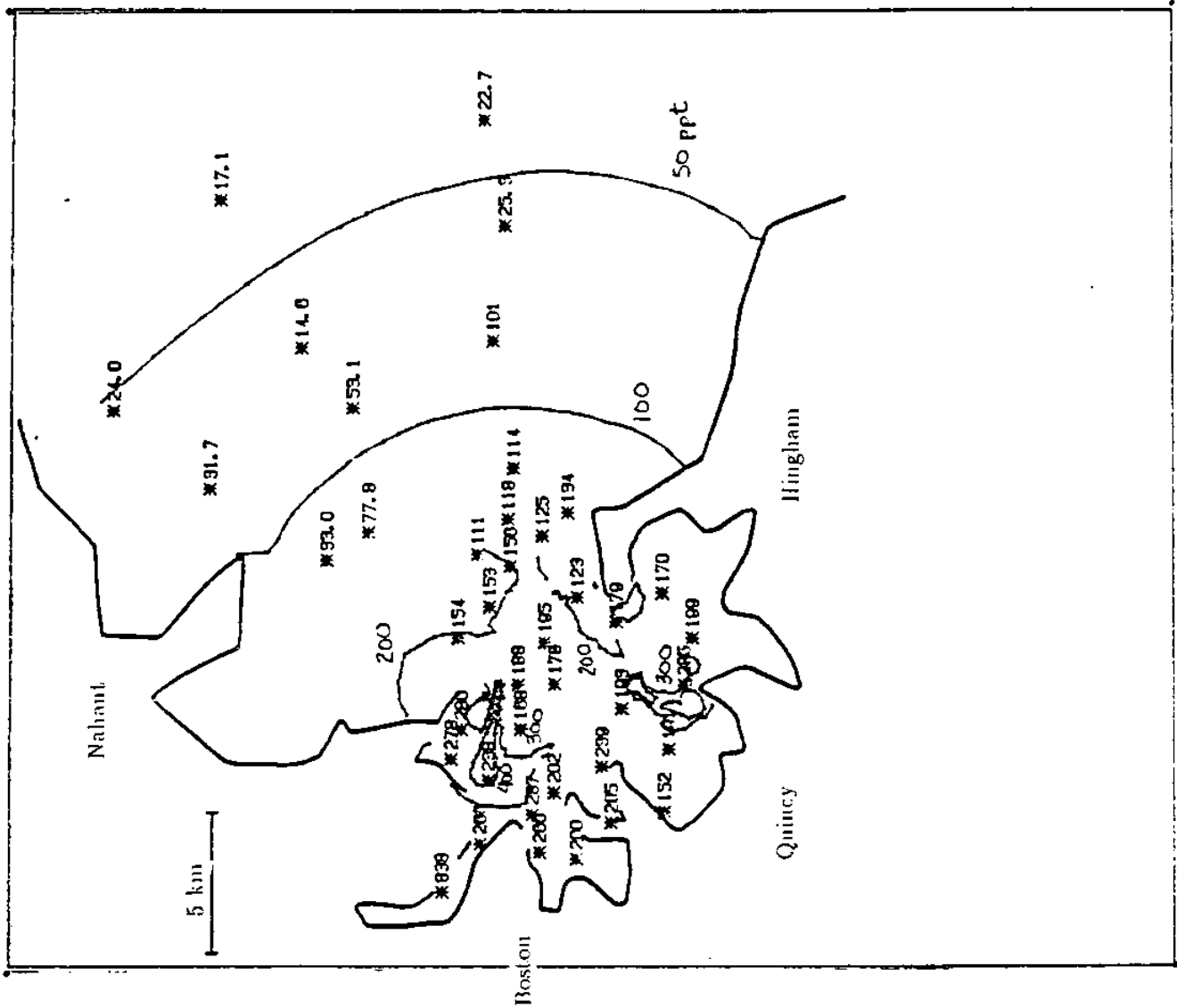


Figure 4.4a Measured concentrations (ppt) of CH_2Cl_2 compared with simulation

April 27, 1987

Boston Harbor/Mass Bay

VHOC Sampling

Methyl chloroform
($\text{ng} \cdot \text{L}^{-1}$)

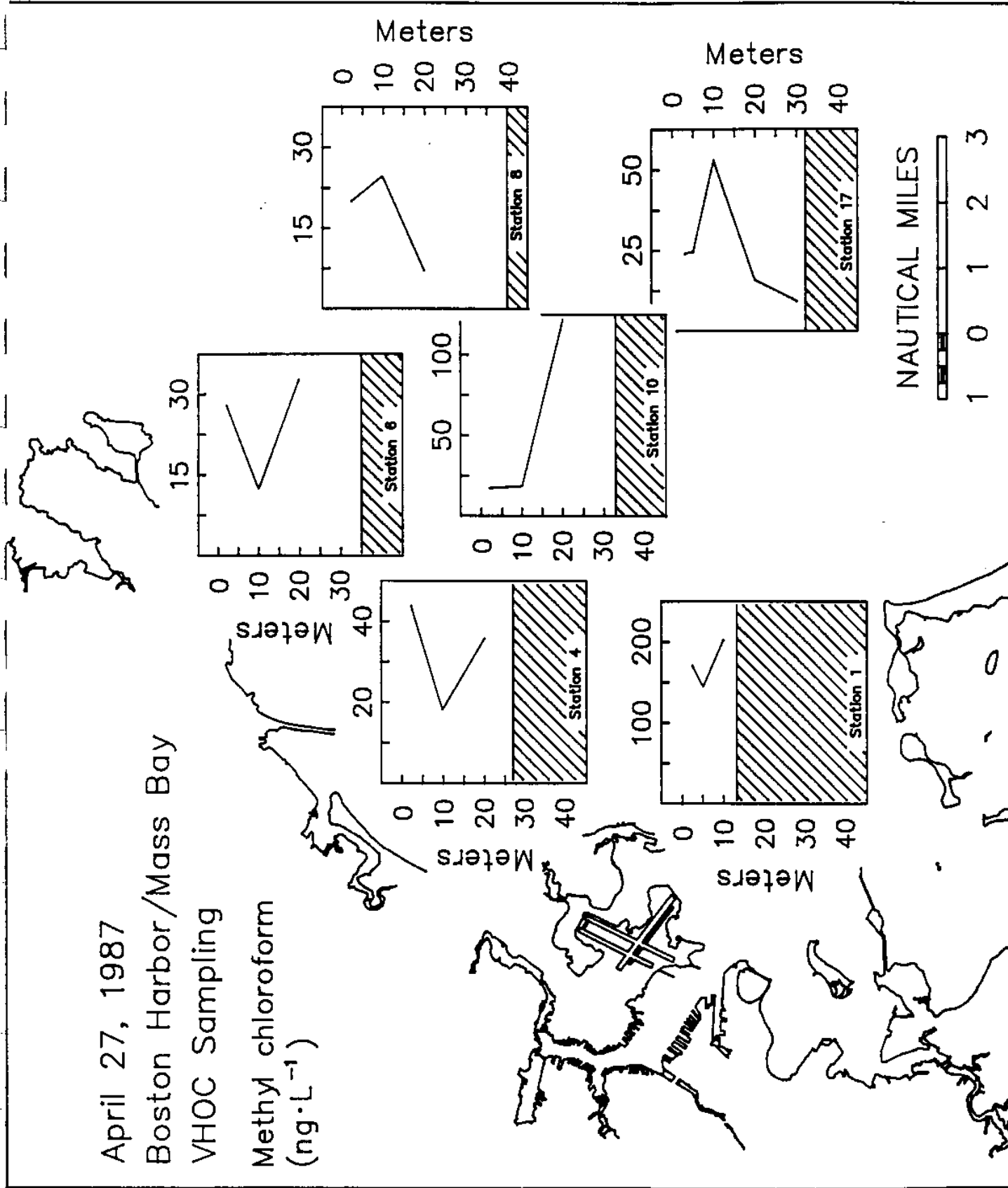


Figure 4.4b Measured vertical concentration profiles of CH_3CCl_3

April 27, 1987
 Boston Harbor/Mass Bay
 VHOc Sampling
 Trichloroethylene
 ($\text{ng} \cdot \text{L}^{-1}$)

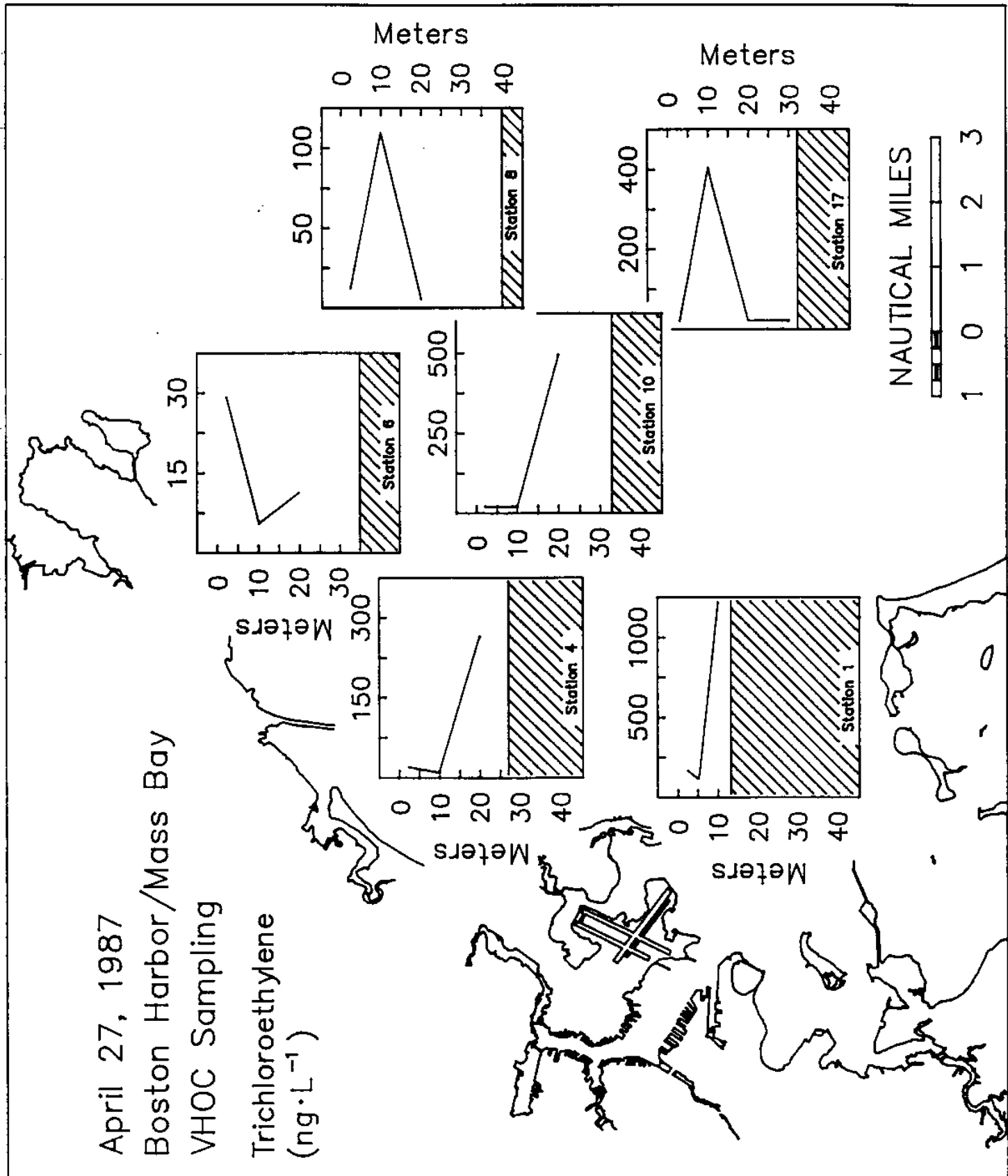


Figure 4.5b Measured vertical concentrations profiles of $\text{CHCl}=\text{CCl}_2$

April 27, 1987
 Boston Harbor/Mass Bay
 VHOc Sampling
 Bromodichloromethane
 ($\text{ng}\cdot\text{L}^{-1}$)

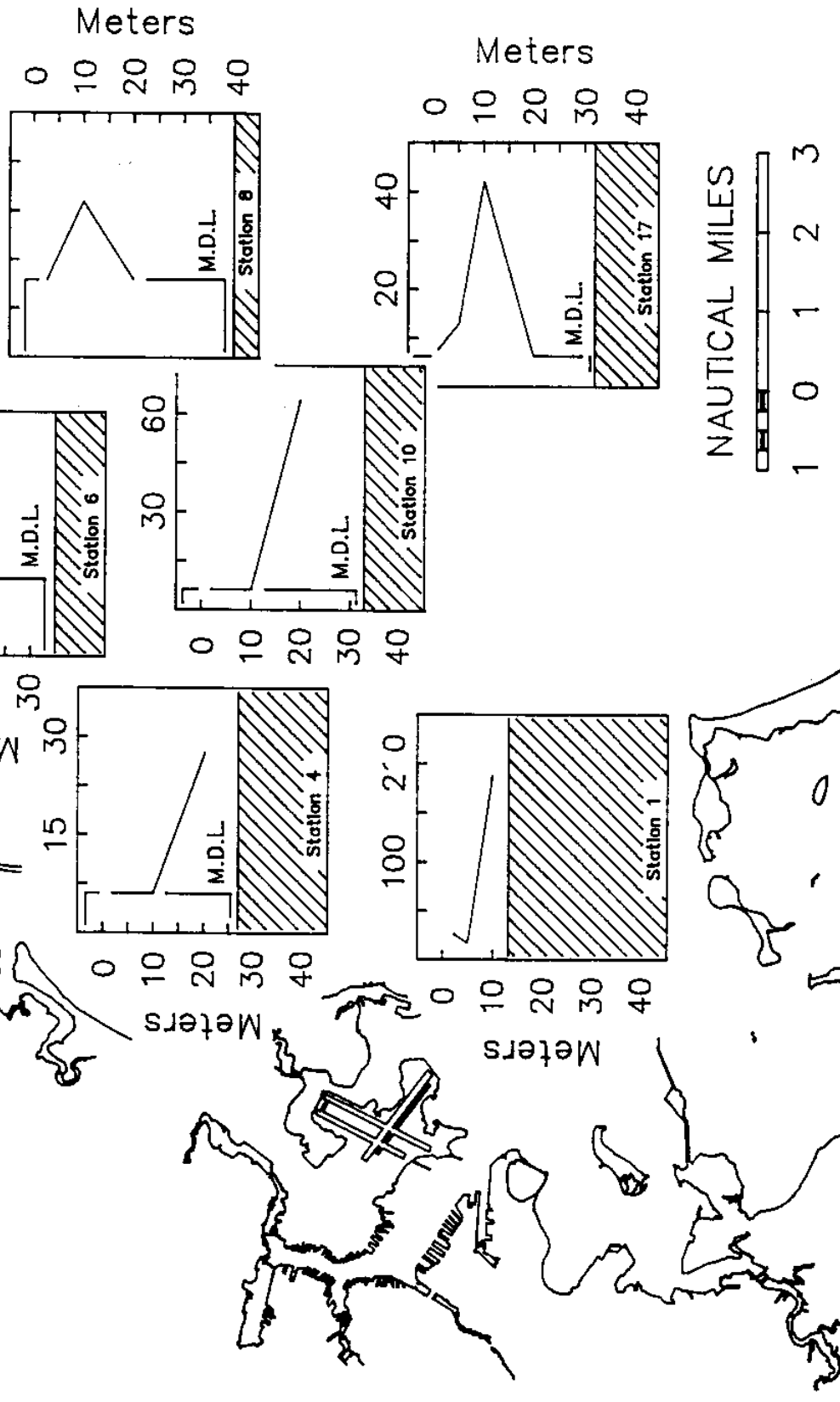


Figure 4.6b Measured vertical concentration profiles of CHBrCl₂

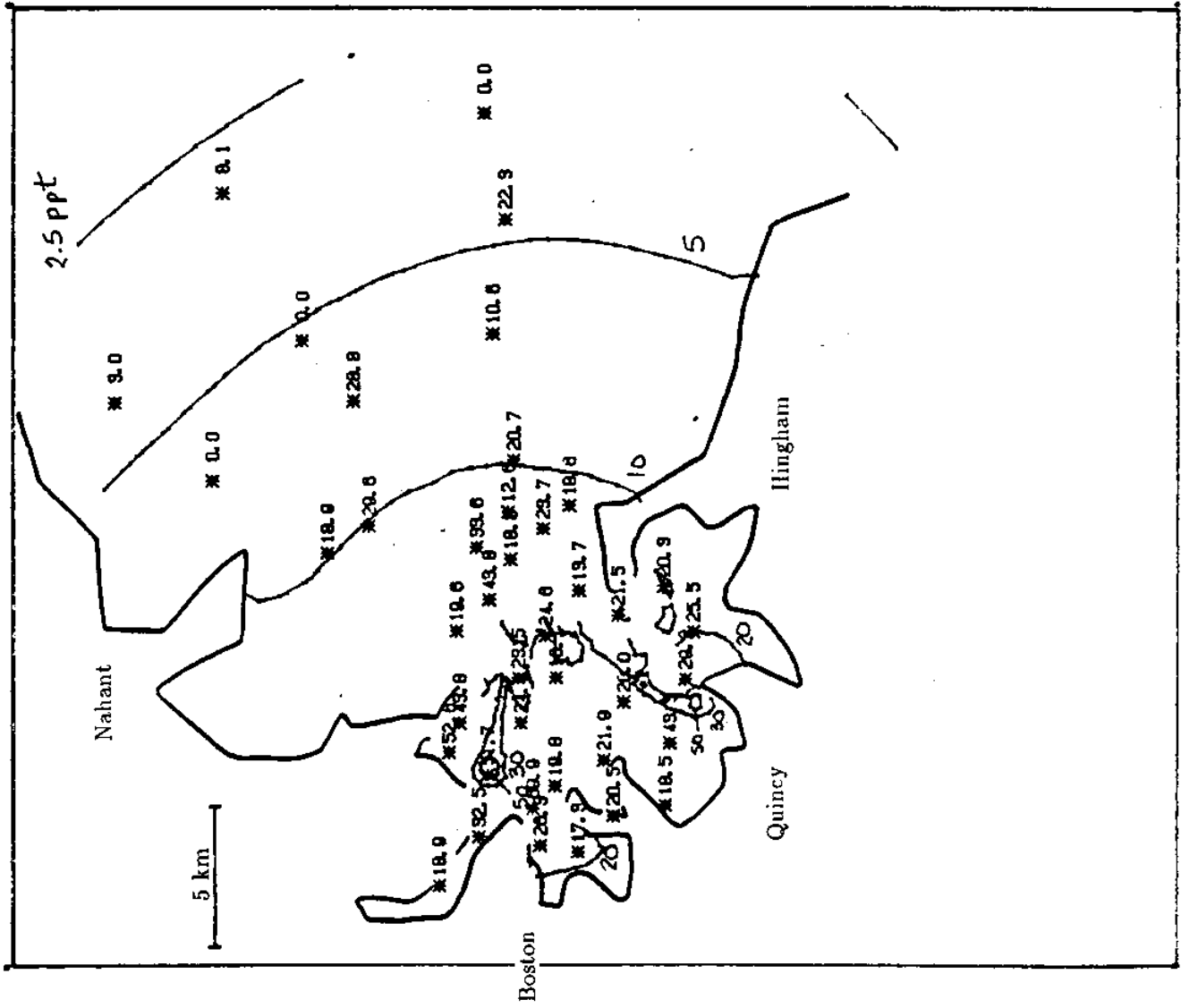


Figure 4.7a Measured concentration (ppt) of CHBr₂Cl compared with simulation

April 27, 1987

Boston Harbor/Mass Bay

VHOC Sampling

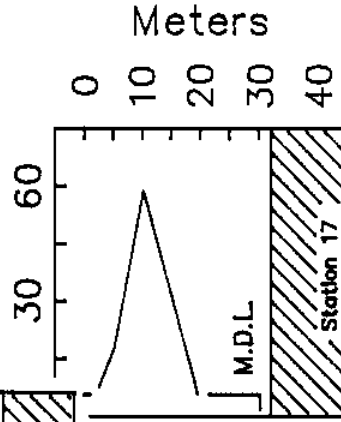
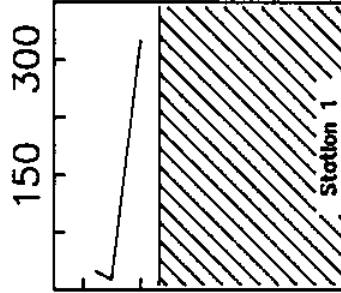
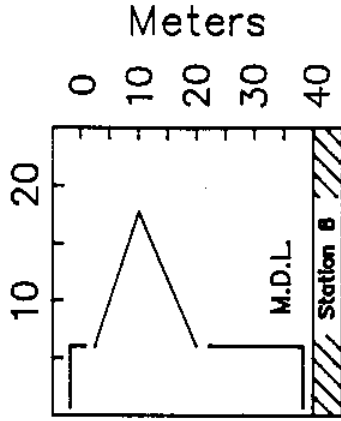
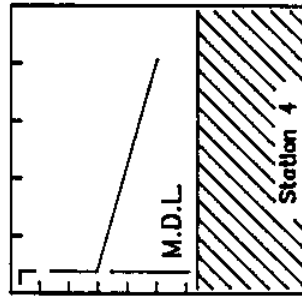
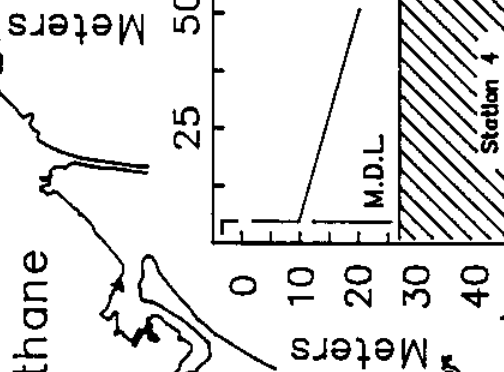
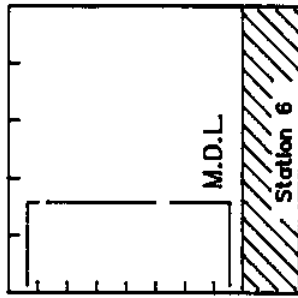
Dibromochloromethane

($\text{ng} \cdot \text{L}^{-1}$)

M.D.L.

Minimum Detection Limit

7.5 15



NAUTICAL MILES

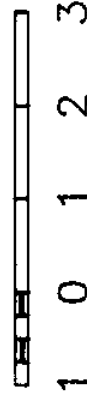


Figure 4.7b Measured vertical concentration profiles of CHBr_2Cl

April 27, 1987

Boston Harbor/Mass Bay

VHOC Sampling

Tetrachloroethylene
($\text{ng}\cdot\text{L}^{-1}$)

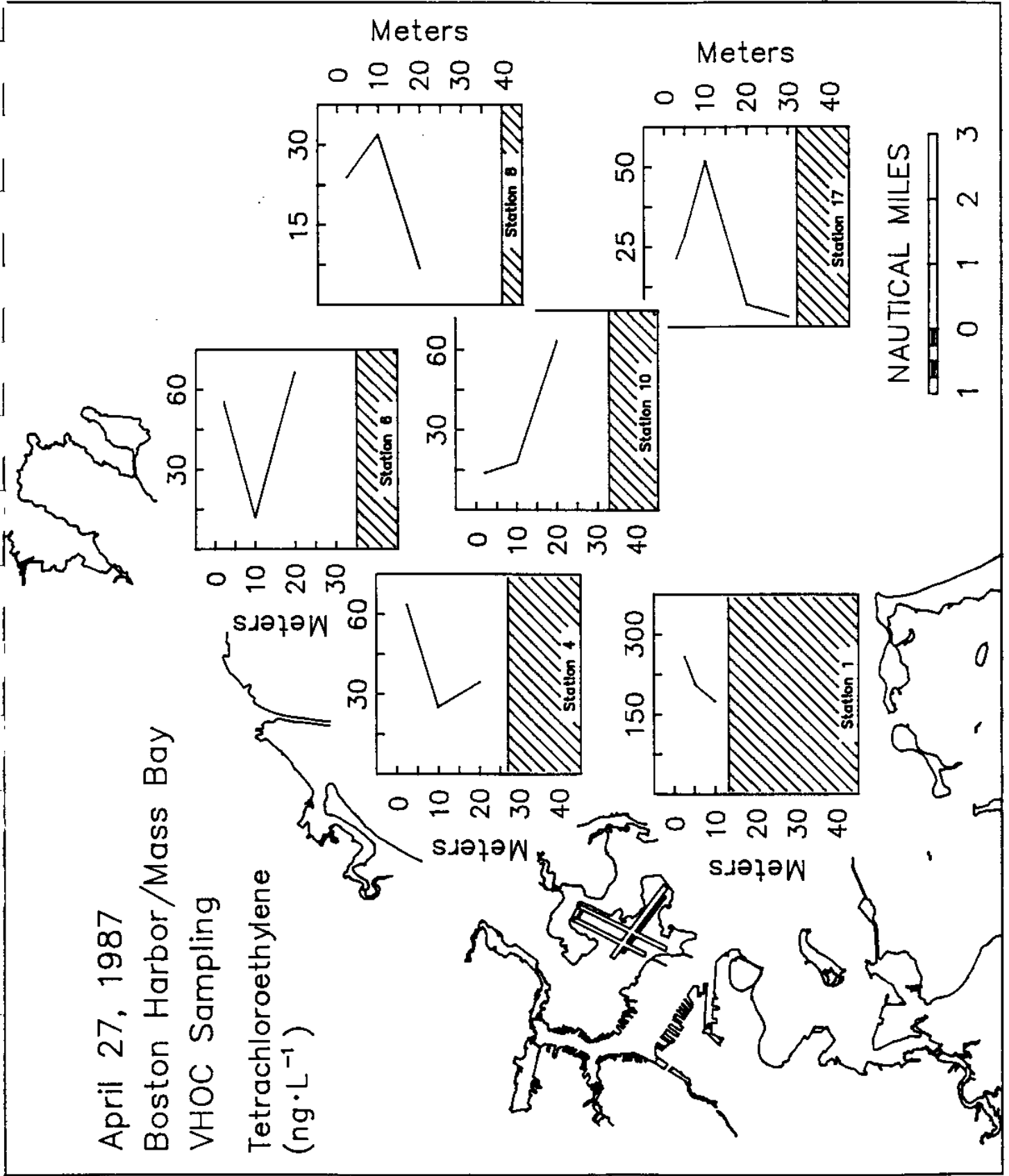


Figure 4.8b Measured vertical concentration profile of $\text{CCl}_2=\text{CCl}_2$

April 27, 1987
 Boston Harbor/Mass Bay
 VHOC Sampling

Carbon tetrachloride
 ($\text{ng} \cdot \text{L}^{-1}$)

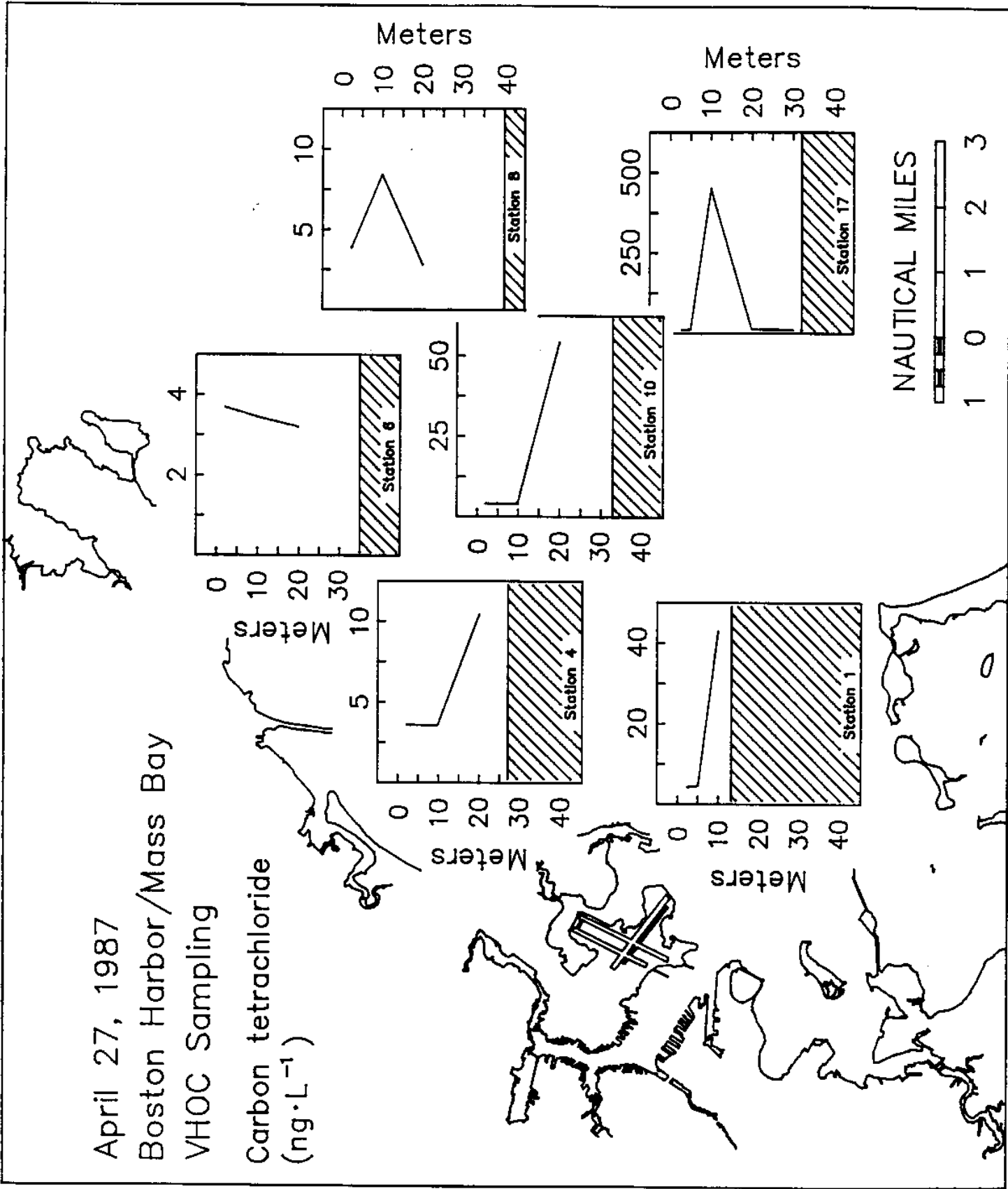


Figure 4.9b Measured vertical concentration profile of CCl_4

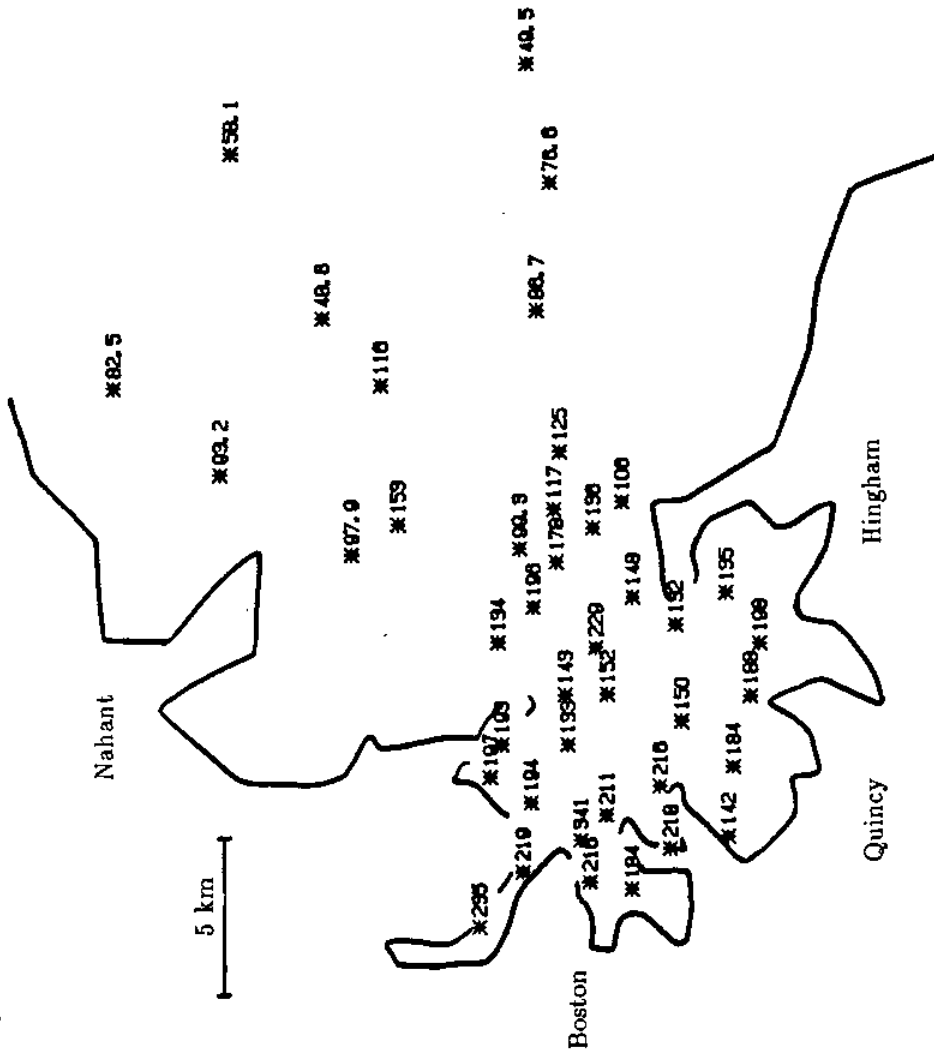


Figure 4.10a Measured concentrations (ppt) of CHBr₃

April 27, 1987

Boston Harbor/Mass Bay

VHOC Sampling

Bromoform
($\text{ng}\cdot\text{L}^{-1}$)

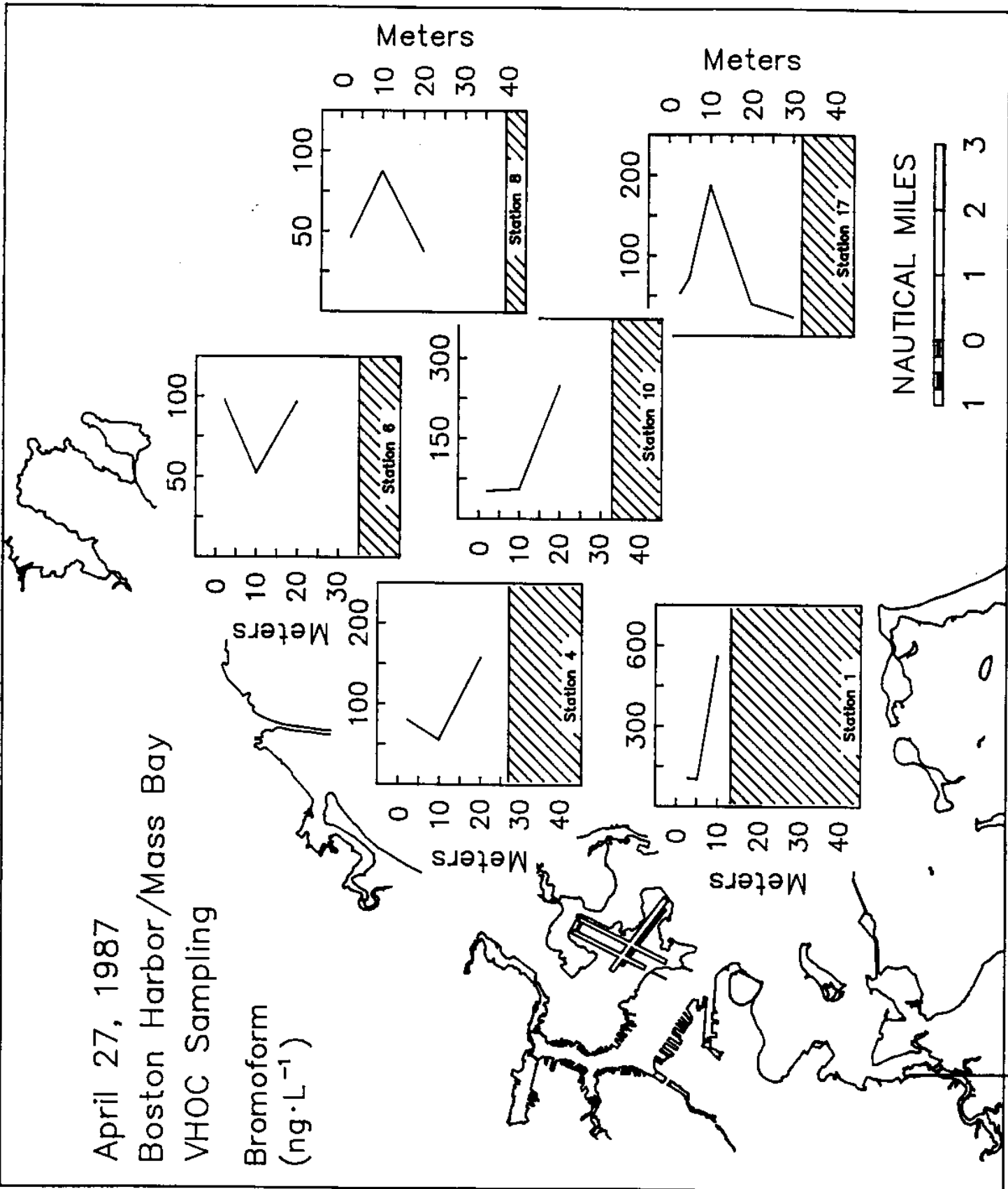


Figure 4.10b Measured vertical concentration profile of CHBr₃

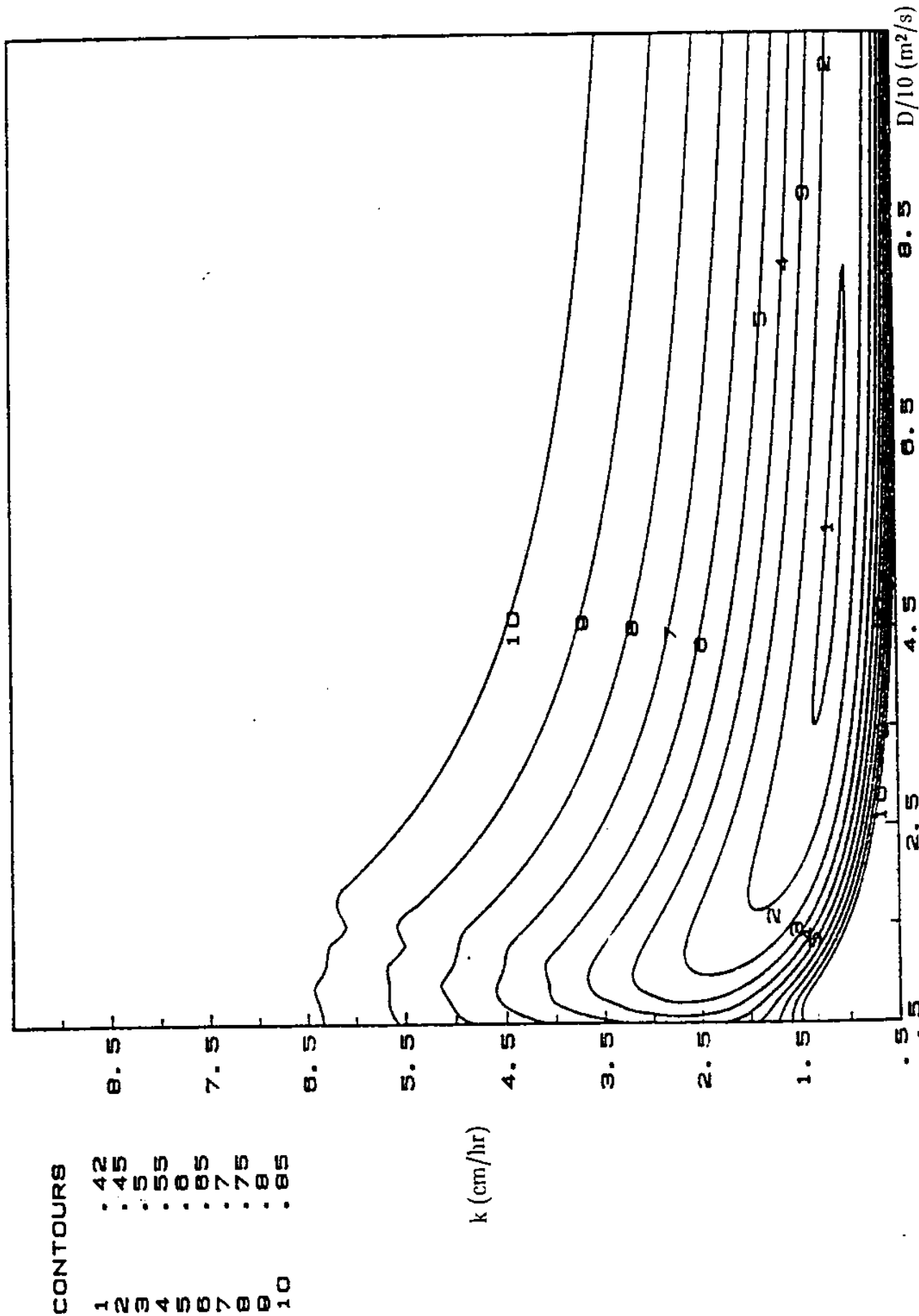


Figure 4.11 Contours of normalized mean square error between measured and simulated depth average concentration, using averaged data for CHBrCl_2 , CHBr_2Cl , $\text{CCl}_2=\text{CCl}_2$, $\text{CHCl}-\text{CCl}_2$, and CH_2Cl_2 , plotted versus volatization piston velocity k and dispersion coefficient D

5. SUMMARY AND CONCLUSIONS

In §2 sensitivity studies showed that ELA calculations are strongly dependent on site location, decay rate, dispersion coefficient, and low frequency (or steady) currents. The model was comparatively less sensitive to precise representation of tidal currents suggesting that most effort in the future analysis of currents be directed towards the low-frequency components. Sensitivity to boundary conditions and near field representation was identified, and it was suggested that these issues be examined further in the context of actual simulations.

In §3, the model was shown to predict the predominant M_2 tides reasonably well (~10-20% error). Worse agreement (~50%) was seen in simulating the non-linear dynamics (M_4 and M_6 tides). Discrepancies could be attributed to difficulties with model convergence and the associated need to use high bottom friction factors in the non-linear model. Further effort on the non-linear model calibration is required, but not a high priority on this project, and it is recommended that simulations be performed in the linear mode using iteration, using a value of $C_F = 0.005$.

Simulated low-frequency (or steady) currents are strongly dependent on specified tilt on the open boundary. Use of a steady 10-cm north-to-south tilt produced currents in the range of 0.3 to 5.7 cm/s in the region of potential outfall sites, in reasonable agreement with the magnitudes of the low frequency components of current meter measurements. Additional current meter data should be examined and spectral and time domain methods should continue to be used to study the correlation among currents and between currents and driving forces.

In §4, the April 1987 VHOC study was described, including a formal procedure for calibrating ELA parameters. The data set collected was much more comprehensive than previous studies—both regarding spatial coverage in the receiving water and regarding

temporal coverage of effluent loading—resulting in a more consistent calibration. However, the study was complicated by the somewhat anomalous condition of extremely high freshwater flow in the preceding month, leading to strong vertical stratification in tracer concentrations in western Massachusetts Bay. The best-fit dispersion coefficient and volatilization piston velocity were, respectively, $D = 45 \text{ m}^2/\text{s}$ and $k = 1.2 \text{ cm/hr}$. Unfortunately, however, computed error measures were quite insensitive in the range of $0.7 < k < 2.0 \text{ cm/hr}$ and $17 < D < 105 \text{ m}^2/\text{s}$ leaving some uncertainty regarding the most appropriate values.

The models TEA and ELA are being used to study both absolute and relative magnitudes of impact associated with alternative discharge locations. Uncertainty in model parameters (e.g., dispersion coefficient) and variability in other inputs (e.g., currents) should affect the simulated impact over the entire Massachusetts Bay for all discharge sites. Hence, the relative impact, associated with different sites, should be far less sensitive to parameter values.

It should also be re-stated that TEA and ELA assume a vertically homogeneous water column. Effects of density induced flows, vertical variations in current or stratification of natural or induced constituents, as well as any structure in the horizontal distributions of flow and concentration are not directly simulated. Additional transport (beyond the depth-averaged advection) caused by these phenomena is accounted for in the dispersion coefficients calibrated from the field surveys. These dispersion coefficients may conceptually be thought of as representing transport processes with a spatial scale of several kilometers (about a tidal excursion) and a temporal scale of about a day. Computed concentrations should be considered as representing averages over these same scales.

Finally, the models have been calibrated to current meter data representing one period of one year and measurement locations limited to the upper northwest corner of Mass Bay. Thus the models can not be considered to be calibrated with respect to Bay-wide circulation patterns or to other seasons of the year.

6. REFERENCES

- Adams, E. E.; R. F. Kossik, and A. M. Baptista. 1986. Source representation in a numerical transport model. 6th Int'l. Conf. on Fin. Elem. in Wat. Res., Lisbon.
- Baptista, A. M., E. E. Adams, and K. D. Stolzenbach. 1985. Comparison of several Eulerian-Lagrangian models to solve the advection-diffusion equation. Proc. of Int'l Symp. on Refined Flow Modeling and Turbulence Measurements, U. of Iowa, Iowa City, Iowa
- Baptista, A. M., E. E. Adams, and K. D. Stolzenbach. 1986. Accuracy analysis of the backwards method of characteristics. 6th Int'l Conf. on Fin. Elem. in Water Resources, Lisbon.
- Baptista, A. M., E. E. Adams, and K. D. Stolzenbach. 1984. The solution of the 2-D unsteady, convective diffusion equation by the combined use of the FE method and the method of characteristics. Report No. 296, R. M. Parsons Lab., MIT.
- Baptista, A. M. 1987. Solution of advection dominated transport by Eulerian-Lagrangian methods using the backwards method of characteristics. Ph.D. Thesis, Dept. of Civil Engineering, MIT
- Battelle Pacific Northwest Laboratories. 1982. Analysis of organohalogen and other organic chemicals in cooling waters discharged from Redondo Generating Station. Report No. 81-RD-127. Prepared for Southern California Edison under Contract 2311204478, January.
- Helz, G. R., and R. Y. Hsu. 1978. Volatile chloro- and bromocarbons in coastal waters. *Limnol. Oceanog.* 23(5):858-869.
- Ketchum, B. H. 1951. The dispersion and fate of pollution discharged into tidal waters, and the viability of enteric bacteria in the sea. Reference No. 51-11, Woods Hole Oceanographic Institution, Woods Hole, Mass.
- Kossik, R. F., P. S. Gschwend, and E. E. Adams. 1986. Tracing and modeling pollutant transport in Boston Harbor. Sea Grant Report No. 86-016, MIT.
- Metcalf & Eddy. 1979. Application for modification of secondary treatment requirements for its Dear Island and Nut Island effluent discharge into marine waters. Prepared for the MDC, Boston, Mass.
- Westerink, J. J., et al. 1984. Users manual for TEA-LINEAR, a linearized harmonic finite element circulation model. Report No. MIT-EL 84-012, MIT Energy Laboratory, Cambridge, Mass.
- Westerink, J. J., K. D. Stolzenbach, and J. J. Connor. 1985. A frequency domain finite element model for tidal circulation. Report No. MIT-EL 85-006, MIT Energy Laboratory.
- Westerink, J. J., J. J. Connor, K. D. Stolzenbach. 1986a. A frequency-time domain finite element model for tidal circulation based on the least squares harmonic analysis method. Submitted to *International Journal for Numerical Methods in Fluids*.
- Westerink, J. J., J. J. Connor, K. D. Stolzenbach. 1986b. A primitive pseudo wave equation formulation for solving the harmonic shallow water wave equations. Submitted to *Advances in Water Resources*.